AEDC TR-96-7

An Analytic Investigation of Accuracy Requirements for Onboard Instrumentation and Film Data for Dynamically Scaled Wind Tunnel Drop Models

K. S. Keen, C. H. Morgret, and R. L. Arterbury
Sverdrup Technology, Inc., AEDC Group

March 1997

Final Report for Period June 1992 — June 1993

ARNOLD ENGINEERING DEVELOPMENT CENTER
ARNOLD AIR FORCE BASE, TENNESSEE
AIR FORCE MATERIEL COMMAND
UNITED STATES AIR FORCE

NOTICES
When U. S. Government drawings, specifications, or other data are used for any purpose other than a definitely related Government procurement operation, the Government thereby incurs no responsibility nor any obligation whatsoever, and the fact that the Government may have formulated, furnished, or in any way supplied the said drawings, specifications, or other data, is not to be regarded by implication or otherwise, or in any manner licensing the holder or any other person or corporation, or conveying any rights or permission to manufacture, use, or sell any patented invention that may in any way be related thereto.
Qualified users may obtain copies of this report from the Defense Technical Information Center.
References to named commercial products in this report are not to be considered in any sense as an endorsement of the product by the United States Air Force or the Government.

This report has been reviewed by the Office of Public Affairs (PA) and is releasable to the National Technical Information Service (NTIS). At NTIS, it will be available to the general public, including foreign nations.

APPROVAL STATEMENT

This report has been reviewed and approved.

LEO R. MARPLE, JR
Aircraft Systems Test Division
Test Operations Directorate

Approved for publication:

FOR THE COMMANDER

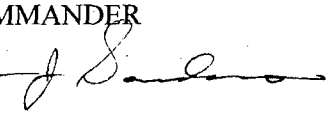

EUGENE J. SANDERS
Technical Director, Aircraft Systems Test Division
Test Operations Directorate

DISCLAIMER NOTICE

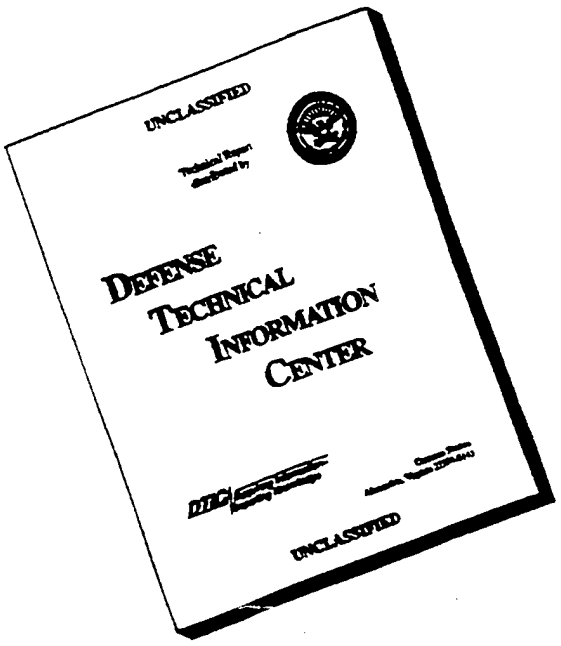

THIS DOCUMENT IS BEST QUALITY AVAILABLE. THE COPY FURNISHED TO DTIC CONTAINED A SIGNIFICANT NUMBER OF PAGES WHICH DO NOT REPRODUCE LEGIBLY.

REPORT DOCUMENTATION PAGE

Form Approved
OMB No. 0704-0188

1. AGENCY USE ONLY (Leave blank)	2. REPORT DATE	3. REPORT TYPE AND DATES COVERED
	March 1997	Final Report for June 1992 - June 1993

4. TITLE AND SUBTITLE

An Analytic Investigation of Accuracy Requirements for Onboard Instrumentation and Film Data for Dynamically Scaled Wind Tunnel Drop Models

5. FUNDING NUMBERS

PN 0675

6. AUTHOR(S)

K. S. Keen, C. H. Morgret, and R. L. Arterbury
Sverdrup Technology, Inc., AEDC Group

7. PERFORMING ORGANIZATION NAME(S) AND ADDRESS(ES)

Arnold Engineering Development Center/DOF
Air Force Materiel Command
Arnold AFB, TN 37389-6000

8. PERFORMING ORGANIZATION (REPORT NUMBER)

AEDC-TR-96-7

9. SPONSORING/MONITORING AGENCY NAMES(S) AND ADDRESS(ES)

ASC/YFFFI
Wright-Patterson Air Force Base, OH 45433

10. SPONSORING/MONITORING AGENCY REPORT NUMBER

11. SUPPLEMENTARY NOTES

Available in Defense Technical Information Center (DTIC).

12A. DISTRIBUTION/AVAILABILITY STATEMENT

Approved for public release; distribution is unlimited.

12B. DISTRIBUTION CODE

13. ABSTRACT (Maximum 200 words)

An analytic study was conducted to evaluate anticipated ranges and required accuracies for onboard linear acceleration and angular rate (or acceleration) measurement equipment to be mounted within dynamically scaled wind tunnel drop models. Generic simulations of the separation motion of a tumbling fuel tank both at full scale and at 1/15th wind tunnel model scale were generated using an analytic trajectory simulation program coupled with a prescribed aerodynamic database. The simulations provide a basis for sizing the required instrumentation for proof-of-concept demonstrations of telemetry techniques in the wind tunnel. The simulations were also used as test cases to demonstrate extraction of aerodynamic information from drop data positions and orientations as read from film records via an inverse solution of the store equations of motion. The studies also aid identification and evaluation of inaccuracies associated with the basic dynamic scaling laws and standard film-based data reduction techniques.

14. SUBJECT TERMS

dynamic scaling
free drop testing
telemetry
trajectory film data
motion simulation
store separation

15. NUMBER OF PAGES

119

16. PRICE CODE

17. SECURITY CLASSIFICATION OF REPORT	18. SECURITY CLASSIFICATION OF THIS PAGE	19. SECURITY CLASSIFICATION OF ABSTRACT	20. LIMITATION OF ABSTRACT
UNCLASSIFIED	UNCLASSIFIED	UNCLASSIFIED	SAME AS REORT

COMPUTER GENERATED

Standard Form 298 (Rev. 2-89)
Prescribed by ANSI Std. Z3918

PREFACE

The work reported herein was conducted at the Arnold Engineering Development Center (AEDC), Air Force Materiel Command (AFMC). The major portion of the effort was sponsored by the store separation effort for the F-22 aircraft at the request of the Aeronautical Systems Center (ASC/YFT), AEDC Project Number 0675. The ASC/YFFIT Project Manager was Mr. Pete Amstutz. The results were obtained by Calspan Corporation/AEDC Operations, operating contractor during the period when the work was conducted for the Aerospace Flight Dynamics effort at the AEDC, AFMC, Arnold Air Force Base, TN. The work was conducted during the period June 1992 through June 1993, and the manuscript was submitted for publication on February 6, 1997.

CONTENTS

ILLUSTRATIONS

TABLES

APPENDIX

1.0 INTRODUCTION

The information contained herein was developed to assist planning for a technology demonstration program in which the capability to instrument a free-falling model in the wind tunnel and transmit the measured data out of the model was demonstrated. Prior to the demonstration effort, an analytic study (the subject of the current report) was conducted to evaluate anticipated ranges and required accuracies for onboard linear acceleration and angular rate (or acceleration) measurement equipment which was to be mounted within the dynamically scaled wind tunnel drop models. Generic simulations of the separation motion of a tumbling fuel tank store both at full scale and at a 1/15th wind tunnel model scale were generated using an analytic trajectory simulation program coupled with a prescribed aerodynamic database. The simulations were also used as test cases to demonstrate extraction of aerodynamic information from drop data positions and orientations as read from film records via an inverse solution of the store equations of motion. The studies also aid identification and evaluation of inaccuracies associated with the basic dynamic scaling laws and standard film-based data reduction techniques. The current report only discusses the analytical aspects of the study. The current report also provides an Appendix detailing the derivation and compromises associated with the various wind tunnel dynamic scaling laws. An overview of results of the follow-on experimental effort using both instrumented telemetry models and standard film reduction techniques is available in Ref. 1.

Normally free-drop data are comprised of store model positions and orientations relative to the aircraft reduced from high-speed film records of the drop events. Typically only the final motion parameters from the experimental drops are measured (i.e., only the 'effects' are defined). In many cases the accuracy of the data reduction is limited by lack of visual access to the model and human error associated with 'reading' the film. Similar data reduction problems (but on a much larger scale) are associated with full-scale flight tests because cameras on the flight-test aircraft, chase aircraft, and ground-based cinetheodolite cameras are often the only instrumentation available to record flight events. Onboard instrumentation would, however, allow direct measurement of the rates and accelerations that are directly related to the aerodynamic 'causes' of the store motion in both the wind tunnel and flight cases and, therefore, provide much more useful information for simulation verification, flight-test and wind tunnel data reduction, and similar purposes.

An opportunity for wind tunnel demonstration of instrumented-model technology was identified in association with the first in a series of wind tunnel drop tests of fuel tank releases from the F-22 aircraft which was conducted in 1994. The F-22 was selected as the aircraft of choice for several reasons: (1) Lockheed - Martin Tactical Aircraft Systems (LMTAS), which maintains responsibility for F-22 weapons integration, has industry's largest experience base in free-drop model design, (2) extracted data from F-22 tank releases were highly desired for validation of analytical trajectory-prediction methods which were to form a large part of the F-22 store-separation program, (3) the F-22 tank at 1/15th-scale represents one of the largest bodies ever used in a wind tunnel free-drop test program and is thus ideal for first demonstration of the miniaturized instrumentation, and (4) a large database of trajectory data for a similar fuel tank from the F-16 aircraft at the same scale is available. No F-22 results are actually presented in this document (F-22 results are available in Ref. 1). Instead, only results from the generic pre-test analytical stud-

ies, which were so fundamental to the understanding that led to the ultimate success of the F-22 experimental program, are presented.

2.0 TRAJECTORY MODELING

Two types of techniques are available for modeling flight drops in a ground-simulation environment. Either a repetitive solution of the six-degree-of-freedom (6-DOF) equations of motion of the separating store can be generated on a computer (using either predicted aerodynamic forces and moments or sub-scale wind tunnel measurements) or a dynamically similar scale model can actually be dropped in the tunnel and its motion recorded. One intent of the current analytic study was to use a computer simulation to emulate both full-scale drops and drops of dynamically scaled wind tunnel models. The analytical simulations are free from data-reduction "noise" of most experiments and allow direct evaluation of the compromises involved in simulating full-scale drops at wind tunnel scale. The simulated analytical trajectories also provide the source data for determining the ranges of accelerations and rates that the instrumentation package must be designed to measure.

2.1 COMPUTER SOLUTION OF EQUATIONS OF MOTION

A simulation program known as the Flow-field/Loads Influence Prediction Trajectory Generation Program (or FLIP TGP) (Ref. 2) was used for the analytical tank release simulations. (The FLIP TGP was selected because it was intended to be a primary tool in the generation of tank trajectories for the production F-22 test program.) For the current effort, only limited capabilities of the FLIP TGP were used to generate the simple analytical drop trajectories. Pitch plane motion (3-DOF) trajectories for a tumbling tank were generated using a simple aerodynamic model of the standard F-15 tank without tail fins. Slosh of the fuel within the tank was assumed not to occur, and the tank moments of inertia were held constant. The tank was oriented at an initial release angle relative to the gravity vector of 8 deg nose up. Mass properties corresponding to a quarter-full fuel tank were used for most simulations.

The free-stream aerodynamic data on the tank used in the computer simulations were based on data for a similar configuration. The free-stream data were obtained over an angle-of-attack range of 12 to -40 deg and were used in an aeroballistic form for the simulations. The free-stream data were extended to extreme angles of attack (0 to 360) using mirroring techniques involving trig functions and by a semi-empirical prediction code known as the Missile Distributed Airloads (MDA) program, which is also an integral component of the FLIP TGP. Rotational aerodynamic damping was simulated using an input damping derivative (C_{mq}) value of -15.0, which was converted to a full-scale damping moment increment based on the pitch rates from the equation-of-motion solutions. The dynamic rotational damping increment was added to the static moments obtained from the free-stream database before each evaluation of the equations of motion. The F-22 tank is being designed for jettison from the aircraft with its pylon attached. Mass properties of the combined pylon/tank assembly were used in the computer simulations but no aerodynamic effects of the pylon were included in the simple aerodynamics model.

2.2 DYNAMICALLY SCALED DROP TESTING

The motion of a full-scale store separating during flight and a small-scale model released in a wind tunnel can be dynamically similar provided two basic criteria are met. First, the aerodynamic forces and moments on the model store must directly scale to flight forces and moments. Second, the inertial motion responses of the wind tunnel model to the applied forces and moments must be directly scalable to flight motion responses. Unfortunately, it is physically impossible to fully satisfy both criteria at the same time for a sub-scale model, and some compromise in selected aspects of the dynamic simulation must be accepted. Of the three major compromised scaling laws available, the so-called "heavy-scaling" laws are generally the most often used for larger wind tunnel models (generally 1/20th scale or greater) and have been selected for the F-22 tank effort. Complete derivations of the scaling laws are provided in Appendix A. The heavy-scaling laws from Appendix A are reproduced below.

PHYSICAL PROPERTIES

gravitational acceleration:	$g' = g$	(1)
time:	$t' = t\sqrt{(\Lambda)}$	
free-stream velocity:	$V_\infty' = V_\infty * \sqrt{(T_\infty'/T_\infty)}$	
Mach number:	$M_\infty' = M_\infty$	
linear dimensions:	(model coords)' = Λ *(full-scale coords)	
mass or weight:	$m' = m*(Q_\infty'/Q_\infty)*\Lambda^2$	
inertias:	$IYY' = IYY*(Q_\infty'/Q_\infty)*\Lambda^4$	
ejector forces:	$FEZ' = FEZ*(Q_\infty'/Q_\infty)*\Lambda^2$	

MOTION PROPERTIES

linear translations:	XFBF' = XFBF *Λ [X'=X *Λ]
linear velocities (except free stream):	UBBI' = UBBI*$\sqrt{(\Lambda)}$ [u'=u*$\sqrt{(\Lambda)}$]
linear accelerations (or velocity derivatives):	DUBBI' = DUBBI [udot'=udot]
angles:	THABF' = THABF [$\theta'=\theta$]
angular rates:	QBBI' = QBBI/$\sqrt{(\Lambda)}$ [q'=q/$\sqrt{(\Lambda)}$]
angular accelerations (or velocity derivatives):	QBBI' = DQBBI/Λ [qdot'=qdot/Λ]

where the primed terms indicate reduced-scale model quantities, and Λ is the scale factor for model linear dimensions. Each of the three major scaling laws involves built-in compromises and errors as described in Appendix A. The major compromise of heavy scaling, for instance, is that the free-stream flow velocity and the motion velocities are scaled in a somewhat inconsistent manner. By performing analytical simulations before the actual test, using both full-scale properties and the dynamically scaled model-scale properties for the wind tunnel experiment, it is possible to evaluate the effects of the scaling compromises on the accuracy of the experimental wind tunnel motions.

The experimental heavy-scaled free-drop models are primarily designed according to the scaling criteria for mass and pitch moment of inertia. A design mass for the model is selected so that the test dynamic pressure, Q_∞', which appears in the mass scaling law, is within the operating limits of the wind tunnel. This requirement often necessitates that free-drop models be built from exotic metals and alloys (such as gold or kinertium) in order to achieve the desired mass density. (Even then, for smaller wind tunnels which necessitate that models significantly smaller than 1/20th scale be used, it is sometimes impossible to find a material dense enough to satisfy the heavy mass scaling, and some other scaling law must be used.) In contrast, non-dense stores such as empty or partially filled fuel tanks necessitate use of light-weight materials such as balsa wood or plastic. The mass must be distributed within the model in such a way as to achieve the scaled moments and products of inertia. Unfortunately, when physically building the wind tunnel drop models, it is often extremely difficult to match mass and all the moments and products of inertia simultaneously. Most often, the cross-products of inertia and the moments of inertia about the roll and yaw axes are not rigorously matched, and only the pitch moment of inertia (which is the dominant inertial term for tumbling tank motion) is considered in the dynamic model design. For the analytical simulations, of course, exact correct scaling can be easily applied to all properties. Packaging of instrumentation within a drop model can be greatly impacted by the locations of the distributed masses within the model, and the contributions of the package itself to the total store mass and moments of inertia must be considered in the model design and mass balancing.

Although scaling relationships have been developed for external ejector forces, these relationships are rarely used in the actual design of an experimental drop model. Normally the full-scale ejector forces are imparted by some type of pyrotechnic device so that the forces are non-linear functions of time or ejector piston stroke length. It is typically very difficult to mechanically simulate the scaled ejector forces as a function of scaled time in the drop test. Instead, an alternate simulation of the ejector is performed in which the spring coefficient of a spring, modeling the ejector, is tuned until the store demonstrates the desired scaled vertical velocity and pitch rate at a position corresponding to the end of the ejector stroke. The exact time history of the ejector force during the stroke is, thus, not simulated but the integrated area (impulse) of the ejector forces as a function of time is properly modeled. For analytical simulations, as is the case with mass properties, the scaling laws can, in contrast, be applied directly and rigorously to the full-scale ejector curves.

Many stores (including fuel tanks) are constrained by some type of rail system or ball-in-socket pivot mechanism during the initial portions of the trajectory. Such mechanisms must be simulated in hardware for drop testing and in software for the analytical simulations. The numerical model of the pivot restraint device used for the analytical study is described in Section 4.3.6 of Ref. 3.

Dynamic models have been mounted on the aircraft in various ways. One of the most common techniques is to hold the store on the aircraft (with the constraint mechanism engaged and the ejector spring compressed) using a small screw known as a "burn bolt." The screw is machined locally to a small diameter at one point and is connected to a high-amperage current source. When store release is commanded, a current of approximately 1,200 amp instantly vaporizes the reduced-diameter portion of the screw, releasing the store and allowing it to respond to

the spring forces. The burn-bolt technique has been used for most dynamic tank drop tests. A typical burn-bolt installation is shown in Fig. 1. It should be noted that on occasion during drop testing, the high-amperage current has been known to "arc" across the grounding pads between the aircraft and store models without vaporizing the burn bolt. Such "misfires" could potentially have disastrous consequences on instrumentation contained within the free-drop model if not properly grounded, and survival of the telemetry package and the transmitted signals during burn-bolt event must be a prime consideration for instrumented model design.

Physical size constraints can also be imposed on the size and placement of instrumentation within wind tunnel drop models as part of the drop model design. To illustrate this point, several models designed and developed by LMTAS (formerly General Dynamics) for an F-16 version of the standard 600-gal tank will be described. The basic contour of the tank is presented in the 1/15th-scale drawing of Fig. 2. Note that the tank has identical nose and tail sections. One proposal for an F-22 version of the tank is illustrated in Fig 3. The aft end of the tank shown in Fig. 3 has been modified to allow entrance of the model support sting for CTS wind tunnel testing. One previously tested design of a heavy-scaled F-16 tank configuration representing a tank fully loaded with fuel is presented in Fig. 4. The forward and aft sections of the tank are made of balsa wood with a solid steel centerbody. The 1/15th-scale model was designed for a tunnel-to-flight dynamic pressure ratio of 0.352 resulting in a scaled model weight of 7.027 lb. The small "J" hook for the pivot mechanism can also be seen. Later designs for drop models of empty tanks with truncated bases at different body lengths are shown in Fig. 5. These models were designed for a somewhat higher dynamic pressure ratio of 0.788 but resulted in low total weights of around 1.22 lb because of the lack of fuel mass. Design weight would be proportionally reduced for lower design dynamic pressure ratios. It is important to point out that it would be highly undesirable from the standpoints of model design and mass balancing for the weight of an instrumentation package to be a significant percentage of the total design weight of an empty-tank drop model. The empty tank models consist of smaller centerbody sections made of aluminum, balsa nose and tail sections, fins, and a ballast-weighted nose tip made of mallory alloy to satisfy pitch/yaw moment-of-inertia constraints. A dynamically scaled model of a tank with partial fuel located in a center tank compartment is shown in Fig. 6. As a further aid to illustrating mass/inertia constraints on the instrumentation, LMTAS model designers developed a prototype design for a minimum-mass (worst-case) empty-tank configuration with generic instrumentation assemblies, shown in Fig. 7. For this generic light-weight design, the tank is molded from plastic, and seven sensor/battery packages are used to distribute the mass within the model. The figure is presented for illustrative purposes only and was not used in wind tunnel testing.

Free-drop events in the wind tunnel are recorded using 16-mm motion-picture cameras with frame rates of 400 frames per second. The cameras are mounted in the tunnel side and bottom walls and provide orthogonal views of the drop event. In some cases the film records themselves are treated as the final test data (if a store hits the aircraft during drop testing, it is considered unsafe for flight testing and no other analysis is performed). In most cases, however, a data-reduction procedure involving "reading" the film records, quantifying the positions and orientations, and re-scaling the data to full-scale flight conditions at full-scale time is performed. Film data are read by projecting each frame of film from each camera on a film reader screen. Crosshairs are manually positioned on each projected frame of film to identify three store-fixed

reference points relative to a common fixed point on the film frame. Two reference points are located at the extreme nose and tail of the store to define the store yaw and pitch angles, and the third reference at a point on the store offset from the line between nose and tail for use in determining store roll angle. If, as is often the case, one or more of the three reference points is visually obstructed by intervening portions of the aircraft or store geometric configuration, the crosshairs are placed according to the best judgment of the film-reader operator. Visual access and the difficulty involved in resolving out-of-camera plane motions (especially roll motion), because of inconsistencies in merging the independently measured reference point positions as identified in the separate side and bottom views, limit the accuracy of the film reading in many cases. Once each frame of data from both cameras and timing marks encoded on the film are read, a data reduction program is used to calculate the position coordinates and angles of the store and to re-scale to full-scale positions and time according to the inverse scaling relations:

$$
\begin{aligned}
&XFBF = XFBF'/\Lambda \qquad [X = X'/\Lambda] \\
&YFBF = YFBF'/\Lambda \qquad [Y = Y'/\Lambda] \\
&ZFBF = ZFBF'/\Lambda \qquad [Z = Z'/\Lambda] \\
&PSIBF = PSIBF' \qquad [\Psi = \Psi'] \\
&THABF = THABF' \qquad [\theta = \theta'] \\
&PHIBF = PHIBF' \qquad [\phi = \phi'] \\
&t = t'/\sqrt{(\Lambda)}
\end{aligned}
\tag{2}
$$

Uncertainties in film-reduced drop model data are obtained by the simple (and very non-statistical) technique of having two separate film-reader operators manually read the same trajectory film. Standard deviations in time on each of the six position and rotation parameters, as well as maximum individual errors at any one time, are quoted as the film data uncertainties. Uncertainties associated with the inability to rigorously scale all of the mass properties directly and those associated with the differences between true flight motions and the re-scaled dynamic drop model motions (which are attributable to the compromises in the scaling laws themselves) are not quoted.

Note that one consequence of the time scaling in Eq. (2) is that the 400-frame-per-sec rate of the camera data (trajectory data defined at a time step of 1/400 = 0.0025 sec model scale) actually corresponds to a full-scale trajectory time increment of $0.0025/\sqrt{(\Lambda)}$ or almost 0.01 sec for a 1/15th-scale model. This rather large full-scale time step has important implications on the ability to extract aerodynamic information from tank free-drop data (as described in the next section) because it is close to the characteristic frequencies of the tumbling tank pitch motions. Film frame-rate limitations on free-drop data extraction will be discussed later in Section 3.3. First, a description of the free-drop data extraction process will be provided in the next section.

2.3 DYNAMIC DROP DATA EXTRACTION

Given the positions and orientations of a store as a function of time, it is possible to extract the aerodynamic forces and moments necessary to cause that motion by an inverse solution of the store equations of motion. A computer program to implement such a solution had previously been developed by the third author of the current report for another effort and was extensively

modified for the current effort. The equation-of-motion package used is identical to that used in forward solutions of the equations as implemented in Ref. 3 and the AEDC captive trajectory tunnel software (Ref. 4). However, rather than integrating the accelerations resulting from the equation-of-motion solutions in order to get the store positions and velocities, the positions from the film-data reduction are instead differentiated to get the velocities and accelerations which are then substituted into the equations of motion to extract the causing forces and moments.

The extraction program is limited to extraction of forces and moments during only the free-falling portion of a trajectory. It is not possible to extract aerodynamics during that portion of a trajectory when the store is constrained by some additional rail or pivot device (although it is possible to extract the velocities and accelerations) because there is no way to determine which portions of the extracted total accelerations of the store are attributable to reaction loads at the restraint and which are attributable to aerodynamics.

The very first step in the free-drop data extraction is to re-scale the reduced film data back to drop scale. As noted in the previous section, the last step of the film reduction program is to scale the drop positions and time to full scale using the relations of Eq. (2). If the extraction process is applied to the scaled-up full-scale positions, however, the extracted properties will represent the aerodynamics and motion properties necessary to generate the full-scale trajectory - not the properties that actually generated the drop trajectory in the tunnel. There are differences between (1) extracting the motion and aerodynamic properties from a scaled-up full-scale drop simulation and (2) extracting all the motion properties from the drop-scale simulation and then scaling them up to full scale. The differences exist because not all motion properties are rigorously scaled in the drop model because of the compromises inherent in the scaling laws. The differences will be illustrated by one of the analytical studies in Section 3.3.

Because the aircraft is always in non-maneuvering flight in a wind tunnel drop test, any aircraft-fixed axis system can be used as an inertial frame of reference for the inverse equation-of-motion solution for free-drop data extraction. Flight-axis positions and orientations from free-drop or flight data have been selected as the primary inputs to the program. Flight axes are the system of choice for the extraction because flight axes are aligned with the wind tunnel axes and, thus, with the axes of tunnel camera systems. Also, flight axes and inertial axes are identical for an aircraft in non-maneuvering flight (always the case for tunnel drop installations). Finally, flight axes are the primary output system for the film data reduction program. Sometimes a film-reading manual error may cause a spike in the reduced flight-axis film position and orientation data; such errors are removed by testing for slope discontinuities and fairing over the suspect points.

The position and orientation data from the wind tunnel drops must, on occasion, be smoothed before being differentiated to get velocities and accelerations. Measurement precision errors in the film readings are greatly exaggerated when the data are twice differentiated and may lead to totally erroneous accelerations if smoothing is not employed. On the other hand, smoothing without destroying some important features such as sharp peaks in the data is also difficult and may also lead to erroneous accelerations. Smoothing is most effective when the store motion amplitudes and frequencies are relatively small (which is, of course, not the case for a tumbling

fuel tank). Smoothing is accomplished in the data extraction program by least-squares curve fits. No smoothing, of course, was necessary for the analytical simulations and, as it turns out, smoothing was also unnecessary for the actual experimental effort (Ref. 1).

The derivatives of the flight-axis linear positions (DXFBF, DYFBF, and DZFBF) are calculated by an Akima spline (Ref. 5) interpolation of the film-reduced flight-axis linear position data (XFBF, YFBF, and ZFBF) as a function of time. The Akima spline represents a localized mathematical spline fit that has several important and useful features. The Akima spline, unlike curve fits, passes through every data point and closely approximates the curves that would be created by an analyst connecting the data points by hand on a plot using a 'French curve' or similar drafting device. Also, the mathematical derivative of the Akima spline is smooth and continuous (unlike finite-difference derivative approximations) and, thus, helps limit the exaggeration of precision errors characteristic of the differentiation process. The flight-axis position derivatives are then projected through a matrix rotation into velocity components (UBBI, VBBI, and WBBI) in the store body-axis directions for actual use in the equation-of-motion evaluations. Advantage is taken of the fact that flight and inertial axes are identical for non-maneuvering drops when projecting the flight-axis derivatives to velocities relative to the inertial system. Linear velocity derivatives (DUBBI, DVBBI, and DWBBI) are then calculated by another call to the Akima routine with the velocity data.

Angular velocities are calculated by a slightly more complicated process. Although it is possible either to take derivatives of the pitch, yaw, and roll angle values directly or to create 3-by-3 direction-cosine matrices from the angles which can then be differentiated for the terms needed to calculate the angular velocities, both processes are fraught with mathematical singularities at pitch, yaw, and roll angles which are multiples of 90 deg. An alternate way of defining rotations using Euler parameters or quaternions (Ref. 3), which avoids mathematical singularities, has been implemented. Euler parameters are first calculated from the smoothed Euler angles at each time step according to:

$$E0BI = \cos(\phi_{BI}/2)\cos(\theta_{BI}/2)\cos(\Psi_{BI}/2) + \sin(\phi_{BI}/2)\sin(\theta_{BI}/2)\sin(\Psi_{BI}/2)$$

$$E1BI = -\cos(\phi_{BI}/2)\sin(\theta_{BI}/2)\sin(\Psi_{BI}/2) + \sin(\phi_{BI}/2)\cos(\theta_{BI}/2)\cos(\Psi_{BI}/2) \quad (3)$$

$$E2BI = \cos(\phi_{BI}/2)\sin(\theta_{BI}/2)\cos(\Psi_{BI}/2) + \sin(\phi_{BI}/2)\cos(\theta_{BI}/2)\sin(\Psi_{BI}/2)$$

$$E3BI = \cos(\phi_{BI}/2)\cos(\theta_{BI}/2)\sin(\Psi_{BI}/2) - \sin(\phi_{BI}/2)\sin(\theta_{BI}/2)\cos(\Psi_{BI}/2)$$

where Eq. (3) is derived as Eq. (4.2.3.5.4.2) in Ref. 3. Derivatives of the four Euler parameters as a function of time (DE0BI, DE1BI, DE2BI, and DE3BI) are then obtained using the Akima routine, and the body-axis components of the rotation rates are obtained from:

$$\begin{aligned} PBBI &= 2(-E1BI\ DE0BI + E0BI\ DE1BI + E3BI\ DE2BI - E2BI\ DE3BI) \\ QBBI &= 2(-E2BI\ DE0BI - E3BI\ DE1BI + E0BI\ DE2BI + E1BI\ DE3BI) \\ RBBI &= 2(-E3BI\ DE0BI + E2BI\ DE1BI - E1BI\ DE2BI + E0BI\ DE3BI) \end{aligned} \quad (4)$$

where Eq. (4) is derived as Eq. (4.2.3.5.5.15) in Ref. 3. Rotational velocity derivatives (DPBBI, DQBBI, and DRBBI) are calculated by taking the Akima derivatives of PBBI, QBBI, and RBBI with respect to time.

The total forces and moments acting on the store (aerodynamic and otherwise) are obtained by solving the equations of motion for free-falling bodies using the derived velocities and accelerations.

$$\begin{vmatrix} FXB \\ FYB \\ FZB \end{vmatrix} = m \begin{vmatrix} DUBBI \\ DVBBI \\ DWBBI \end{vmatrix} + m\,[\tilde{\omega}\,BBI] \begin{vmatrix} UBBI \\ VBBI \\ WBBI \end{vmatrix} \tag{5}$$

$$\begin{vmatrix} MXB \\ MYB \\ MZB \end{vmatrix} = [\tilde{\omega}\,BBI]\,[\,I\,]_{BB} \begin{vmatrix} PBBI \\ QBBI \\ RBBI \end{vmatrix} + [\,I\,]_{BB} \begin{vmatrix} DPBBI \\ DQBBI \\ DRBBI \end{vmatrix} \tag{6}$$

where Eq. (5) is derived as Eq. (4.1.1.11) and Eq. (6) as Eq. (4.2.1.33) in Ref. 3, $[\,I\,]_{BB}$ represents the moment of inertia tensor of the body [(defined in Eqs. (4.2.1.23) and (4.2.1.19) of Ref. 3)], and $[\tilde{\omega}\,BBI]$ represents the skew-symmetric rotational velocity cross-product operator defined by:

$$[\tilde{\omega}\,BBI] = \begin{bmatrix} 0 & -RBBI & QBBI \\ RBBI & 0 & -PBBI \\ -QBBI & PBBI & 0 \end{bmatrix} \tag{7}$$

The expressions of Eqs. (5) and (6) allow determination of the total forces and moments of the store. These totals consist of restraint-reaction, weight, ejector-force, and aerodynamic load contributions which can be expressed as follows:

$$\begin{vmatrix} FXB \\ FYB \\ FZB \end{vmatrix} = \begin{vmatrix} RXB \\ RYB \\ RZB \end{vmatrix} + \begin{vmatrix} FXB_{AERO} \\ FYB_{AERO} \\ FZB_{AERO} \end{vmatrix} + \begin{vmatrix} WXB \\ WYB \\ WZB \end{vmatrix} + \begin{vmatrix} FEXB \\ FEYB \\ FEZB \end{vmatrix} \tag{8}$$

and

$$\begin{vmatrix} MXB \\ MYB \\ MZB \end{vmatrix} = \begin{vmatrix} MXB_{AERO} \\ MYB_{AERO} \\ MZB_{AERO} \end{vmatrix} + \begin{vmatrix} RLB \\ RMB \\ RNB \end{vmatrix} - \begin{vmatrix} XBBH \\ YBBH \\ ZBBH \end{vmatrix} X \begin{vmatrix} RXB \\ RYB \\ RZB \end{vmatrix} + \begin{vmatrix} MEXB \\ MEYB \\ MEZB \end{vmatrix} \tag{9}$$

where the {RXB} and {RLB} vectors denote reaction forces and moments at the restraint point, {WXB} is the store weight vector, the $\{\ \}_{AERO}$ vectors denote the store aerodynamic forces and moments, and the {FEXB} and {MEXB} vectors denote forces and moments imparted to the store by the ejector [thrust forces and moments are not included in Eqs. (8) and (9)]. Provided the weight and ejector forces are known and given the totals from Eqs. (5) and (6), the combined

sum of the aerodynamic and reaction forces and moments can be determined from Eqs. (8) and (9). Unfortunately it is impossible to separate the aerodynamic and reaction terms from one another (except to realize that reaction terms go to zero and only aerodynamic forces remain after pivot release). The weight components are determined from:

$$\begin{vmatrix} WXB \\ WYB \\ WZB \end{vmatrix} = [TRNBI]\,[TRNIE] \begin{vmatrix} 0.0 \\ 0.0 \\ WT \end{vmatrix} = [TRNBE] \begin{vmatrix} 0.0 \\ 0.0 \\ WT \end{vmatrix} \tag{10}$$

where [TRNIE] is the direction cosine matrix describing the orientation of inertial axes relative to earth gravity axes (which is almost always an identity for free-drop experiments in the wind tunnel), and [TRNBI] is the body-axis-relative-to-inertial-axis direction cosine matrix which corresponds to the Euler parameters (E0BI, E1BI, E2BI, and E3BI) or the sequential rotation angles (Ψ_{BI}, θ_{BI}, and ϕ_{BI}). The ejector forces and moments that are subtracted out of the totals of Eqs. (8) and (9) are determined by an analytical input model of the ejector force as a function of ejector stroke or ejector displacement. For drop models using springs to simulate the ejector, the model may be as simple as specifying a simple linear function of ejector stroke according to Hook's law. The equations used to calculate the ejector stroke at each time in the film-data trajectory are described in Section 4.3.8.1 of Ref. 3. After subtracting the ejector and weight terms from the totals in Eqs. (8) and (9), the remainder represents pure aerodynamic forces and moments only after the reaction forces from pivot or rail restrained-motion devices go away. A test to see when restrained motion is ended is to calculate the movement of the rail hook point downrail or to calculate the movement of a pivot device out of its socket. These parameters are calculated from the reduced film position and orientation data using equations derived in Section 4.3 of Ref. 3. For instance, Eqs. (4.3.6.18) and (4.3.6.19) were used to determine the pivot release point of the analytical and experimental tank drop simulations for the F-22 data analysis.

Aerodynamic forces and moments after pivot release may be reduced directly to non-dimensional coefficients based on store flight conditions and the appropriate full-scale or model-scale reference lengths and areas. The forces and moments are reduced to coefficients based on the dynamic pressure experienced by the store (dynamic pressure, defined by $1/2 * \rho_\infty * V_\infty^2$, is a measure of the energy in the flow that can be imparted to the store). The free-stream density is specified by the tunnel operating conditions for dynamic drops and is usually supplied by a standard atmosphere model or balloon data for full-scale flight. There is an added complication for the velocity term in store separation, however, in that the store velocity in both the full-scale flight simulations and in dynamic tunnel drops is different from the velocity of the aircraft because of the relative motion between store and aircraft. It is necessary to determine the store velocity relative to the wind mass in both the tunnel and flight cases to determine the true store velocity and store dynamic pressure. First, the body-axis components of the velocity of the inertial axis system relative to the moving air mass in the tunnel or the relatively fixed air mass (neglecting winds) in flight are calculated according to:

$$\begin{vmatrix} UBIW \\ VBIW \\ WBIW \end{vmatrix} = [TRNBI] \begin{vmatrix} UIIW \\ 0.0 \\ 0.0 \end{vmatrix} \tag{11}$$

where UIIW is the free-stream flight velocity, V_∞, of the aircraft at the instant of release (i.e., the tunnel free-stream velocity for the dynamic drop case). The body-axis components of the "idealized" velocity of the body-axis system relative to the air mass are then:

$$\begin{vmatrix} UBBW \\ VBBW \\ WBBW \end{vmatrix} = \begin{vmatrix} UBIW \\ VBIW \\ WBIW \end{vmatrix} + \begin{vmatrix} UBBI \\ VBBI \\ WBBI \end{vmatrix} \quad (12)$$

The {UBBW} vector is "idealized" in the sense that it represents the total velocity of the store relative to the undisturbed air mass far away from the aircraft. (The local velocity disturbances caused by the near-field presence of the parent aircraft are ignored.) The idealized aerodynamic angles of attack and sideslip of the store body relative to the wind mass are then:

$$ALPHAS = Tan^{-1} \{WBBW/UBBW\} \quad (13)$$

and

$$BETAS = \sin^{-1} \{VBBW/VTOTBW\} \quad (14)$$

where VTOTBW represents the total magnitude of the velocity of the store body axes relative to the wind mass:

$$VTOTBW = SQRT(UBBW^2 + VBBW^2 + WBBW^2) \quad (15)$$

Using the total resultant store velocity and the wind tunnel or flight free-stream density, as appropriate, the dynamic pressure for non-dimensionalizing the aerodynamic forces and moments is:

$$QA = 1/2 * \rho_\infty * VTOTBW^2 \quad (16)$$

The reduced aerodynamic force coefficients are:

$$C_A = - FXB_{AERO} /(QA*S) \quad (17)$$
$$C_Y = FYB_{AERO}/(QA*S)$$
$$C_N = -FZB_{AERO}/(QA*S)$$

where the negative signs are necessary because, by convention, positive normal force is directed up and positive axial force is directed aft, whereas the corresponding ZB and XB directions are down and forward, respectively.

An effort is made to remove some of the effects of store rotational motion in the flow field from the aerodynamic moment coefficients based on constant input damping coefficient derivatives. Only the primary rotational moment damping terms are removed because other dynamic rotational terms, such as forces caused by rotational rates and moments about one axis caused by rotations about another axis, are typically negligible. Use of constant damping derivatives results in good agreement for the extracted data from the generic analytical simulations in this study and

would also agree well with wind tunnel captive trajectory simulations since the rotational effects are added into such simulations in the first place based on constant damping derivatives. (More advanced options in the FLIP TGP simulation program that calculate rotational dynamic effects directly without assuming constant damping will be used in production F-22 simulations.)

$$C_l = MXB_{AERO}/(QA*S*XLL) - CLP*\{(PBBI*XLL)/(2*VTOTBW*\sqrt{(\Lambda)})\}$$
$$C_m = MYB_{AERO}/(QA*S*XLM) - CMQ*\{(QBBI*XLM)/(2*VTOTBW*\sqrt{(\Lambda)})\}$$
$$C_n = MZB_{AERO}/(QA*S*XLN) - CNR*\{(RBBI*XLN)/(2*VTOTBW*\sqrt{(\Lambda)})\} \quad (18)$$

The $1/\sqrt{(\Lambda)}$ factor is included only for the one analytical test case described in Section 3.3 when reduced data, obtained by taking a free-drop simulation and re-scaling the results according to the inverse scaling laws, are used as input to the extraction program. The factor is necessary to account for the heavy-scaling ratio between the rotational rates for the small-scale model and the rates obtained from differentiating the re-scaled film data.

3.0 RESULTS AND DISCUSSION

Results of various phases of the numerical experiment are discussed in the next several sections. Simulations using full-scale inertial and mass properties and using dynamically scaled properties according to the heavy-scaling laws are described in Section 3.1. The simulations provide a basis for determining the range of measurements that onboard sensors would have to be capable of providing for a tumbling fuel tank. The accuracy with which dynamically scaled sub-scale models can emulate flight for a tumbling fuel tank is discussed in Section 3.2. Section 3.3 describes the extraction of aerodynamic forcing functions from the simulated drops using the inverse solutions of the equations of motion; this section also illustrates some of the limitations associated with the framing rates of current camera systems.

3.1 COMPARISON OF FULL-SCALE SIMULATIONS WITH RAW DATA FROM 1/15TH-SCALE DYNAMICALLY SCALED MODEL SIMULATIONS

The trajectory simulations at full and model scales were generated for a pivoted tank release at a Mach number of 0.9 for an aircraft in an 11.4-deg climb relative to the earth horizontal and a 2-deg angle of attack relative to the air mass. The initial pitch incidence of the tank was -3.4 deg nose down relative to the aircraft at its installed position. As a result, the initial orientation of the tank relative to earth horizontal was 8.0 deg nose up. The design release angle of the tank pivot mechanism was -15 deg pitched down from its carriage attitude. Each of the trajectories was generated for a 1/4th-full fuel load and an aft tank center-of-gravity position without any sloshing fuel effects.

Only free-stream aerodynamics of the tank were included. No interference aerodynamic effects associated with the presence of the aircraft were included. Identical aerodynamic coefficients were used for the full-scale and sub-scale simulations. Aerodynamic contributions of the pylon attached to the tank were not included, but the mass and inertia properties and the slight vertical offset of the tank center of gravity were modeled. Cross products of inertia associated

with the off-center mass of the pylon were set to zero because only pitch-plane motion was simulated.

The baseline trajectory (identified as run 101), which was used as a standard of comparison for all other simulations, was generated using the full-scale mass, inertia, and ejector properties presented in Table 1. The trajectory was generated using an equation-of-motion time step of 0.00125 sec, and digital data were output to the plot file at every 0.01 sec.

Two different dynamically scaled model designs were developed to emulate the motion of the baseline full-scale run at drop scale by applying the heavy scaling ratios, Eq. (1), to the full-scale properties for run 101. One-fifteenth-scale models were designed using a tunnel static temperature to flight temperature ratio of 1.0 and tunnel to flight dynamic pressure ratios of 1.0 and 0.3 which bound the range of most drop tests. The scaled properties for the two dynamic model designs are identified as runs 201 and 202 in Table 1. The simulated trajectories for the dynamic drop models were generated using equation-of-motion time steps of 0.00032275 sec, and digital data were output to the plot files at intervals of 0.002582. The time steps were obtained by applying the time scaling laws to the time steps used for the full-scale simulation. Plotted comparisons of the motion parameters from the baseline full-scale run and the two dynamically scaled runs are provided in Fig. 8. Before getting into detailed discussion of the individual parameters, it should be noted that the dynamically scaled models, based on the two different dynamic pressure ratios, show identical trajectory motions. Each of the motion parameters is shown plotted versus time from release, and the compression of time in the dynamic scaling process is readily apparent. Discussions of the comparisons between full-scale and dynamically scaled motion parameters from Fig. 8 are provided in the next several paragraphs.

The basic position and orientation parameters as they would be read from film records before being re-scaled through the film data-reduction software are presented in Figs. 8a and b. Pylon-axis parameters are presented. Positive values of the tank linear positions (XPBP, YPBP, and ZPBP) represent tank motion forward of, to the right of, and down from the initial carriage position, respectively. Likewise, the pylon-axis pitch angle (yaw and roll are zero for the simple pitch-plane analytical trajectories) represents an angle relative to the initial tank-installed orientation. A pitch angle, NUBP, defined in the pitch-yaw-roll sequence is shown rather than the yaw-pitch-roll sequence angle, THABP. Differences between the two sequences are described in Section 1.3 of Ref. 3, although the sequence has no bearing on the present study because yaw and roll are zero.

Body-axis components of the linear and angular velocities from the baseline full-scale simulation and the simulated dynamic drops are presented in Figs. 8c and d. The linear velocities, UBBI and WBBI, represent the body-axis projections of the inertial velocity of the tank center-of-gravity relative to an inertially fixed point. Linear velocities at points other than the store cg must include additional contributions to account for the cross products of the tank angular velocities with the distance from the point to the cg. The pitch rate, QBBI, represents the body-axis projection of the inertial rotation rate of the store. The projected body-axis pitch rate is the property that would normally be measured by orthogonally mounted rate gyro instrumentation within the body if that type of instrumentation is selected. Note that the value of the pitch rate of the

dynamically scaled model is much larger in magnitude than the corresponding full-scale property. Based on Fig. 8d, a range of at least 150 rad/sec will be required of angular rate instrumentation for 1/15th-scale tank drops.

The linear and angular accelerations of the full-scale and model-scale tanks are indicated in Figs. 8e and f. The linear accelerations of the tank body-axis system are actually defined in terms of the derivatives of the body-axis projected velocities and rates to be more consistent with the manner in which the equations of motion are posed. These velocity derivatives are the result of the solutions of the tank equations of motion at each time step. The velocity derivatives of Figs. 8e and f are the properties that are integrated over time in the simulations to produce the velocities and positions previously shown in Figs. 8a through d. The parameter, DQBBI, is related to the angular acceleration that would be measured by an onboard angular accelerometer if that form of instrumentation is selected over the rate-gyro alternative. Some adjustment of the angular acceleration terms would have to be accomplished, however, to account for rotating reference frames before direct comparisons with angular accelerometer readouts can be obtained. In general, it can be seen that the angular acceleration range required for the 1/15th-scale model reaches almost 6000 rad/sec^2, whereas much smaller rotational accelerations occur in full-scale flight.

Linear accelerometers typically do not measure all components of the full acceleration of the body relative to an inertially fixed point because they do not respond to the acceleration of gravity as noted in Section 2.0 of Ref. 3. Accelerometers also measure accelerations directly and do not measure the derivative-of-body-velocity term which appears in the store equations of motion [Eq. (5)]. Accelerometers are also often calibrated to measure accelerations in units of g's (acceleration in ft/sec^2 divided by the nominal value of the earth gravitational acceleration, 32.174 ft/sec^2). The relationship between true acceleration and the derivative-of-body-velocity at the store center of gravity is expressed by:

$$\begin{vmatrix} DUBBI \\ DVBBI \\ DWBBI \end{vmatrix} = -[\tilde{\omega}BBI] \begin{vmatrix} UBBI \\ VBBI \\ WBBI \end{vmatrix} + 32.174 \left(\begin{vmatrix} GAXMBBI \\ GAYMBBI \\ GAZMBBI \end{vmatrix} + [TRNBE] \begin{vmatrix} 0.0 \\ 0.0 \\ GG/32.174 \end{vmatrix} \right) \tag{19}$$

which is derived as Eq. (4.1.1.12) of Ref. 3. The {GAXMBBI} vector in Eq. (19) is the acceleration in g's that would be measured by onboard three-axis accelerometers. The right-most term is the component of gravitational acceleration that would not be sensed by the accelerometer (GG is the actual value of gravitational acceleration at the particular point of measurement on the earth). The velocity derivatives (measured in ft/sec^2) from Fig. 8e are converted (by subtracting out the inertial coupling and gravitational contributions) to body-measured accelerations at the tank center of gravity (measured in g's) in Fig. 8g. Accelerations of up to 50 g's at the cg are indicated. The body-measured linear accelerations and angular accelerations correlate well with the aerodynamic forces and moments (when not dominated by the ejector forces) as can be seen by comparing Fig. 8g with 8h and Fig. 8f with 8i.

If the body-axis accelerometers are mounted at positions other than the store center-of-gravity (which will probably be the rule rather than the exception for free-drop models), then body-axis accelerations must include rotational coupling terms to account for the offset. The acceleration transfer equations to transfer measured accelerations from the cg point, B, to an off-cg point, N, are:

$$32.174 \begin{vmatrix} GAXMBNI \\ GAYMBNI \\ GAZMBNI \end{vmatrix} = 32.174 \begin{vmatrix} GAMXBBI \\ GAMYBBI \\ GAMZBBI \end{vmatrix} + [\tilde{\omega}\,BBI]\,[\tilde{\omega}\,BBI] \begin{vmatrix} XBNB \\ YBNB \\ ZBNB \end{vmatrix} + [\,D\tilde{\omega}\,BBI] \begin{vmatrix} XBNB \\ YBNB \\ ZBNB \end{vmatrix} \tag{20}$$

which is derived as Eq. (3.0.9) of Ref. 3. $[D\tilde{\omega}\,BBI]$ in Eq. (20) is another skew-symmetric matrix of the form of Eq. (7) but using the angular velocity derivatives rather than the angular velocities to form the terms in the matrix. To illustrate the magnitude of the difference that accelerometer location can make on measured accelerations, Fig. 9 presents a plotted comparison of the acceleration at the cg previously shown in Fig. 8 and the measured acceleration at a point axially offset to the tank nose. As can be seen, the axial component of measured acceleration increases from a maximum of about 4 negative g's to slightly over 500 g's because of the offset accelerometer location. Based on Fig. 9, a range of at least 500 g's will be required of linear accelerometers for 1/15th-scale tank drops. Slightly higher ranges would be necessary for nose-mounted accelerometers on a lower-mass empty tank; however, a requirement to offset the accelerometer all the way to the tank nose is not anticipated.

The 1/4th-full aft center-of-gravity tank case exhibits rather extreme pitch motions. Another case was generated for a full 600-gal tank to demonstrate the motions for a more benign condition that does not result in tank tumble. The full- and model-scale simulations for the full tank were generated with the parameters listed for runs 104 and 206 in Table 1 and are plotted in Fig. 10. The range of the velocities and accelerations for the full tank are greatly reduced from the 1/4th-full case. Instrumentation range requirements of plus to minus 30 rad/sec on rotation rates, 600 rad/sec^2 on angular accelerations, and 20 g's on linear accelerations are indicated. This reduced range of instrument requirements (up to 6000 rad/sec^2 for the 1/4th-full tank as opposed to 600 rad/sec^2 for the full tank) may have large implications on accuracy of the measurements. Typically, the accuracy of an instrument is quoted in terms of a percentage of the total range that it is designed to cover. As a consequence, the instrumentation required for a tumbling tank may not be as accurate as that for the full, non-tumbling tank. If so, separate instrumentation packages with different range specifications may be necessary, depending on the expected severity of the motion, in order to obtain the best possible measurements.

3.2 COMPARISON OF FULL-SCALE SIMULATIONS WITH FINAL DATA REDUCED FROM 1/15TH-SCALE DYNAMICALLY SCALED MODEL SIMULATIONS

Final data from dynamically scaled drop tests usually consist of positions and orientations read from the film records and re-scaled to flight scale according to the inverse scaling laws [Eq. (2)]. The same scaling laws can be applied to the simulations of dynamically scaled drops described in the previous section with the exception that no film-reading errors are introduced. The re-scaled versions of the dynamically scaled simulations, therefore, represent "perfect" drop data with no data reduction errors and illustrate how well-reduced dynamic data can reproduce flight under the best of circumstances. The information presented in this section is relevant to the subject of instrumented free-drop models in the sense that the proposed "more-perfect" onboard instrumentation will actually be used within a dynamically scaled model which only approximately emulates the motion of the full-scale flight store.

The simulation for the heavy-scaled model at a dynamic pressure ratio of 0.3 (curve 3 of Fig. 8) was re-scaled according to the inverse heavy-scaling laws and is compared with the baseline full-scale simulation in Fig. 11. Although normally only the linear and angular positions read from the film are re-scaled for final drop data, inverse scaling was done for all available parameters from the simulated heavy drop, including velocities and accelerations. The scaled vertical drop position is in almost perfect agreement with the full-scale simulation in Fig. 11a, whereas the rearward tank movement is somewhat over-simulated. Pitch angle is also generally over-simulated, as shown in Fig. 11b.

Disagreements of this nature are typical of dynamically scaled drop testing and are a consequence of the compromises inherent in the derivation of the scaling laws. The compromises, as mentioned in Section 2.2, are caused by the inability to simultaneously satisfy requirements to match flight and model aerodynamics and requirements to match the responses of the flight store and the model to the applied aerodynamic loads. The heavy-scaling approximation allows the rotational velocities to be underdamped (indicated by the larger amplitudes of the scaled pitch angles in Fig. 11b) but does not properly account for the dynamic or "induced" angles of attack associated with the linear velocities of the tank as it moves through the flow field. Beyond the expected differences attributable to the factors of non-simulation in the derivation of the heavy-scaling laws, the heavy-scaled model qualitatively reproduces the full-scaled simulation fairly well. The accuracy of the scaled comparisons shown in Fig. 11 represents the upper bound on "goodness" of a scaled tank simulation - in this case, an error in axial position grows to as much as 5 ft, and average over-rotations in pitch of about 15 deg are indicated. Barring fortuitous favorable data-reduction errors in the film data reduction, no better reproductions of flight should be possible in an actual drop test of the heavy-scaled tank.

Given the pitch angle differences indicated in Fig. 11b, a philosophy about how free-drop data would be used in the overall integrated experimental/computational procedure that was then being developed for the F-22 store clearance effort (Ref. 1) was developed. It was decided that the computational trajectory-simulation capabilities such as FLIP TGP, which were proposed as tools in the F-22 effort, would be validated and verified against drop data using only simulations at drop scale without first re-scaling the drop data positions and time according to the inverse

scaling laws. After verification, the trajectory simulations could then be regenerated at full scale with higher confidence factors than would be possible using re-scaled dynamic drop data alone.

3.3 EXTRACTION OF AERODYNAMIC DATA FROM LINEAR AND ANGULAR POSITION DATA

Extraction of aerodynamic data using differentiation of trajectory position and orientation data as a function of time followed by inverse solutions of the store equations of motion was performed on both the full-scale and model-scale generic analytical trajectories. Because the original trajectories were numerically generated based on the defined aerodynamic model, it should be anticipated that extracted aerodynamics using the positions and angles from the analytical trajectories as input would be identical to the input aerodynamics used to generate the original trajectories. Smoothing was turned off in the extraction because the input motion histories were assumed to be perfect data with no errors, and loss of information due to smoothing of sharp peaks was not desirable for the numerical experiment.

The baseline full-scale trajectory positions and orientations versus time were input to the extraction program as a first test case. Extracted linear and angular velocities obtained by differentiating the positions and orientations are compared with the velocities from the original simulation in Figs. 12a and b. Note a small "glitch" in the pitch rate around the 0.30-sec mark. The linear and angular velocity derivatives obtained by differentiating the velocities are compared with the same properties from the original simulation in Figs. 12c and d. Note again small glitches in the pitch velocity derivative, DQBBI. The extracted coefficients from the inverse equation-of-motion solutions are presented in Figs. 12e and f. Disregarding the first 0.15 sec over which the ejector and pivot reaction forces are acting, note that the desired near-exact agreement is not obtained in any of the coefficients. Axial-force coefficient, especially, is in rather poor agreement. An effort to identify possible causes for the inability to exactly extract the aerodynamic coefficients was initiated. It was soon realized that although an integration time step of 0.0025 sec had been used in the actual generation of the baseline trajectory, motion parameters at only every 4th integration step (corresponding to a time step of 0.01 sec) had actually been transferred to the output data files. The data extraction had been attempted using the 0.01-sec time-step positions and orientations as input to the extraction program. To investigate sensitivity of the extractions to the "sampling rate" of the position and orientation data, the baseline trajectory simulation was regenerated without changes except that the output parameters at every integration step were output to the file. The extraction program was then exercised against the higher sampling-rate position and orientation data, resulting in the accuracy shown in Fig. 13. The extracted coefficients are in the desired near-perfect agreement with the original data. Three small glitches appear in the extracted axial-force coefficients (Fig. 13e) and pitching-moment coefficients (Fig. 13f) at time values of 0.25, 0.35, and 0.57, which can be correlated with similar glitches in the numerical derivative for DQBBI (Fig 13d) and pitch angles near 90 and -90 deg. Otherwise, agreement is excellent.

The inability to adequately extract aerodynamics from the full-scale run using input data at a time-step of 0.01 has serious implications on the ability to extract aerodynamic data from free-drop testing because of the compression of time involved in drop scaling. The full-scale time

increment of 0.01 sec for which the extraction was not fully successful corresponds to a dynamically scaled time increment of 0.002582 sec for a 1/15th-scale model, which is virtually identical to the 0.0025-sec framing rate of the cameras currently used for drop data recording. This implies that even if the drop film were read with 100-percent accuracy, data samples are not available at a frequency necessary to adequately extract drop aerodynamics for a tumbling tank. On this basis, faster film frame rates should be investigated and onboard instrumentation should be designed for sampling rates much faster than current film frame rates. (Eventually the experimental telemetry systems were designed with a sampling rate of 10,000 samples/sec but this high rate introduced other problems such as extremely large data volumes, which were hard to store and reduce - in retrospect, a compromise in the neighborhood of 2000 samples/sec seems optimal.)

The data extraction program was next run on the re-scaled-to-full-scale data from the dynamically scaled drop simulation (again using every available time increment). The extracted data are shown in Fig. 14. Note that the extracted aerodynamics from the re-scaled simulation represent the aerodynamics required to cause a full-scale store to have the same motion as that derived from scaling motions which actually occurred for a reduced-scale model. Because dynamic simulations cannot exactly reproduce full-scale simulations in the areas of velocities and pitch rates (see Section 3.2), the aerodynamics extracted from the re-scaled simulation are not in exact agreement with the aerodynamics from either the model-scale simulation or the flight simulation. This again illustrates the point that the data-extraction procedure should be applied to drop-scale data, after which all of the drop data, including the extracted velocities and accelerations, can be scaled up to full scale.

The data extraction program was next run on the un-scaled position and orientation data from the 1/15th-scale drop simulation to illustrate the extraction of aerodynamic data from raw film data as suggested in the previous paragraph. The extracted data are shown in Fig. 15. The extracted coefficients are in excellent agreement with the original simulation after the point of release from the tank pivot mechanism.

4.0 CONCLUDING REMARKS

1. Instrumentation for a heavy-scaled 1/15th-scale tumbling drop tank should be capable of accurate measurements of linear accelerations of up to 50 g's (up to 500 g's if the accelerometers are mounted at the nose and tail away from the tank center of gravity), angular velocities of up to 150 rad/sec, and angular accelerations of up to 6000 rad/sec^2. Instrumentation ranges for full-scale flight tanks should cover the rotational acceleration range from minus to plus 400 rad/sec^2 or the rotational rate range of -40 to 40 rad/sec. Full-scale linear acceleration range at the cg is the same as model scale. Instrumentation requirements for non-tumbling full tanks are greatly reduced: plus to minus 30 rad/sec on rotation rates, 600 rad/sec^2 on angular accelerations, and 20 g's on linear accelerations.

2. Because moment coefficients are directly related to rotational accelerations and force coefficients are directly related to body-measured linear accelerations at the cg, a 1-percent error in any measured acceleration should result in a 1-percent error in the corresponding extracted aerodynamic coefficient. After discussion with various vendors, such accuracies

seem to be within reach of the current state-of-the-art. It is important to emphasize, however, that the accuracy of an instrument is typically quoted in terms of a percentage of the total range that it is designed to cover. As a consequence, the instrumentation required for a partially full tumbling tank may not be as accurate as that for a full, non-tumbling tank. If so, separate instrumentation packages with different range specifications may be necessary, depending on the expected severity of the motion, in order to obtain the best possible measurements. At this point the tendency to expend a large amount of resources or time in an effort to overly define instrumentation accuracy requirements (such as specifying a desire for some magical criteria such as measurements within 1 percent of actual values) should be avoided. Such efforts tend to cloud the fact that even the less accurate instrumentation would seem to be orders-of-magnitude better than the film systems currently used. Therefore, it is recommended that most emphasis be placed on reducing the mass and size of the package (or packages) and increasing usability and flexibility of the telemetry system.

3. Where convenient, it is desirable to place linear accelerometers as close to the store center-of-gravity as possible because the magnitudes of the accelerations are smallest at that point (there are no additional acceleration components arising from the cross products of the store angular velocities with the positions of the accelerometers relative to the store rotation center). As a result, instrumentation with smaller ranges and corresponding higher accuracies can be used.

4. The mass of the entire model-scale instrument package should be manageable relative to a design weight of approximately 1 lb for an empty tank model.

5. For the high rotational rates typical of dynamic drops of fuel tank models in the wind tunnel, even if the positions and orientations are reduced without error from the film data, the 400 frame per second framing rate of current cameras is not adequate to define data at a small enough frequency to allow unbiased extraction of all force and moment coefficients. Errors in extracted coefficients are most evident in the coefficient of least interest (axial force) and appear to be driven by inertial-coupling considerations associated with high rotation rates. Four hundred frames/sec may be more acceptable for stable stores which do not exhibit such extreme motion at such small frequencies and for stores at larger scales which do not involve as much time compression from the dynamic-scaling.

6. Onboard instrumentation should have sampling rates faster than current film rates to resolve the high-frequency motions characteristic of tumbling tanks especially at scaled model time (2000 samples/sec is recommended).

7. The potential for use of high-resolution/high-speed video equipment has been under consideration for some time at the AEDC. Film (or video) frame rates should be increased beyond the current 400 frame/sec in any future upgrades to the wind tunnel optical systems.

8. If drop simulations are to be used to validate analytical prediction methods, the predictions should be run at drop scale, and no direct comparisons should be made between full-scale

predictions and drop data that have been scaled up to full-scale using the inverse scaling laws.

9. The free-drop data extraction process should only be applied to drop data at drop scale and not to scaled-up data.

REFERENCES

1. Howell, G. A. "Store Separation Test and Analysis Techniques Employed on the F-22 Program." Paper presented at the 76th AGARD Fluid Dynamics Panel Meeting and Symposium on Aerodynamics of Store Integration and Separation, Ankara, Turkey, April 24-28, 1995.

2. Sickles, W. L., Rist, M. J., Morgret, C. H., Keeling, S. L., and Parthasarathy, K. N. "Separation of the Pegasus XL from an L-1011 Aircraft." AIAA Paper 94-3454, August 1994.

3. Keen, K. S. "Equations for Store Separation Motion Simulations and Instrumented Model Data Reduction." AEDC-TR-95-12, August 1996.

4. Carman, J. B., Jr., Hill, D. W., Jr., and Christopher, J. P. "Store Separation Testing Techniques at the Arnold Engineering Development Center, Volume II - Description of Captive Trajectory Store Separation Testing in the Aerodynamic Wind Tunnel (4T)." AEDC-TR-79-1 (AD-A087561), June 1980.

5. Akima, Hiroshi. "A New Method of Interpolating and Smooth Curve Fitting based on Local Procedures." *Journal of the Association for Computing Machinery*, Vol. 17, No. 4, October 1970, pp. 589-602.

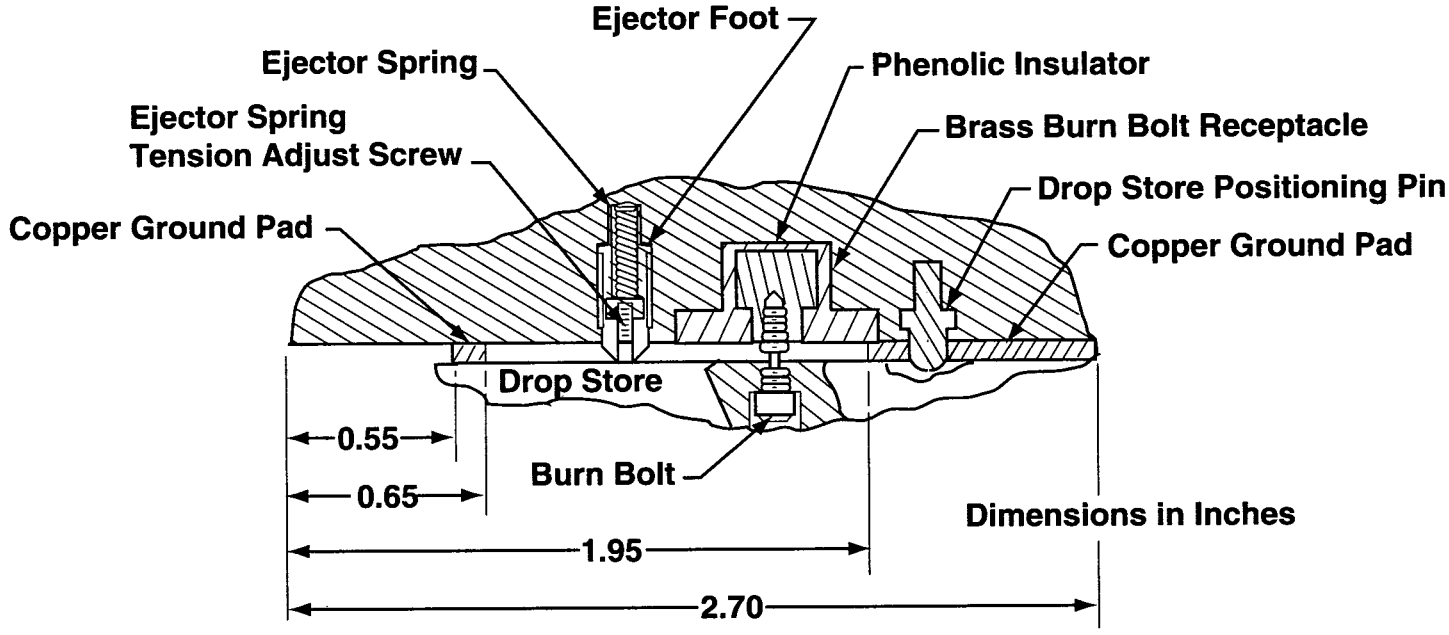

Figure 1. Typical burn-bolt installation.

600-Gal Wind Tank Geometry

T.S.	RAD.	T.S.
0.0	0.0	17.333
0.067	0.066	17.266
0.133	0.102	17.200
0.200	0.134	17.133
0.267	0.163	17.066
0.333	0.190	17.000
0.667	0.309	16.666
1.000	0.411	16.333
1.333	0.502	16.000
1.667	0.584	15.666
2.000	0.659	15.333
2.333	0.727	15.000
2.667	0.791	14.666
3.000	0.846	14.333
3.333	0.893	14.000
3.667	0.932	13.666
4.000	0.964	13.333
4.333	0.992	13.000
4.667	1.015	12.667
5.000	1.034	12.333
5.333	1.049	12.000
5.667	1.061	11.666
6.000	1.071	11.333
6.333	1.078	11.000
6.667	1.083	10.666
7.000	1.086	10.333
7.333	1.087	10.000

CONSTANT

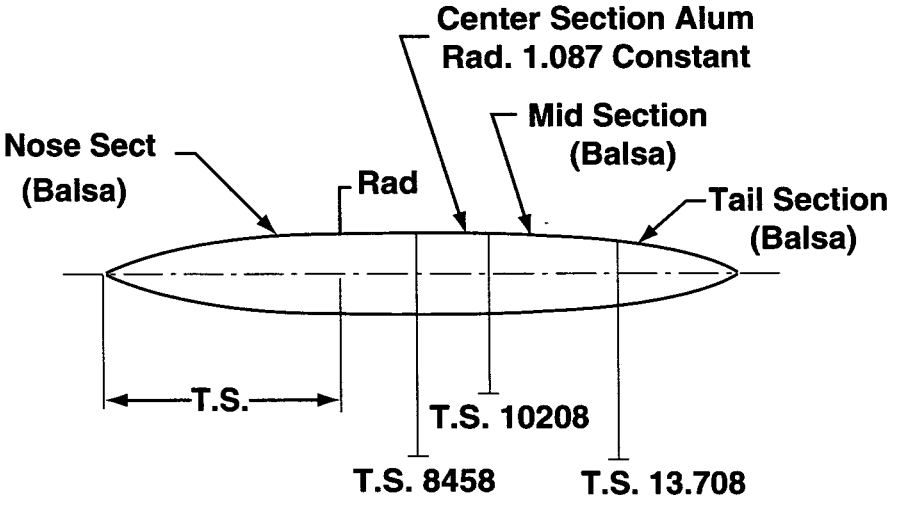

Figure 2. 1/15th-scale 600-gal tank dimensions.

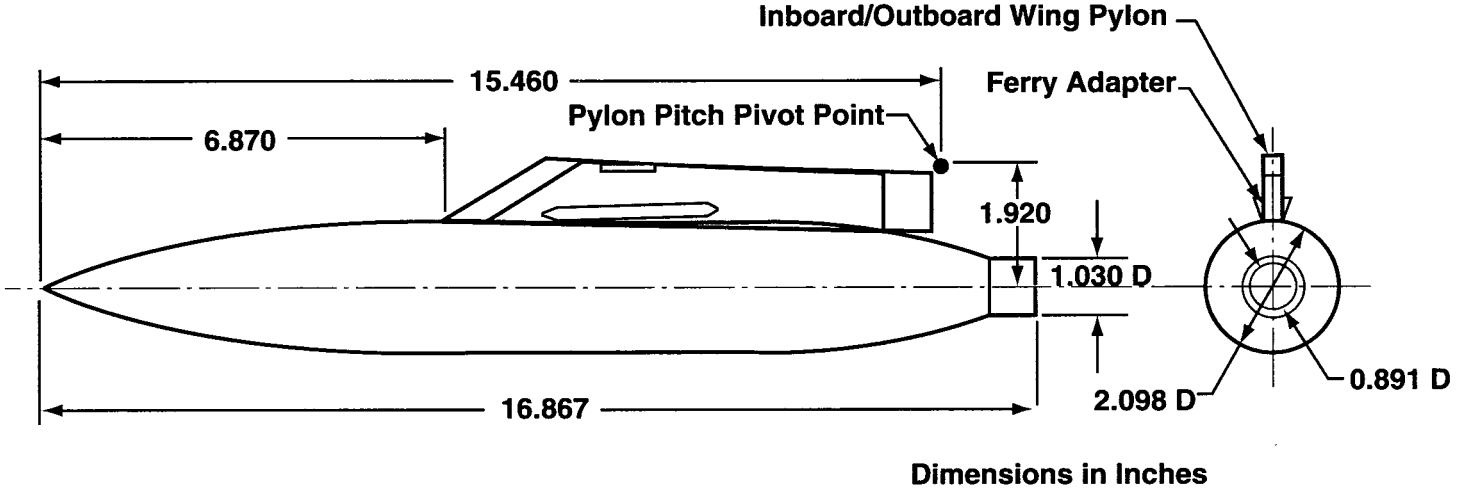

Figure 3. Early proposal for 600-gal tank for F-22.

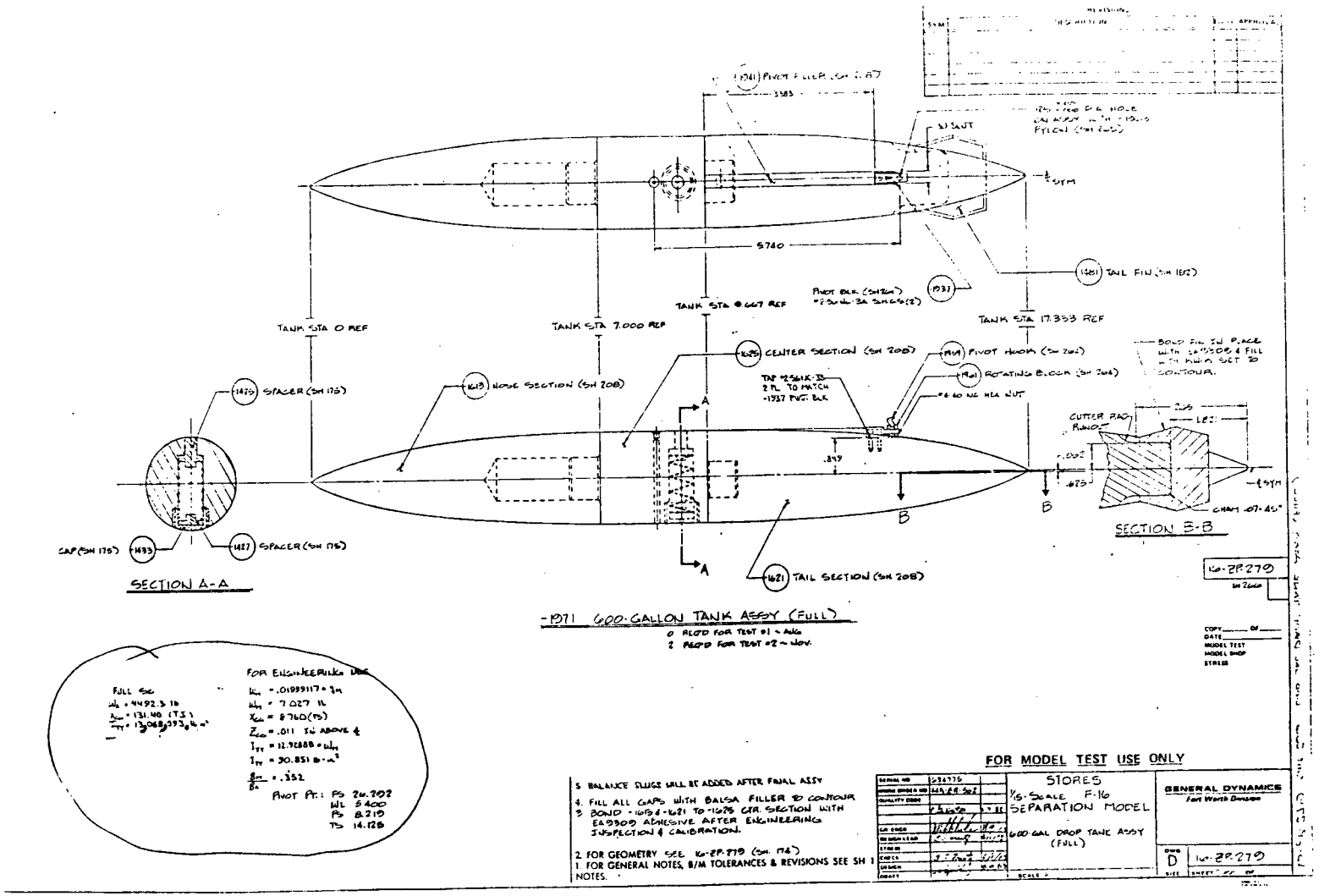

Figure 4. Mass scaled design for a full fuel tank with Q′/Q = 0.352.

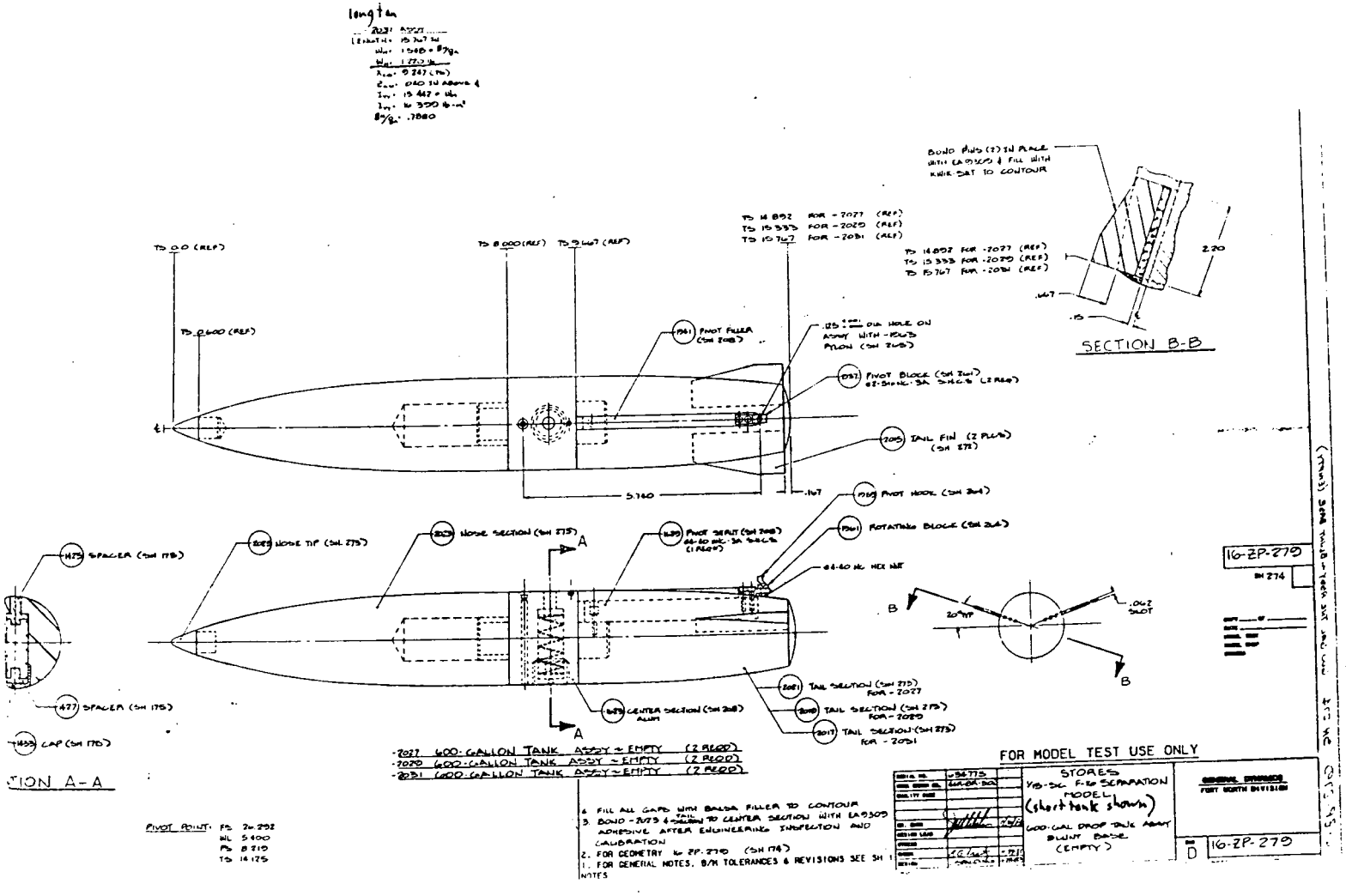

Figure 5. Mass scaled design for an empty fuel tank with Q′/Q = 0.788.

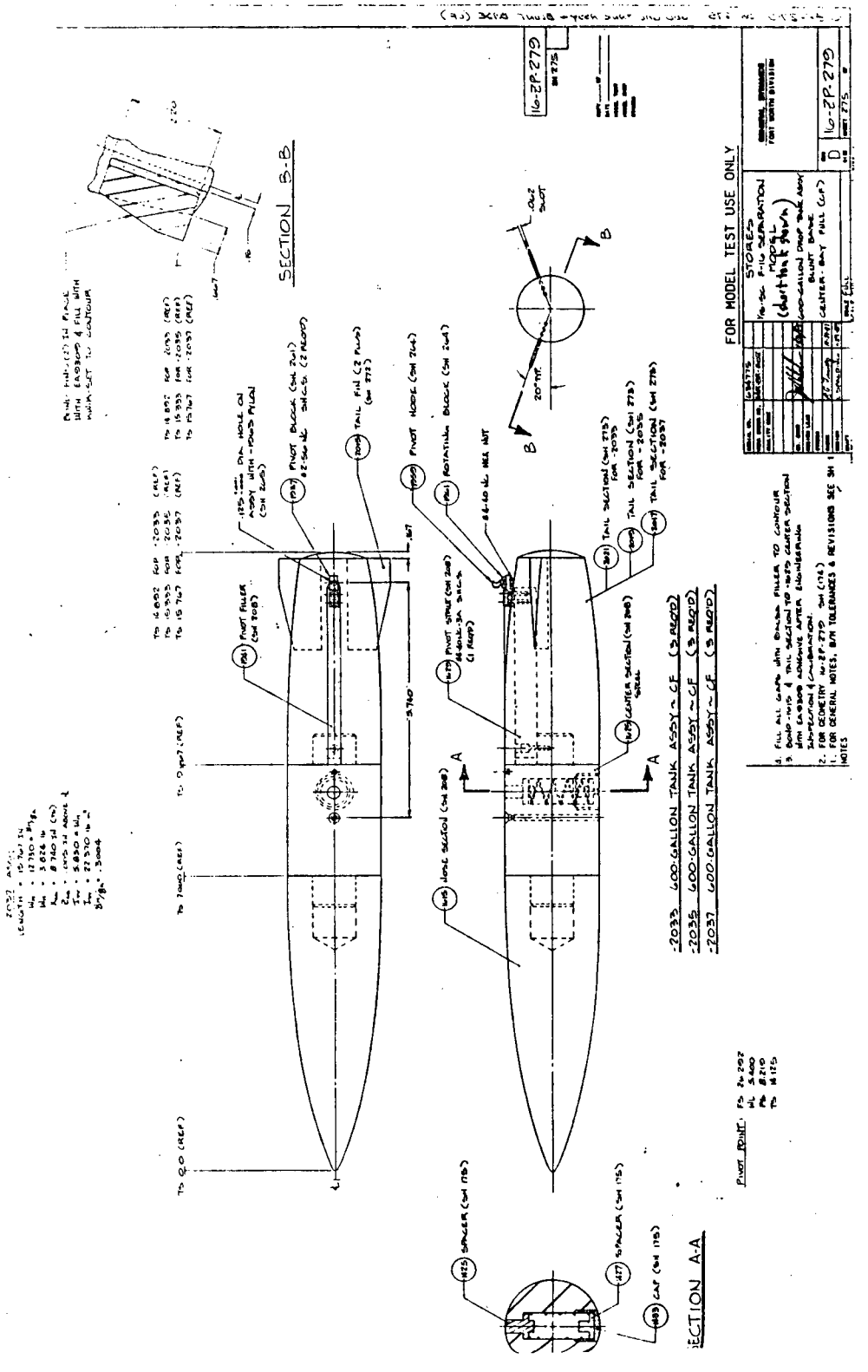

Figure 6. Mass scaled design for tank with partial fuel in center tank section.

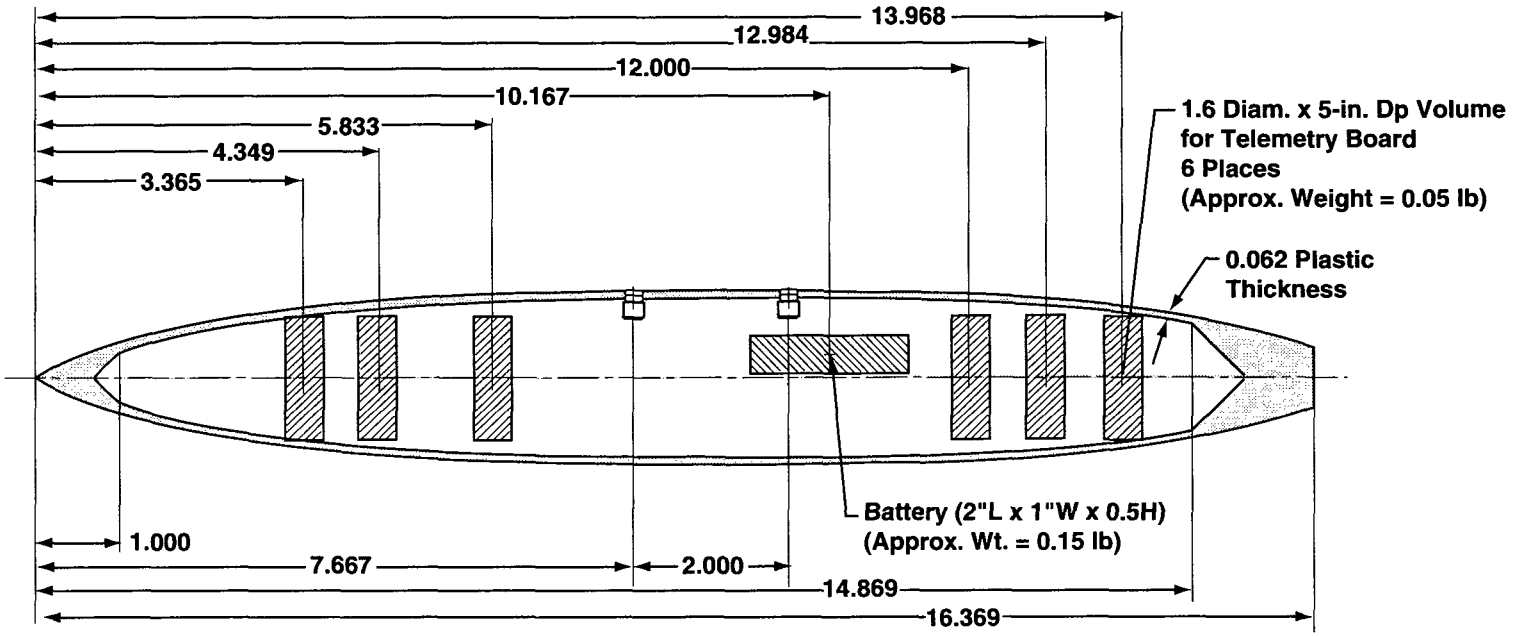

600-gal Tank (Empty) Drop Store for Telemetry

Full-Scale Store Design:
- WT = 344 lb
- Xcg = 141.05 in.
- Zcg = +0.931
- Iyy = 275 slug-ft^2

Model-Scale Store Design:
(Not F22 Design as Shown)
- WT = 0.765 lb
- Xcg = 9.403 in.
- Zcg = +0.062
- Iyy = 12.6 lb-in.^{2}
- q'/q = 0.500636

Figure 7. Generic design for F-22 instrumented drop tank (pylon omitted).

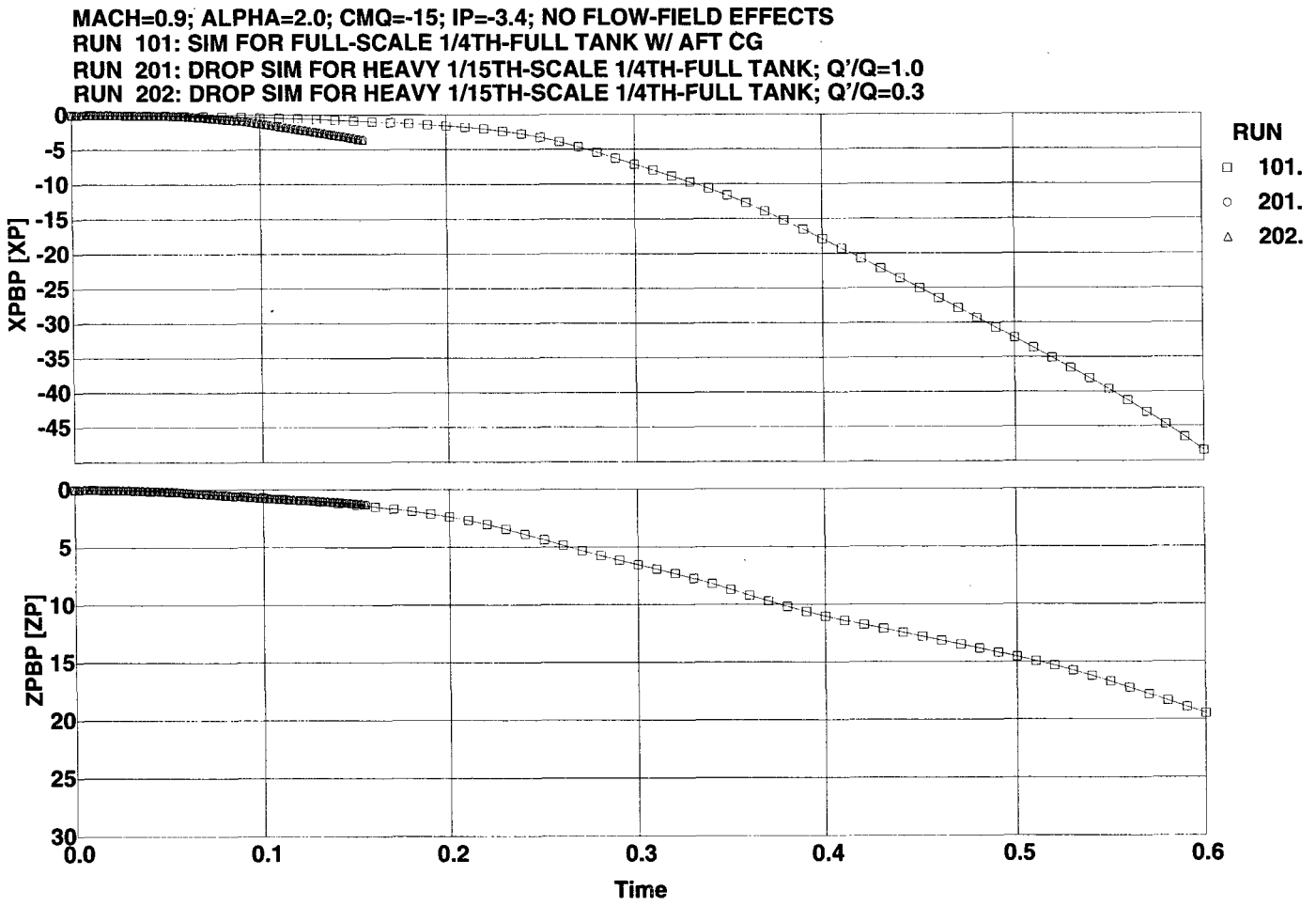

a. Axial and vertical positions

Figure 8. 1/4th-full tank simulations at full scale and 1/15th scale.

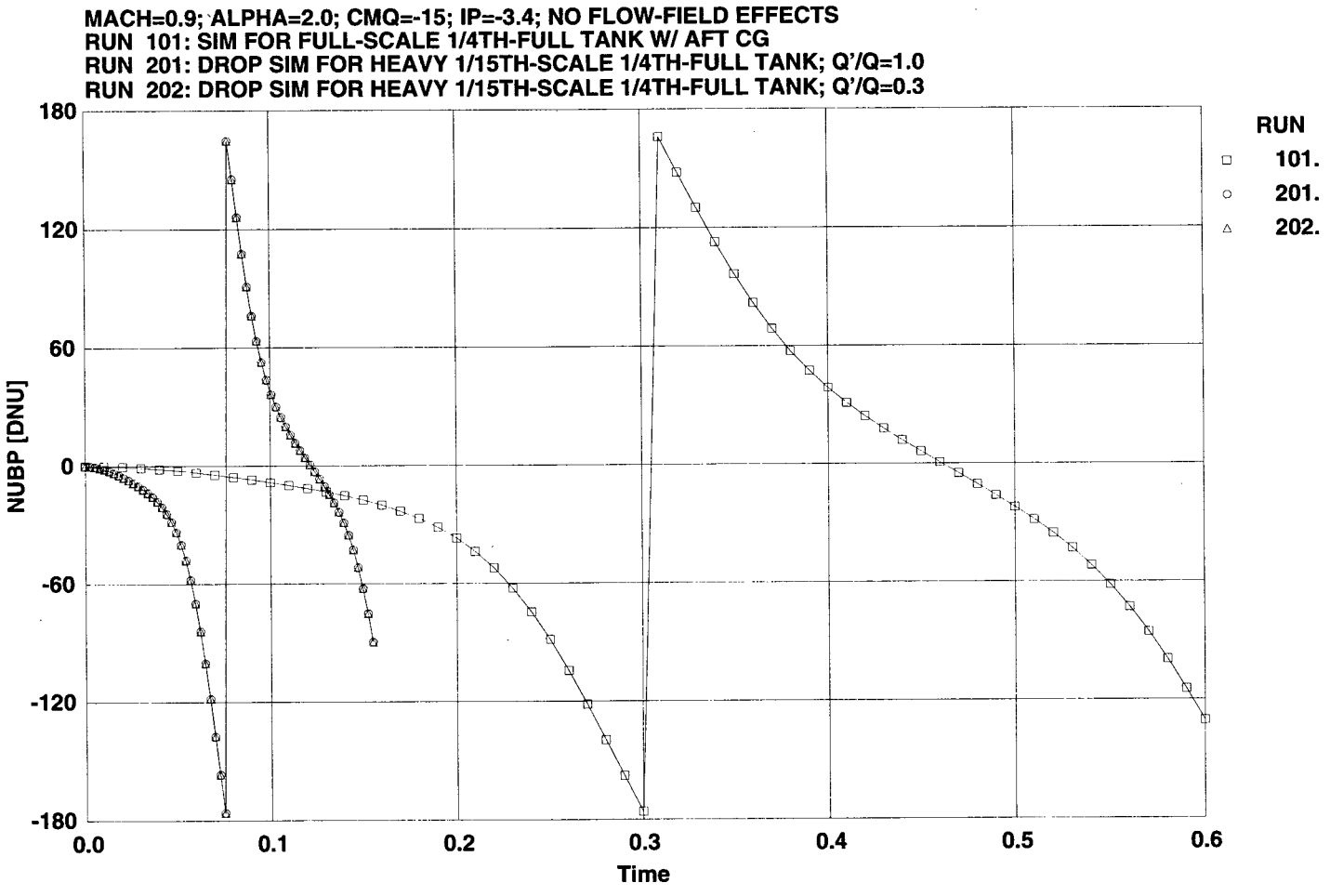

b. Pitch orientation

Figure 8. Continued.

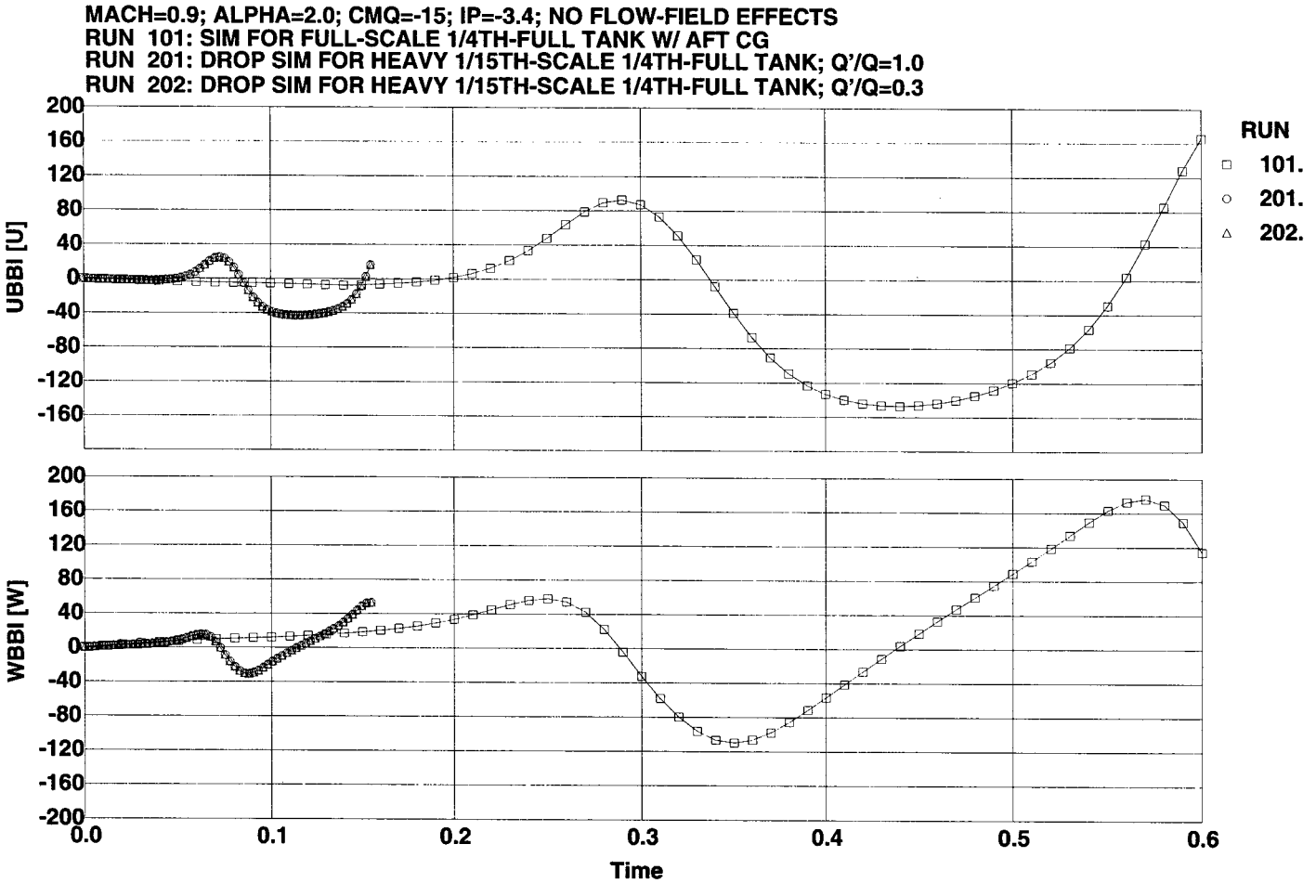

c. Axial and vertical linear velocities
Figure 8. Continued.

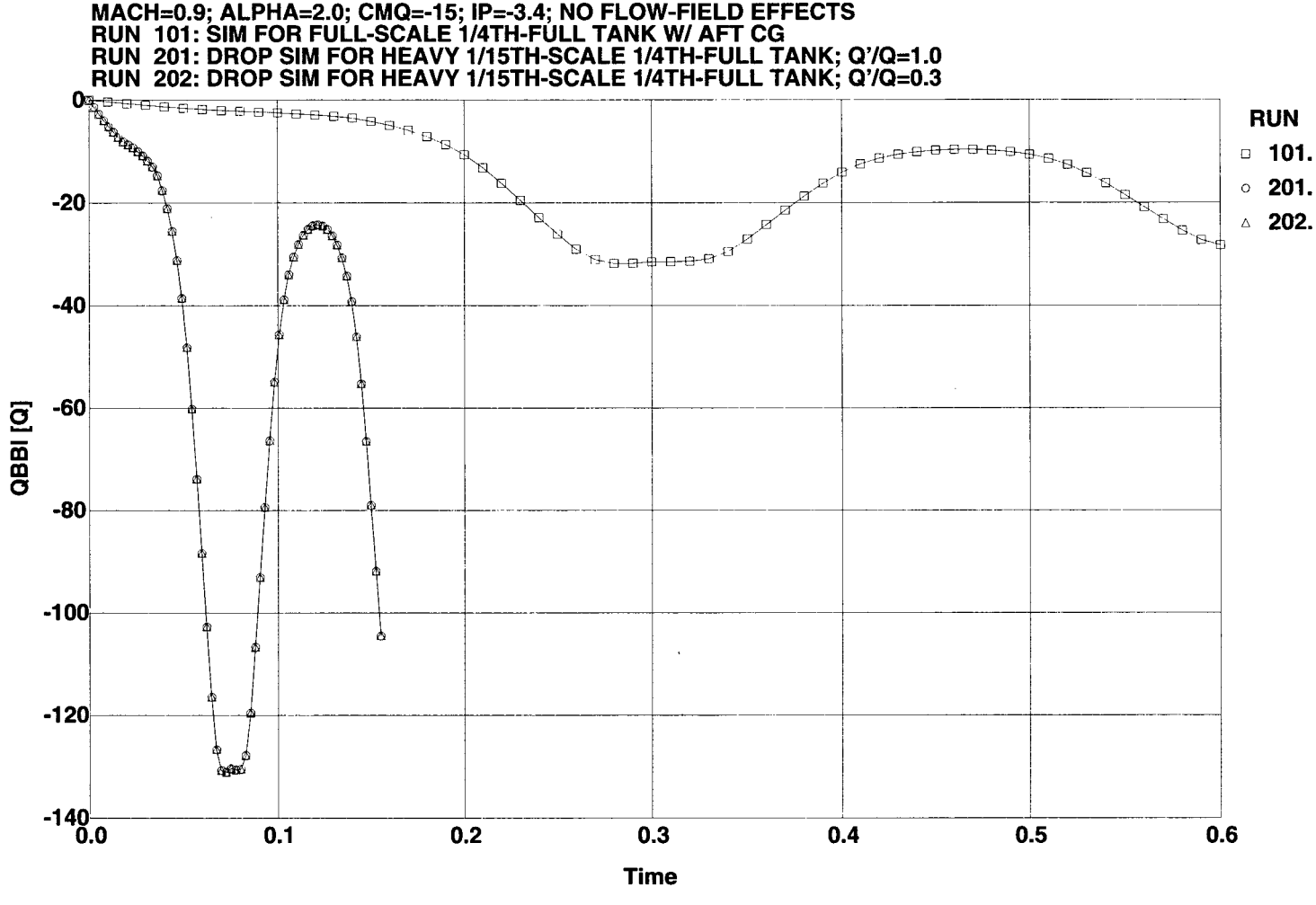

d. Pitch angular velocity
Figure 8. Continued.

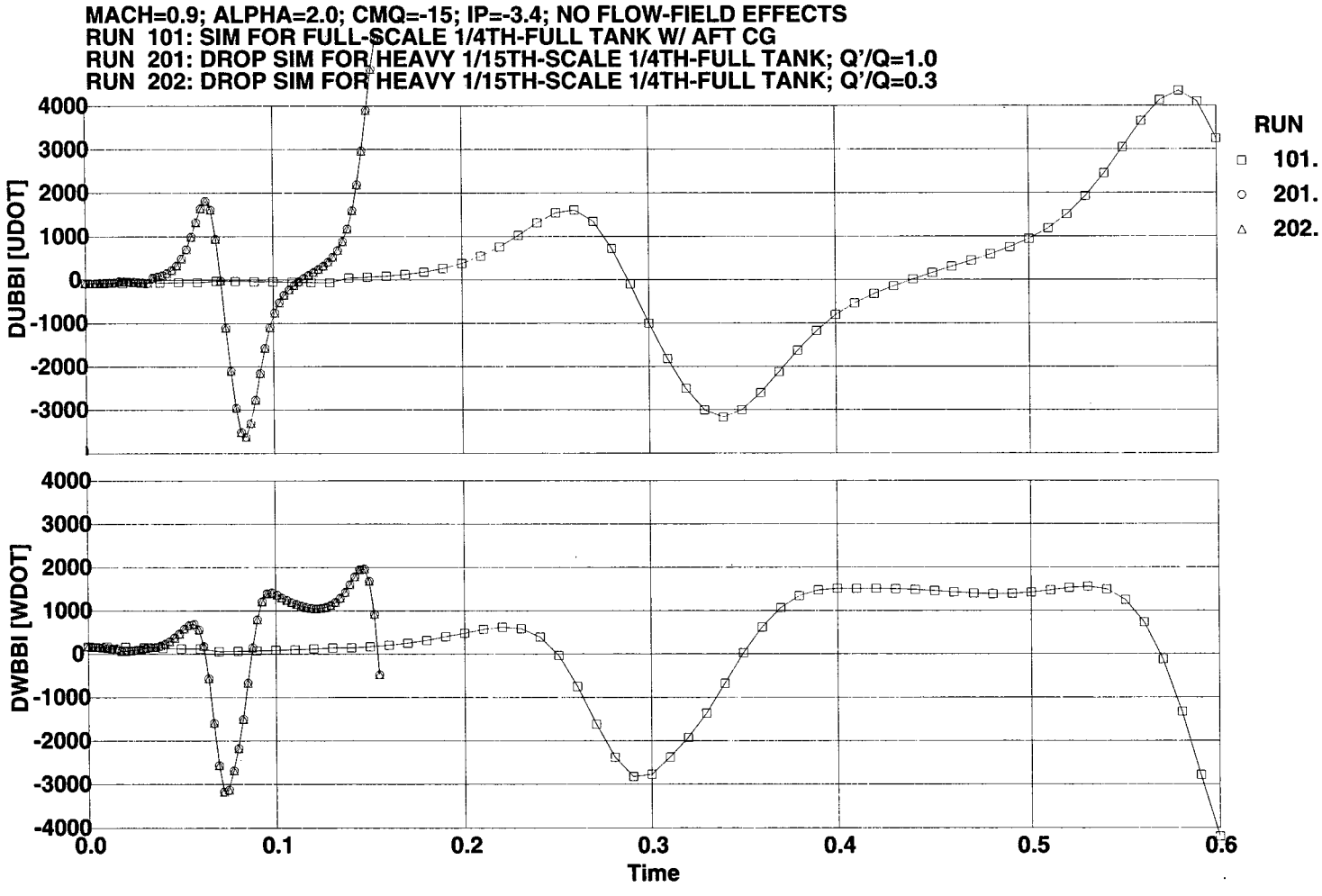

e. Axial and vertical linear velocity derivatives

Figure 8. Continued.

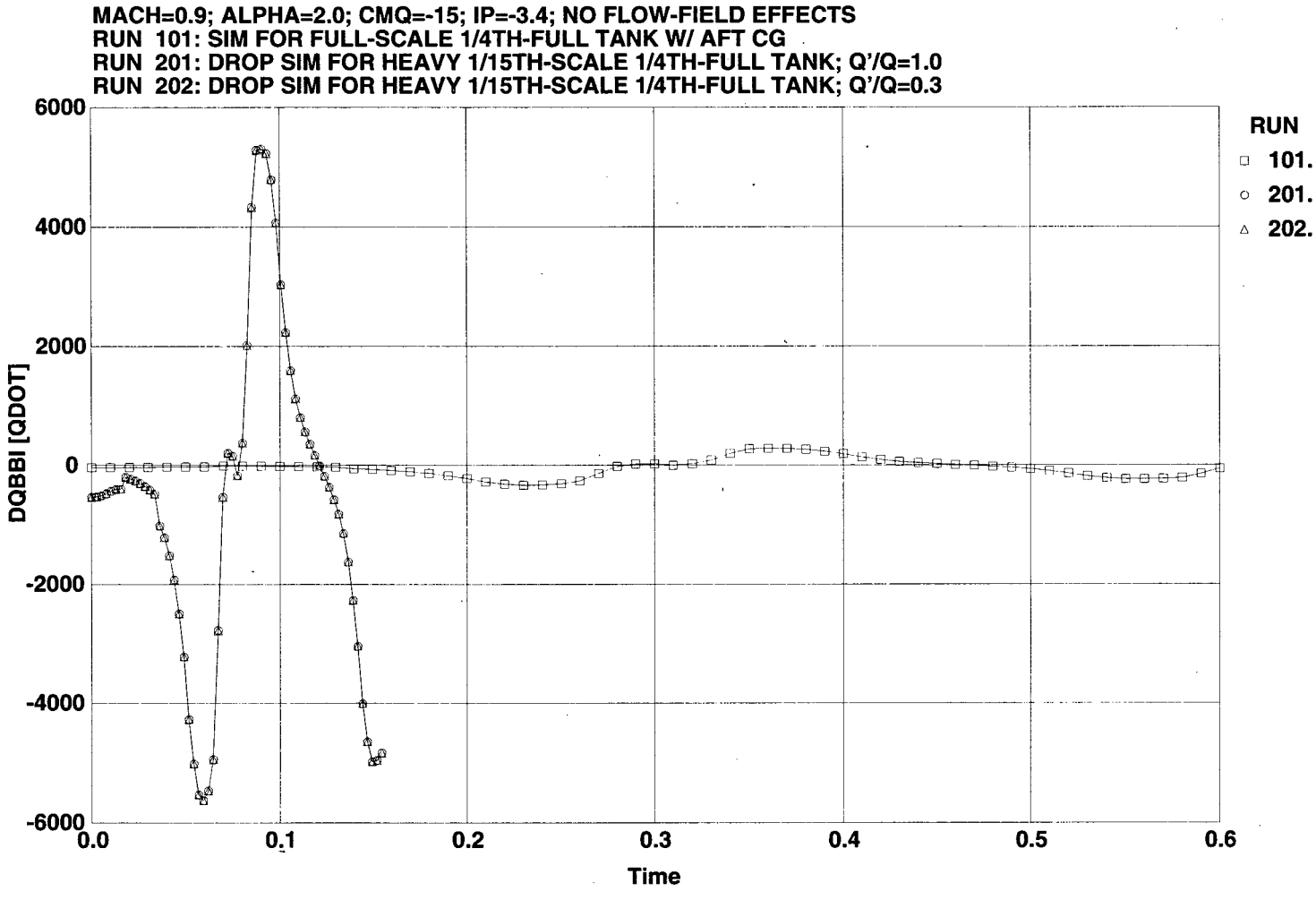

f. Pitch angular velocity derivative

Figure 8. Continued.

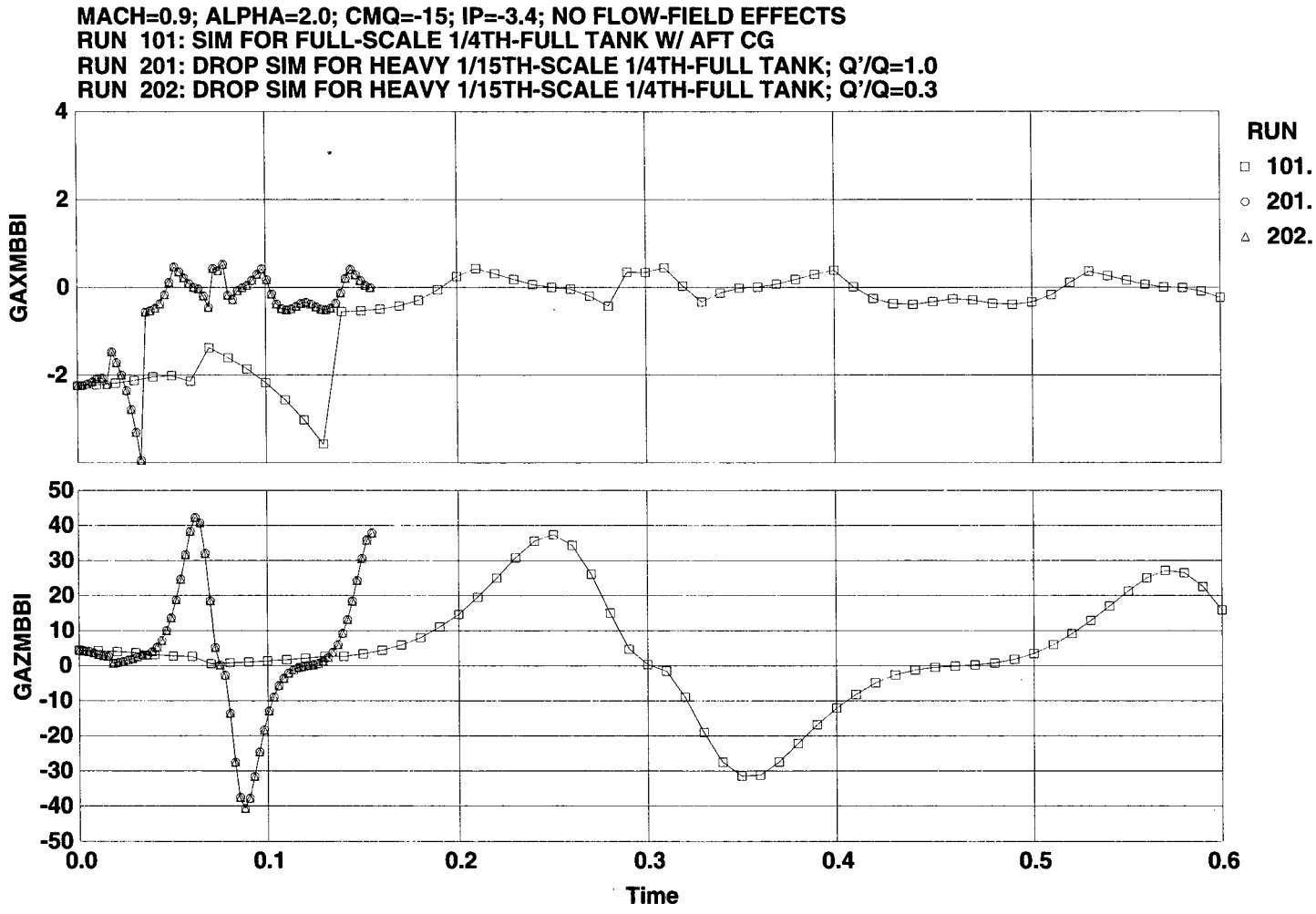

g. Body-measured accelerations at the cg

Figure 8. Continued.

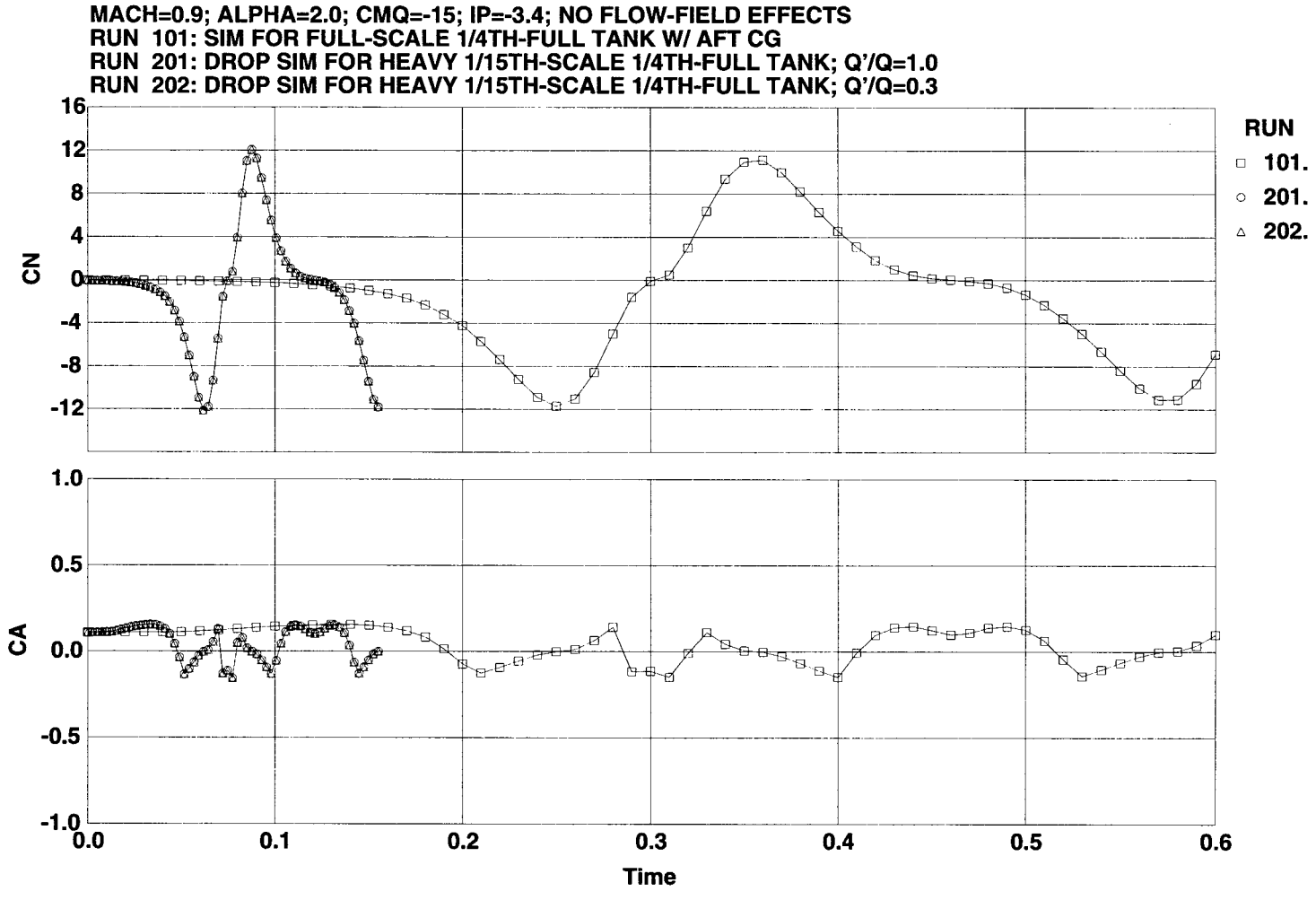

h. Normal and axial force coefficients

Figure 8. Continued.

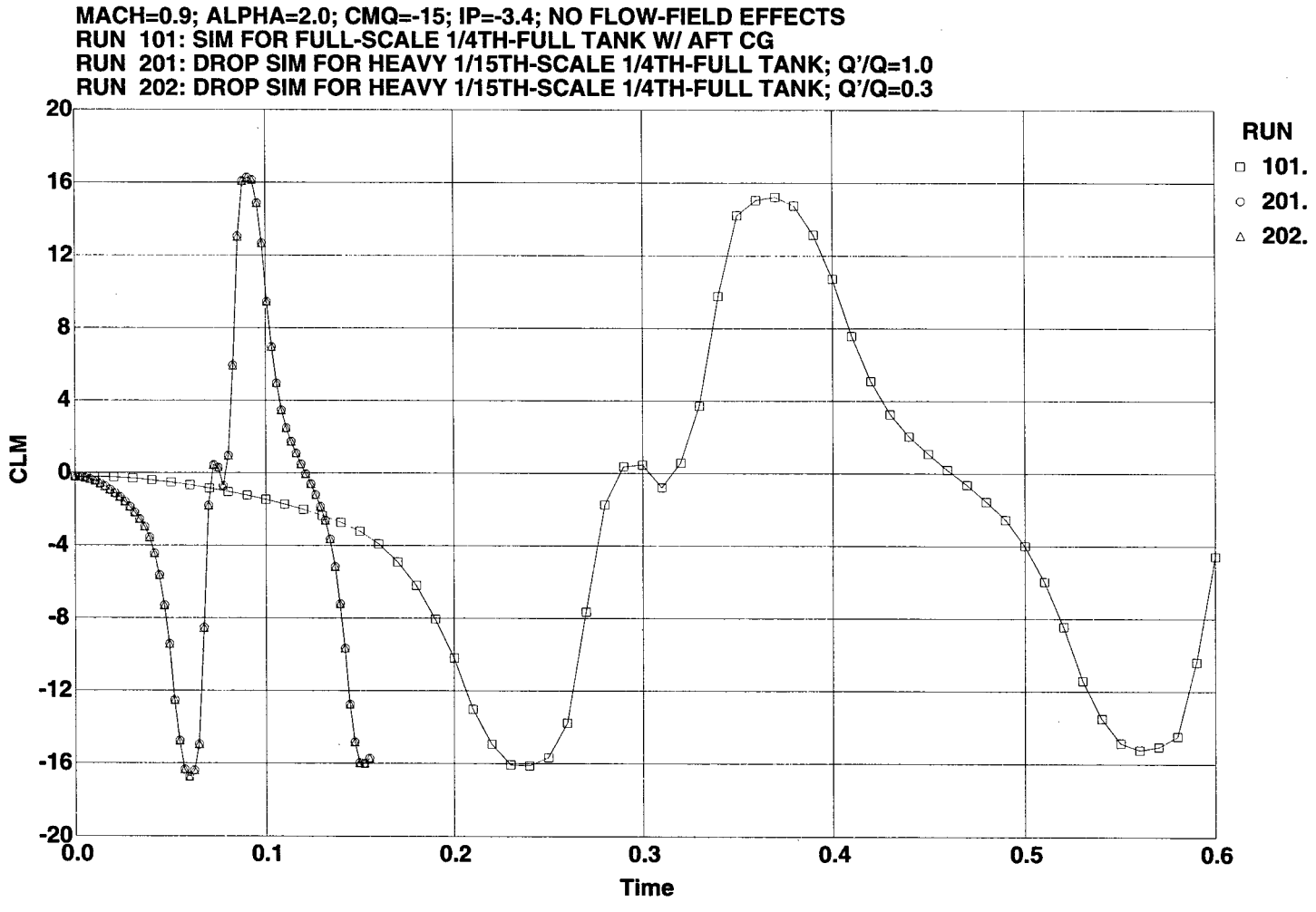

i. Pitching moment coefficient

Figure 8. Concluded.

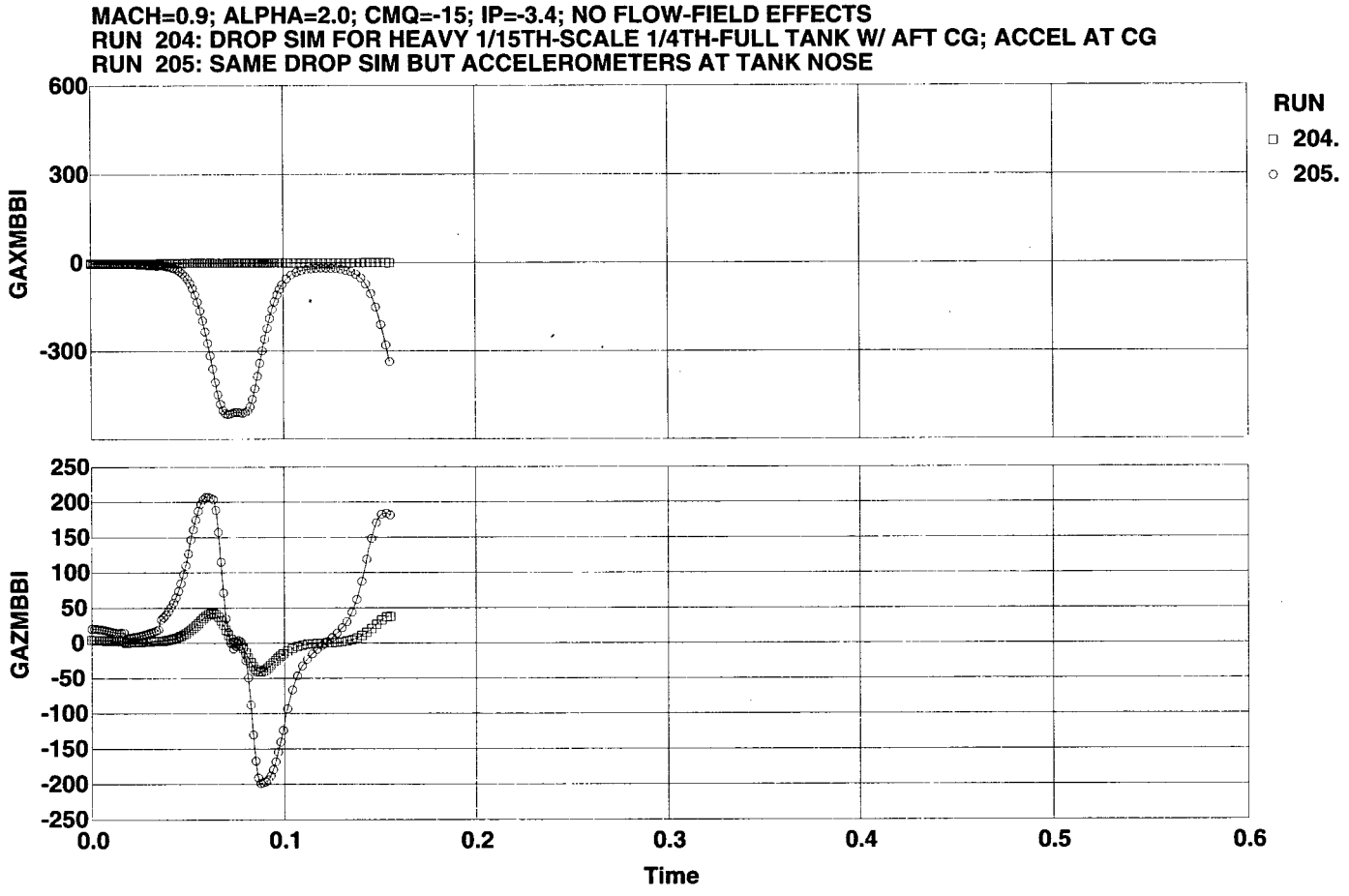

Figure 9. Body-measured accelerations at tank cg and at tank nose.

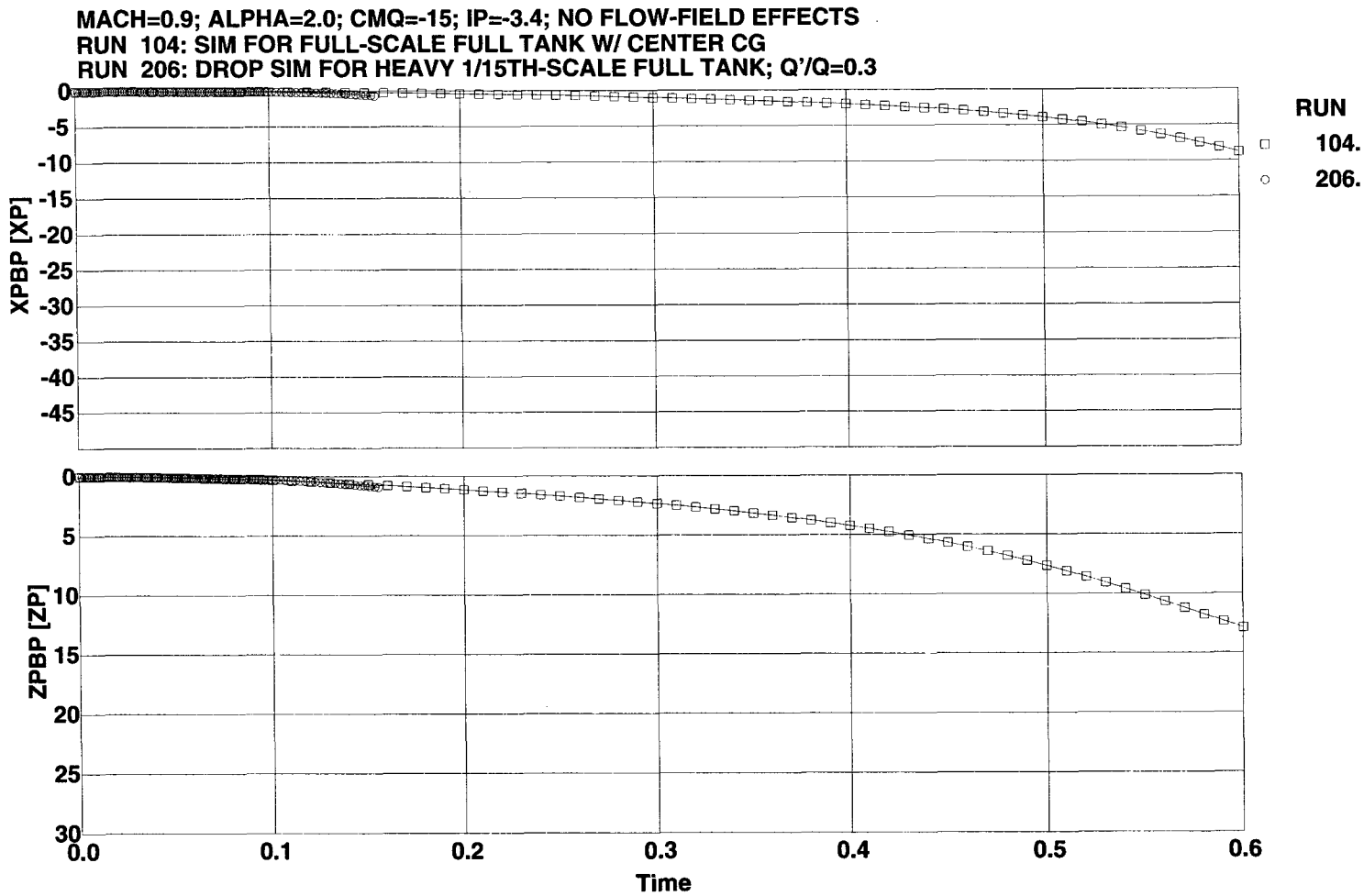

a. Axial and vertical positions

Figure 10. Full-tank simulations at full scale and 1/15 scale.

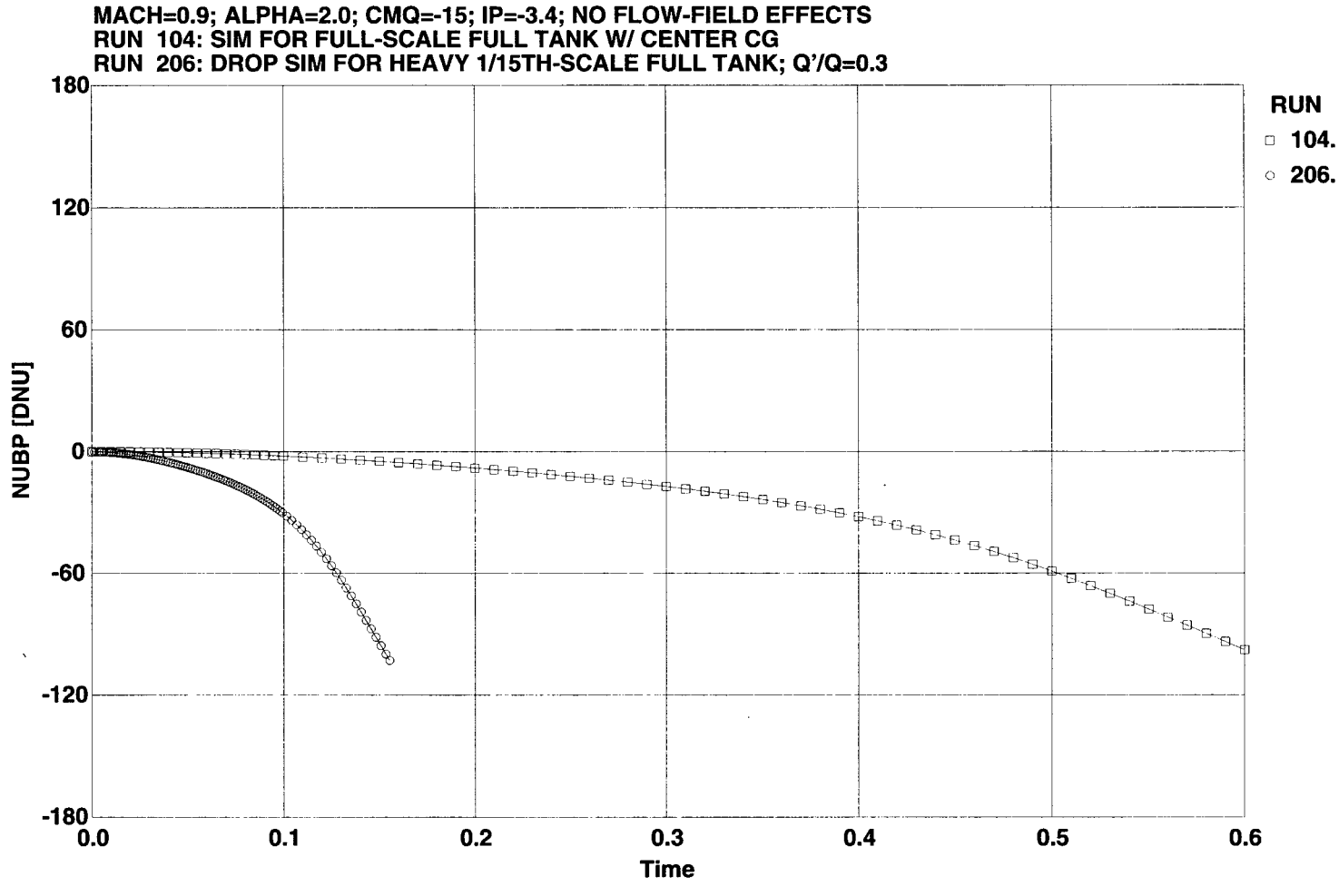

b. Pitch orientation

Figure 10. Continued.

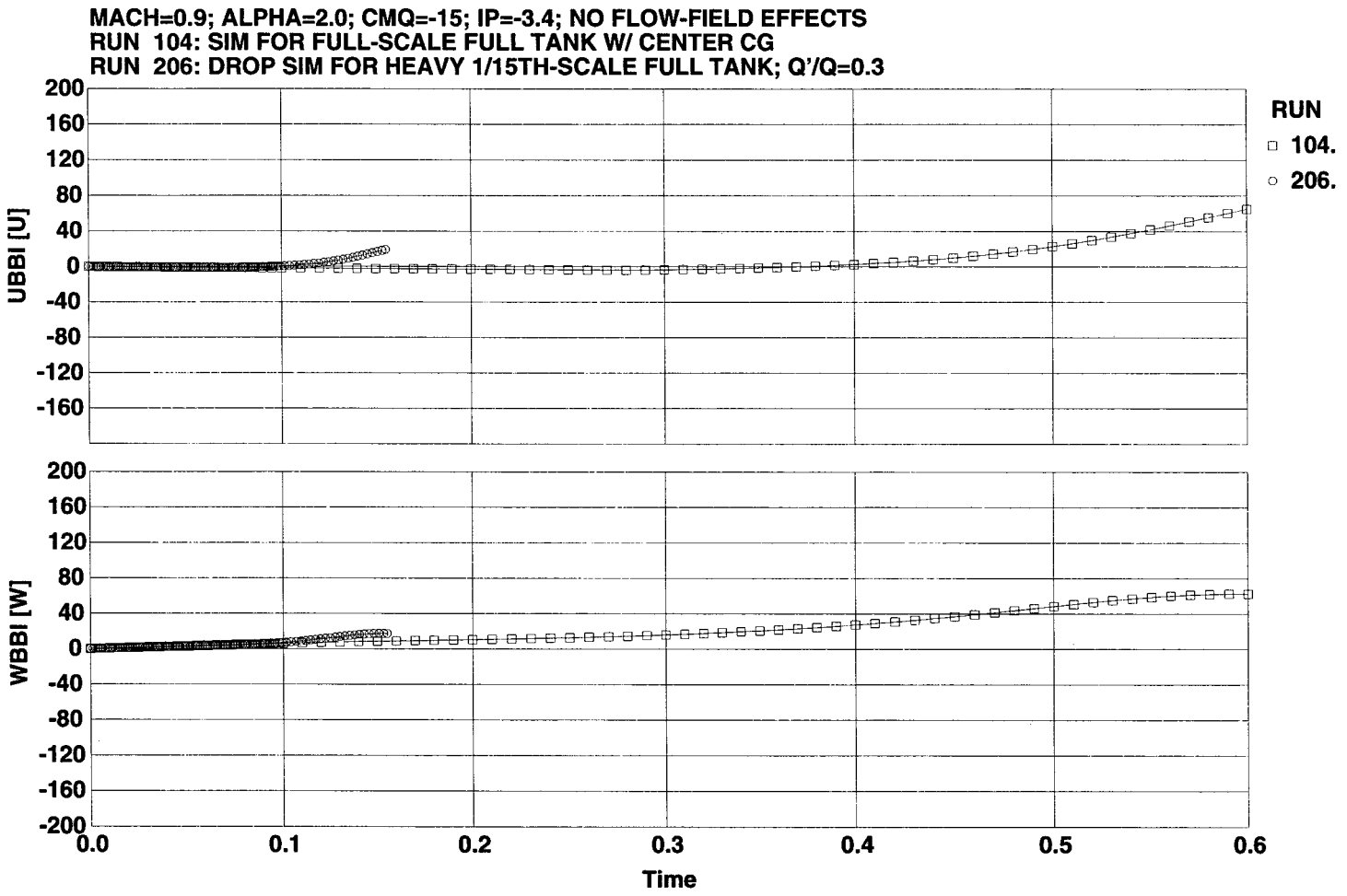

c. Axial and vertical linear velocities

Figure 10. Continued.

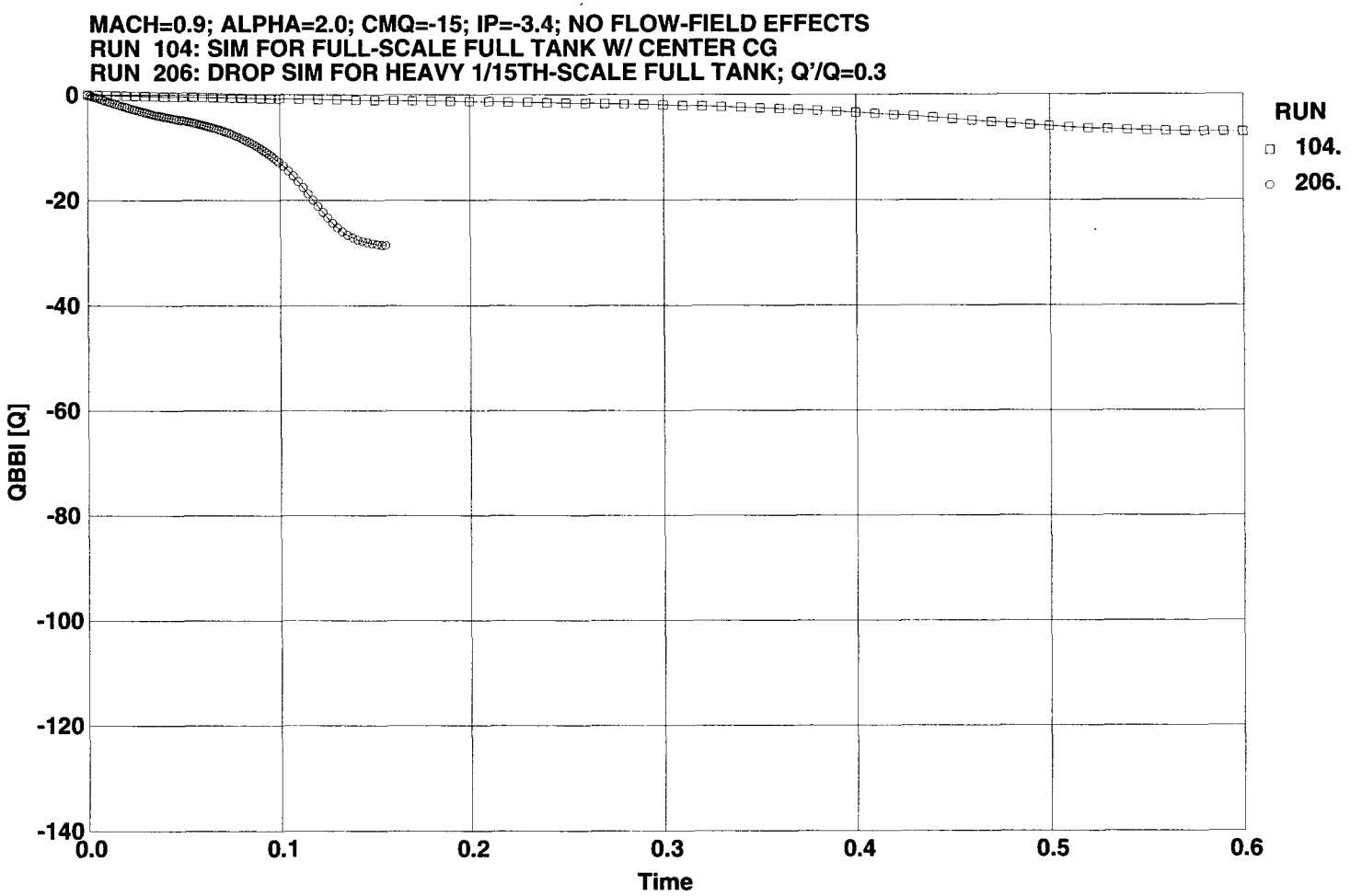

d. Pitch angular velocity
Figure 10. Continued.

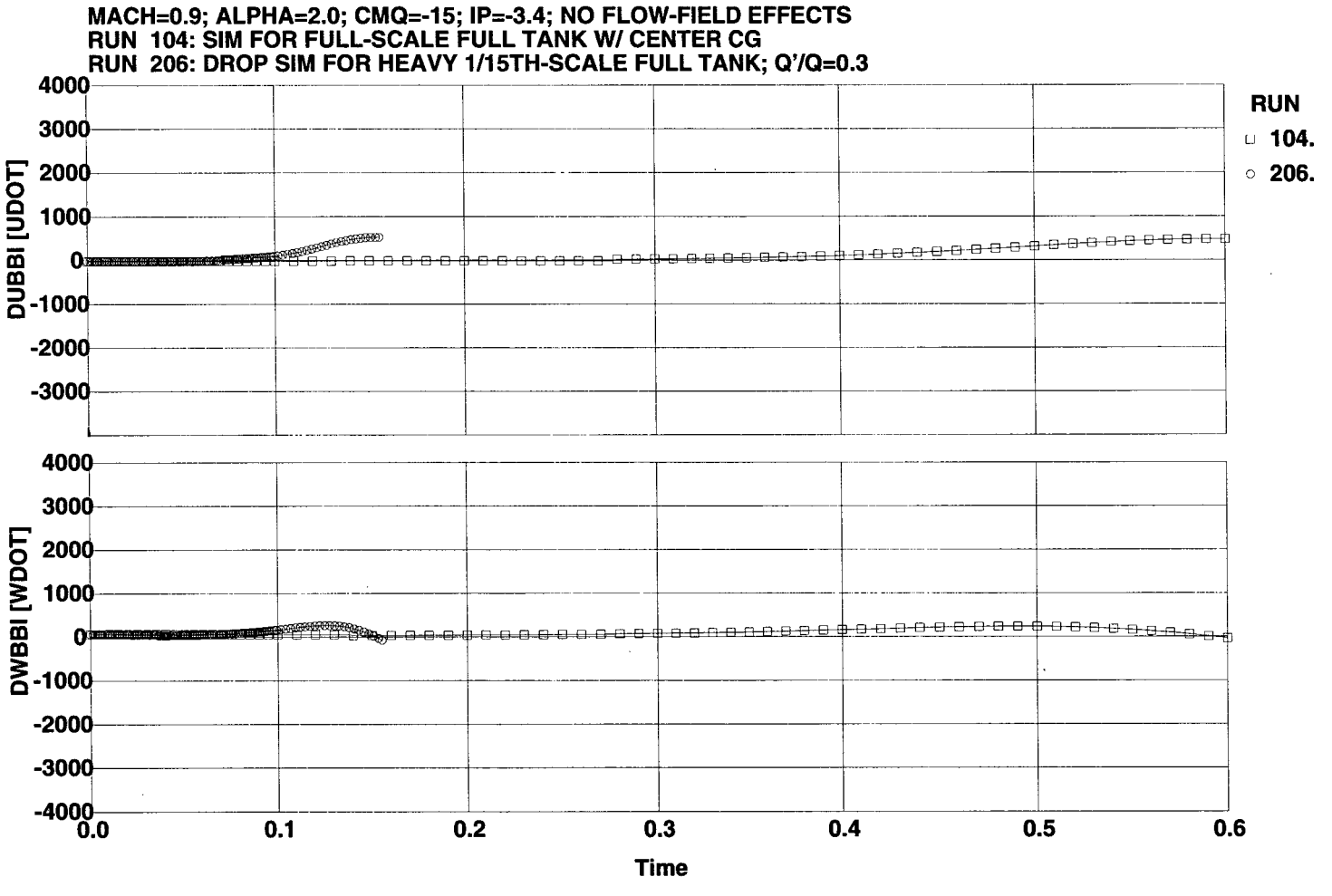

e. Axial and vertical linear velocity derivatives

Figure 10. Continued.

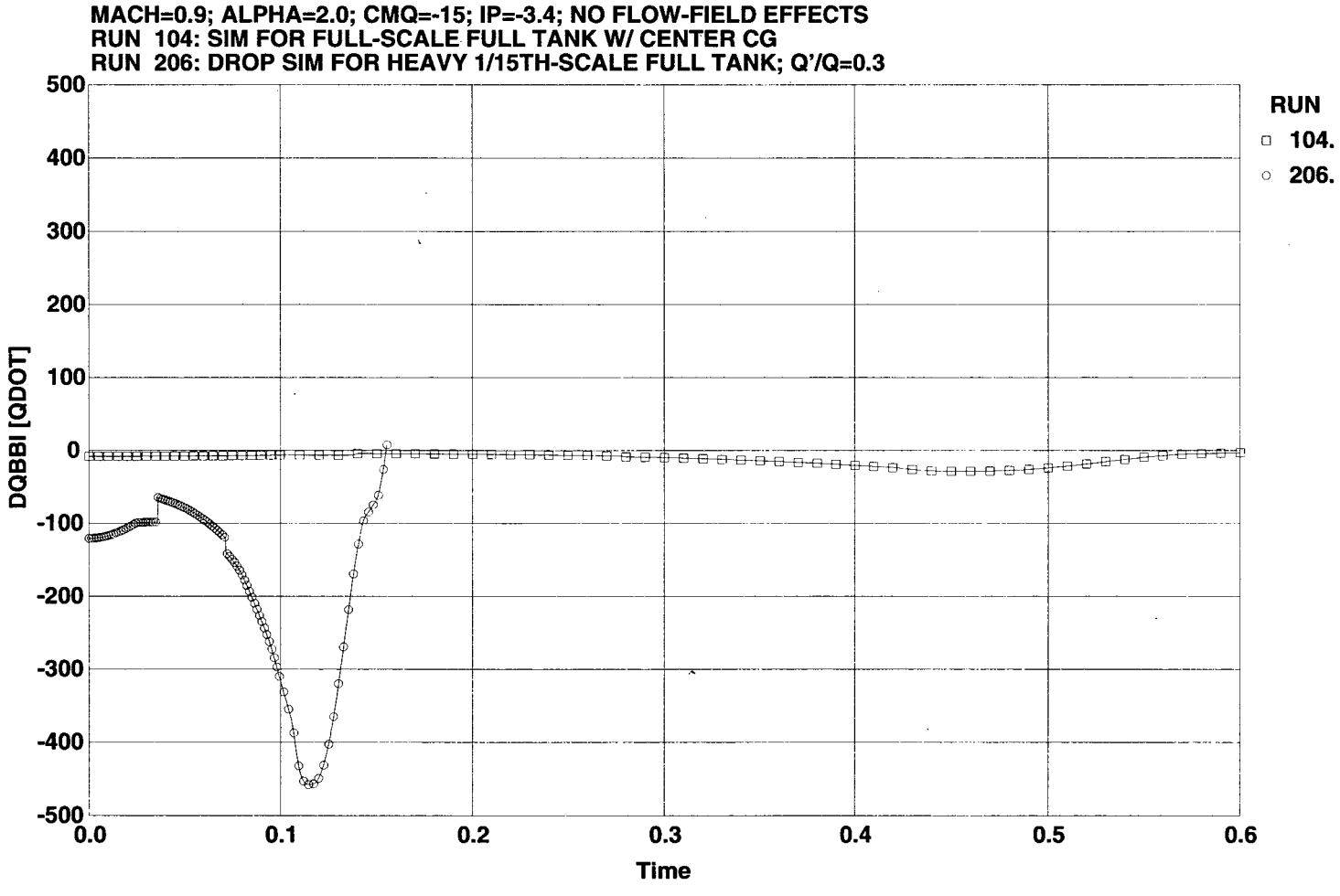

f. Pitch angular velocity derivative
Figure 10. Continued.

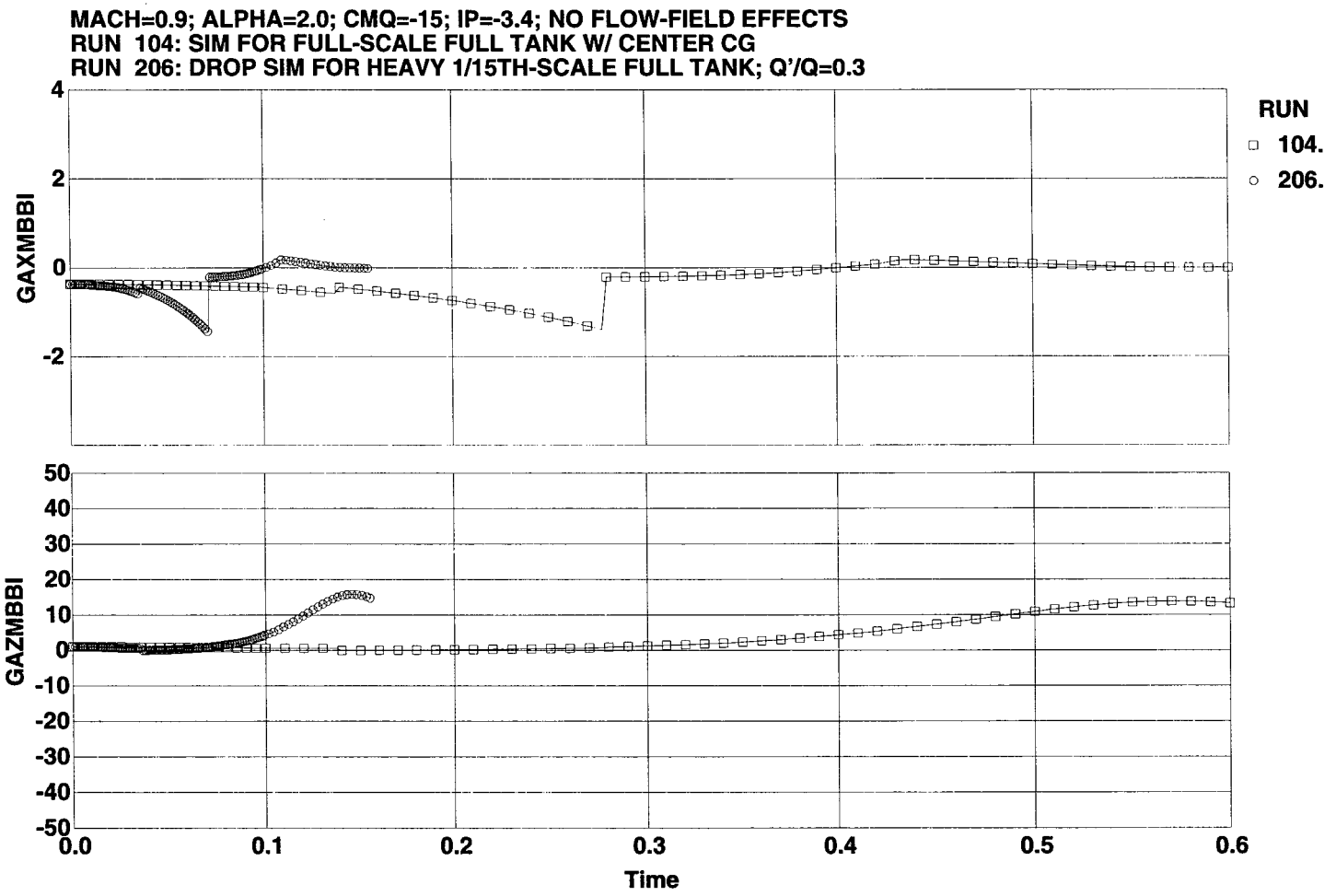

g. Body-measured accelerations at the cg

Figure 10. Continued.

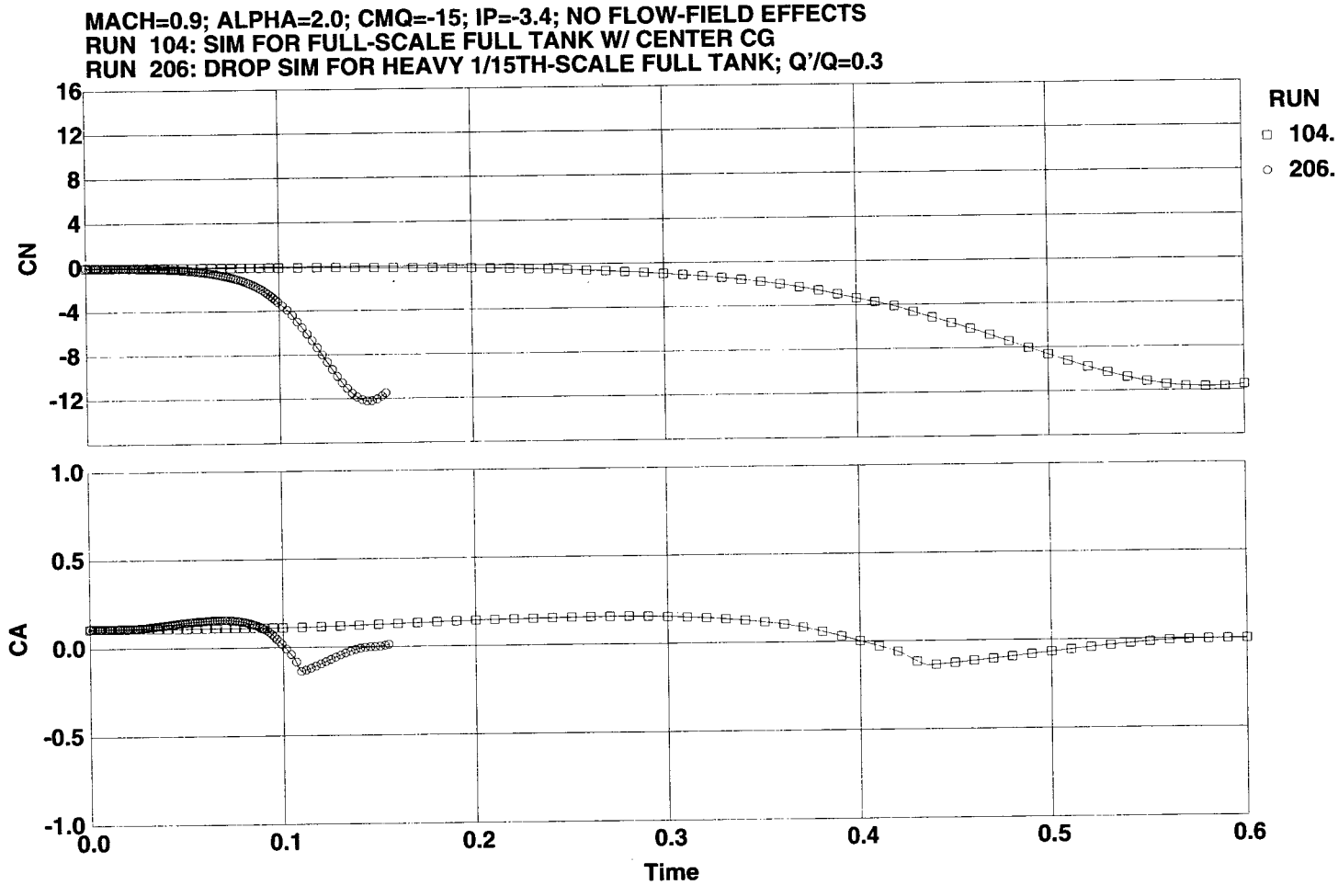

h. Normal and axial force coefficients

Figure 10. Continued.

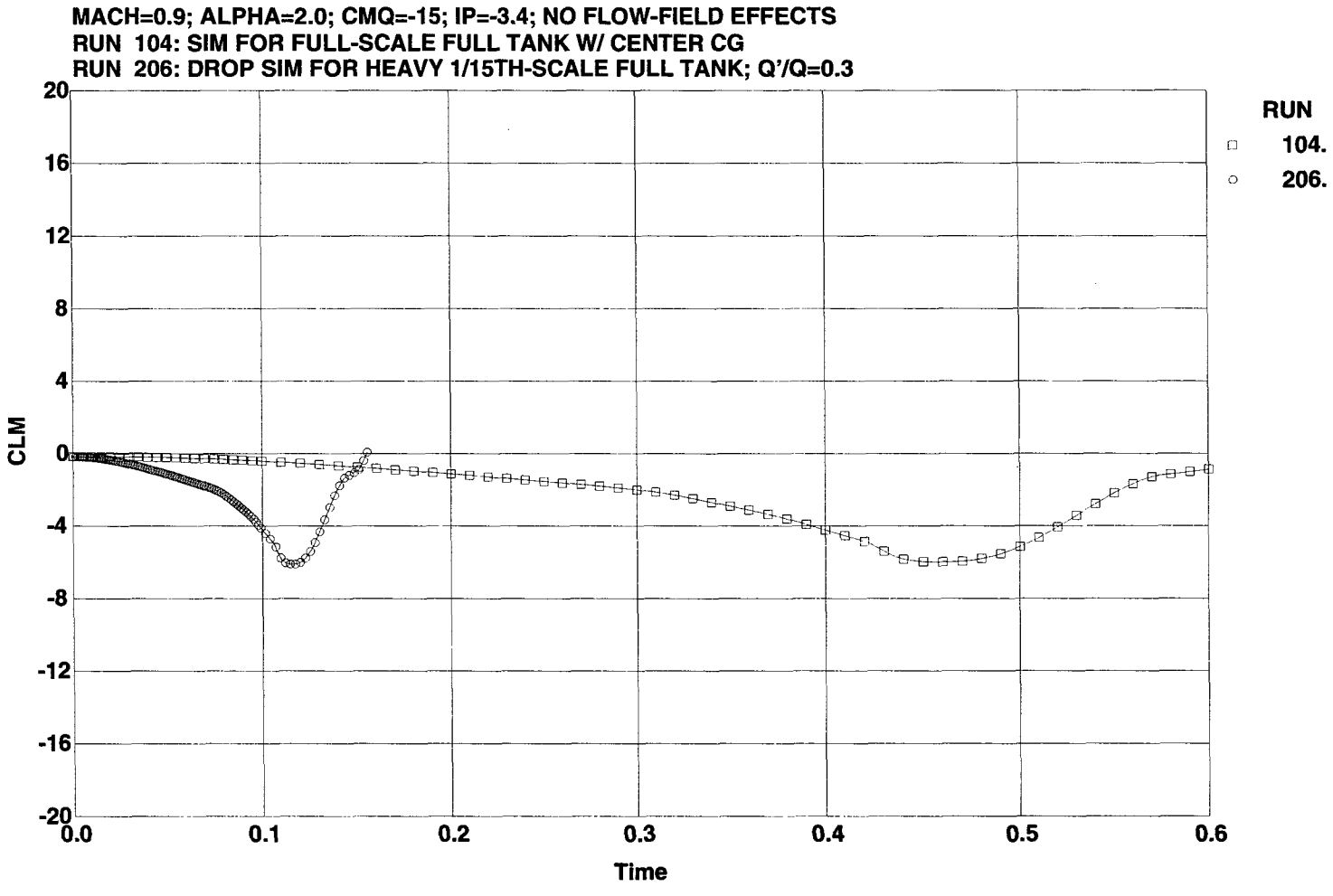

i. Pitching moment coefficient

Figure 10. Concluded.

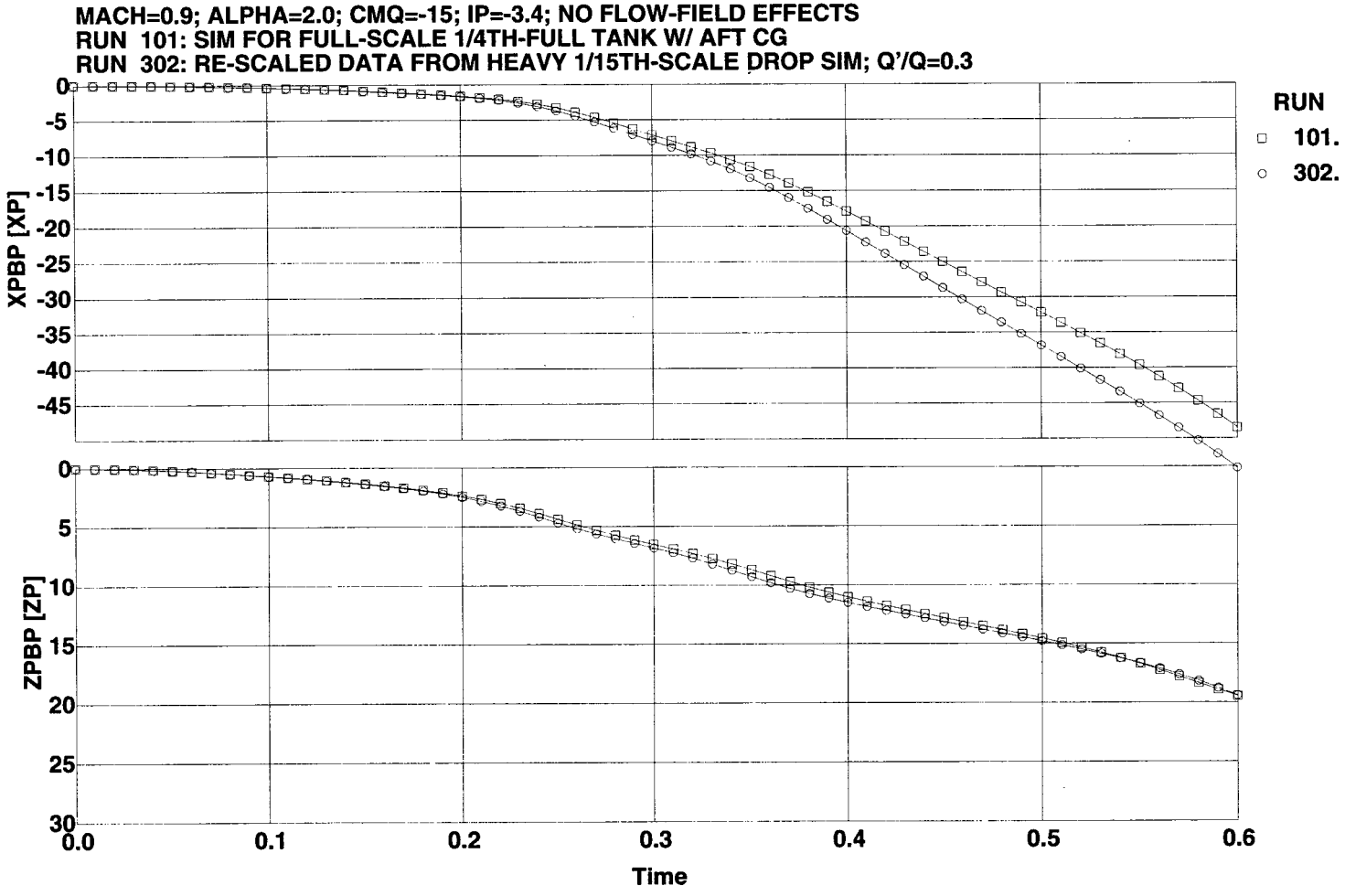

a. Axial and vertical positions

Figure 11. Comparison of full-scale simulation and re-scaled 1/15th-scale simulation.

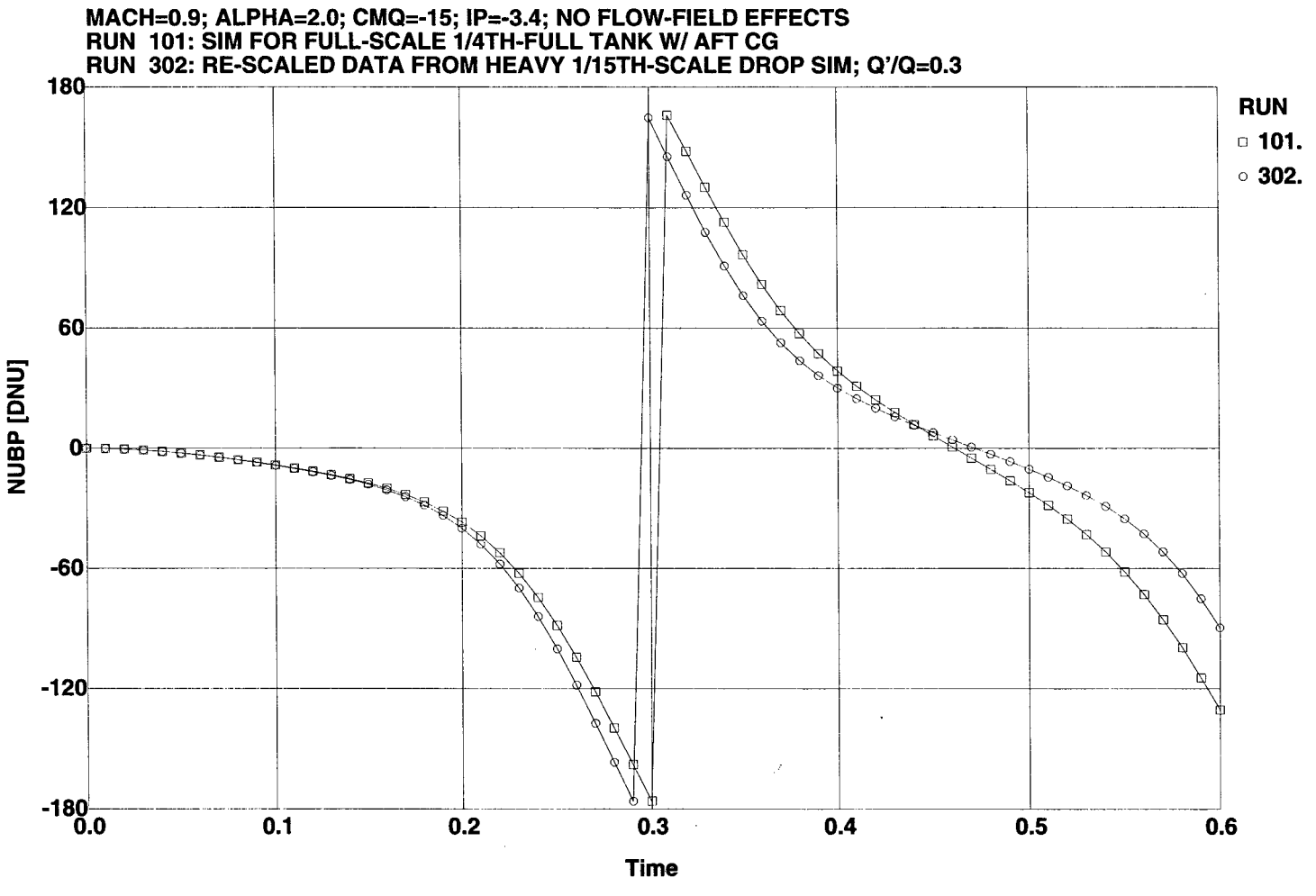

b. Pitch orientation

Figure 11. Continued.

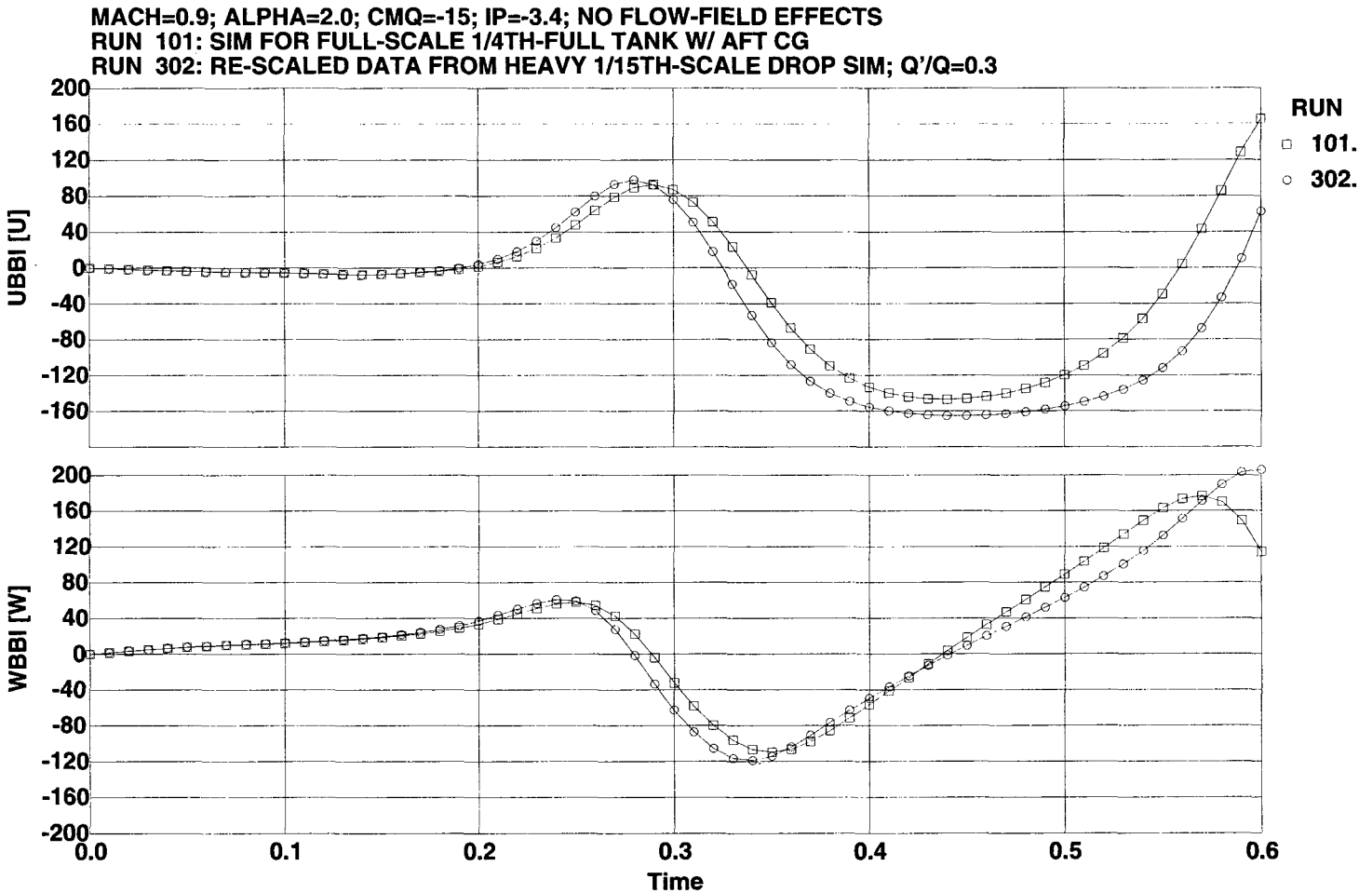

c. Axial and vertical linear velocities
Figure 11. Continued.

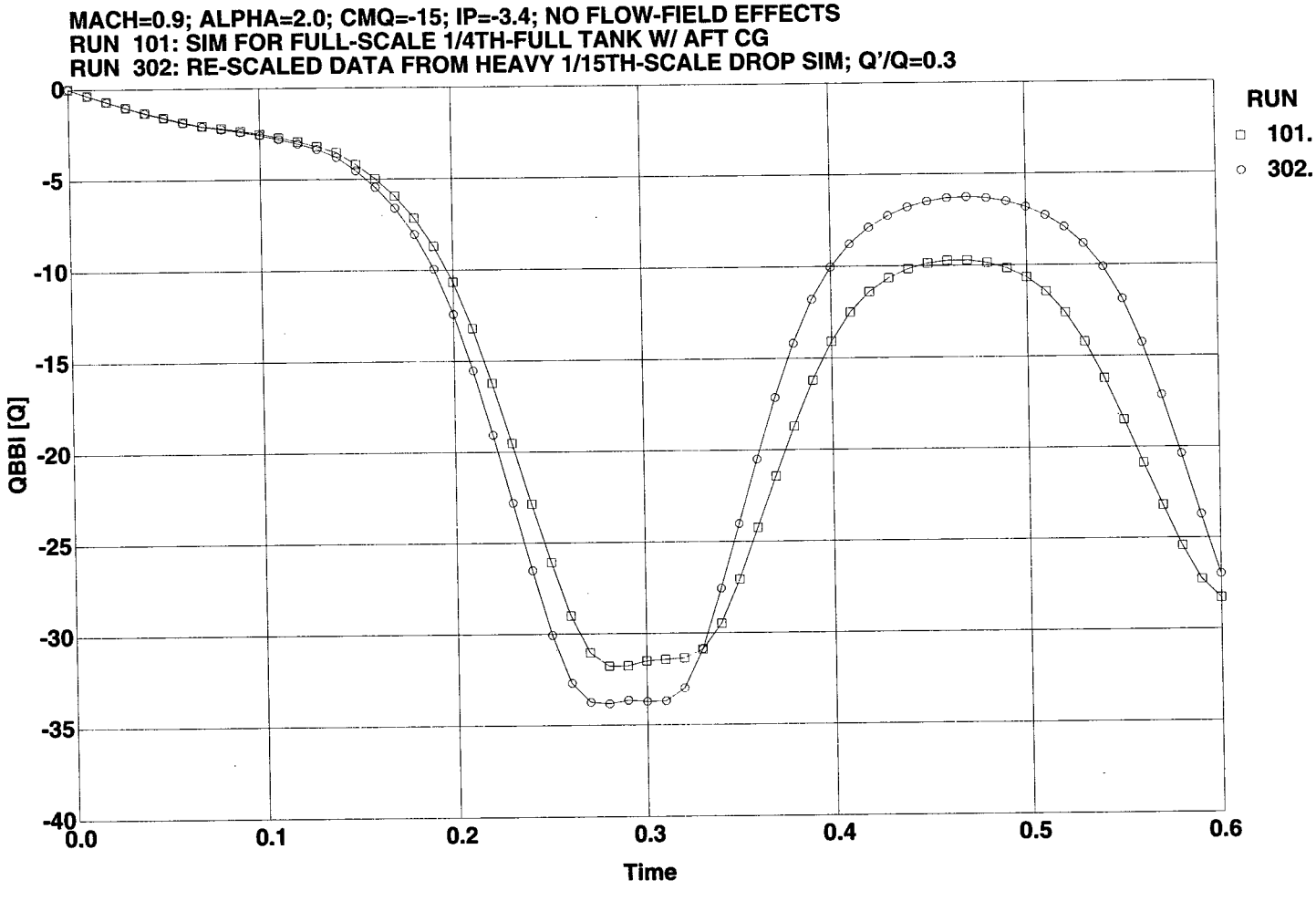

d. Pitch angular velocity

Figure 11. Continued.

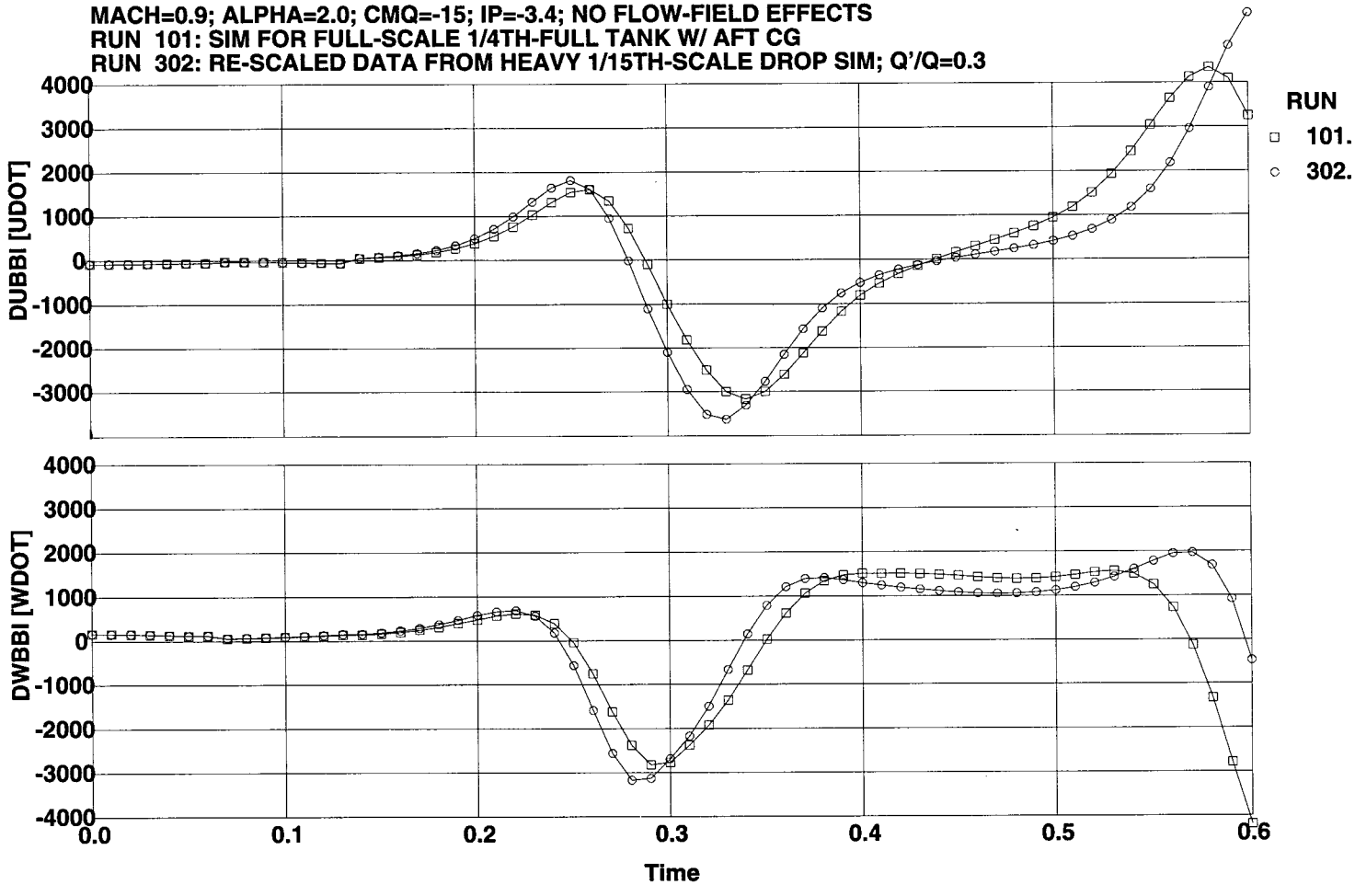

e. Axial and vertical linear velocity derivatives
Figure 11. Continued.

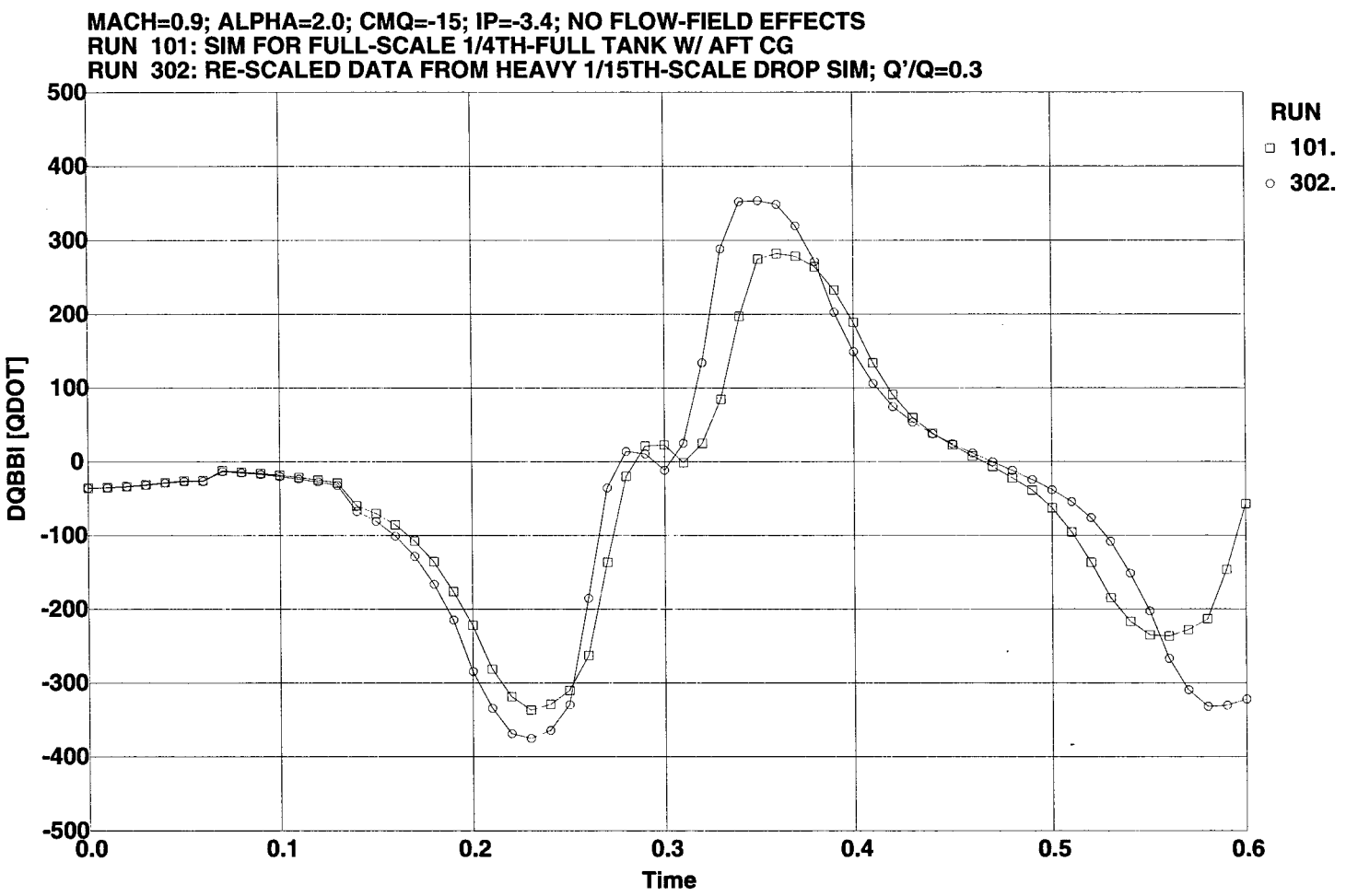

f. Pitch angular velocity derivative

Figure 11. Continued.

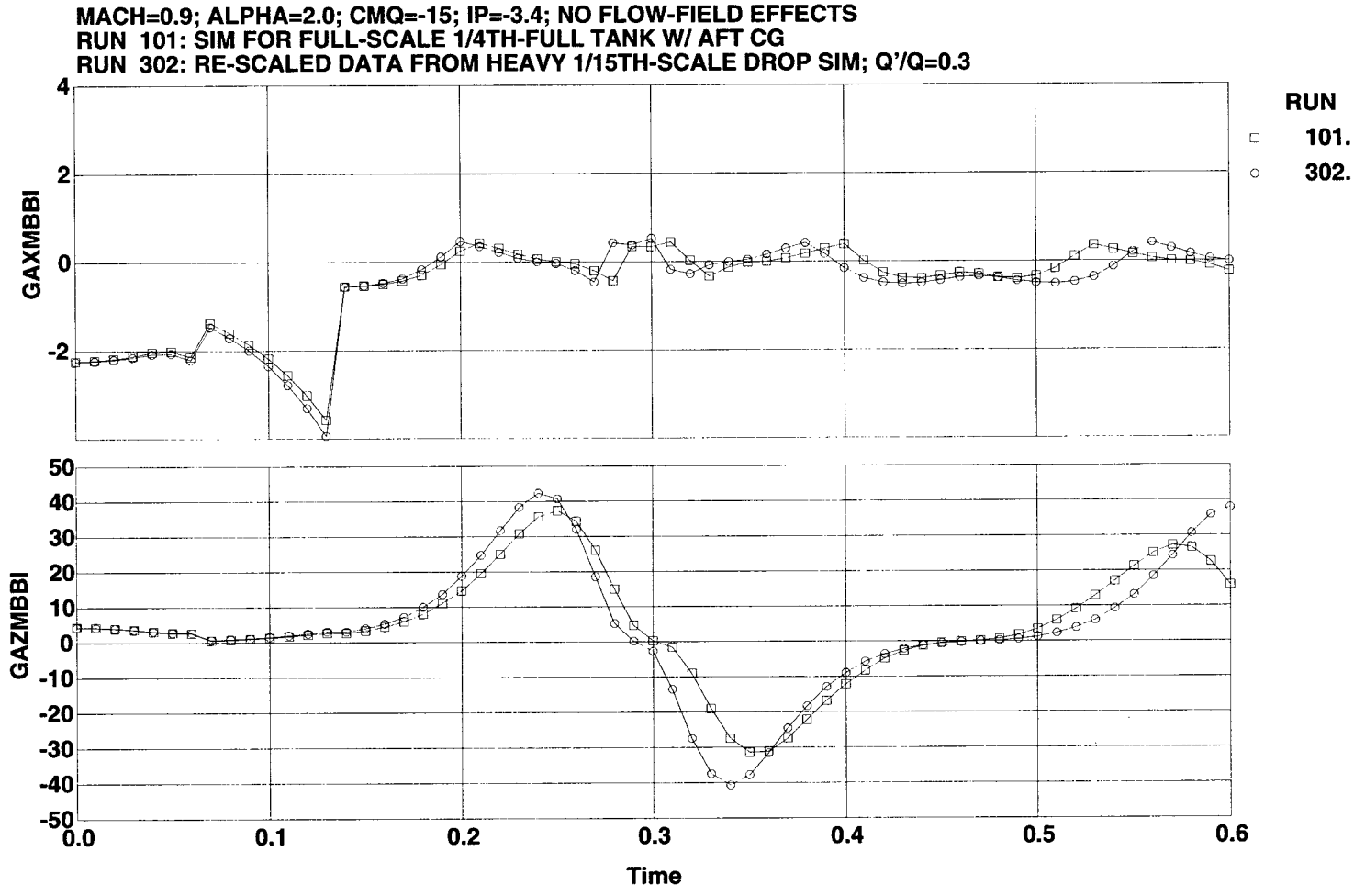

g. Body-measured accelerations at the cg

Figure 11. Continued.

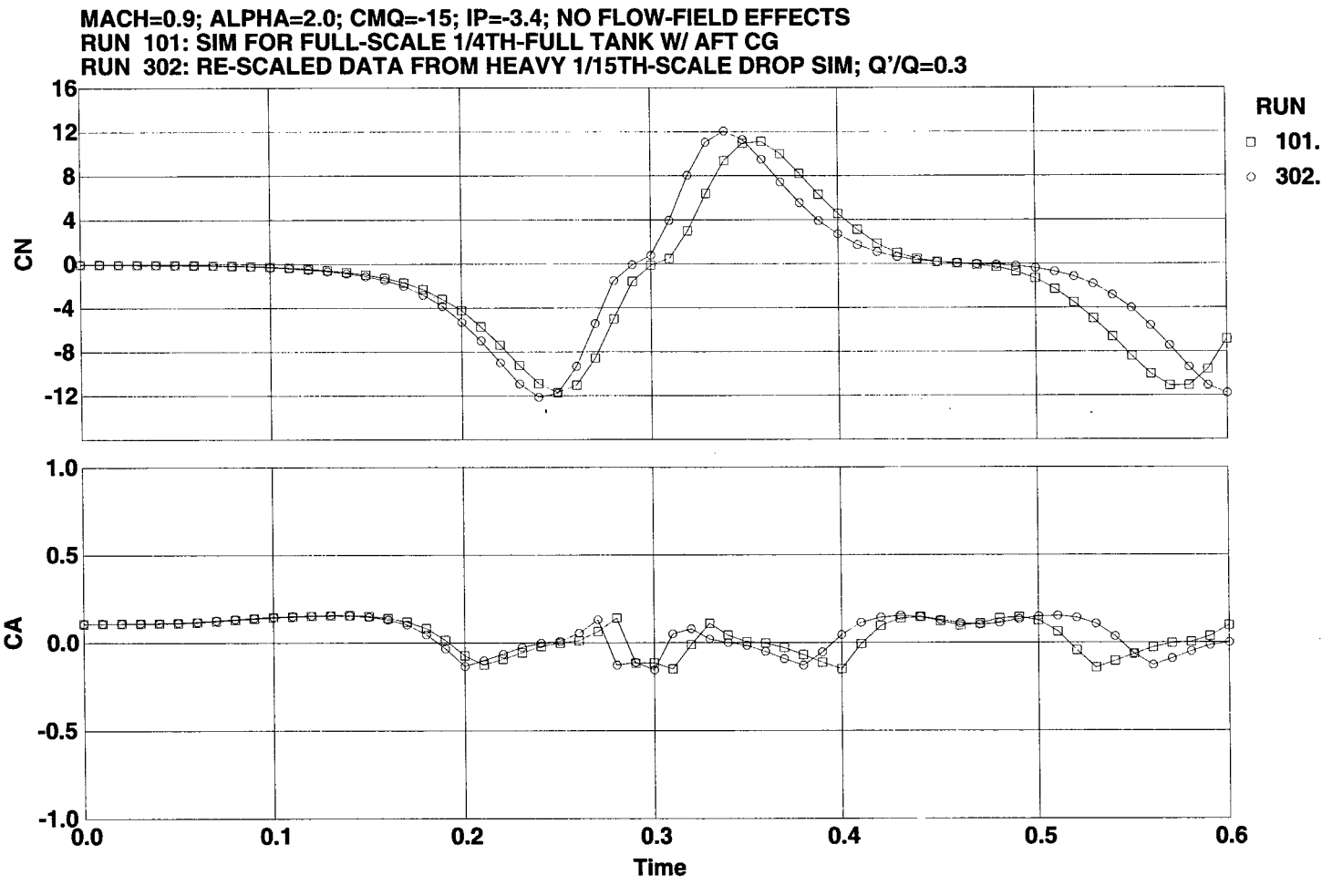

h. Normal and axial force coefficients

Figure 11. Continued.

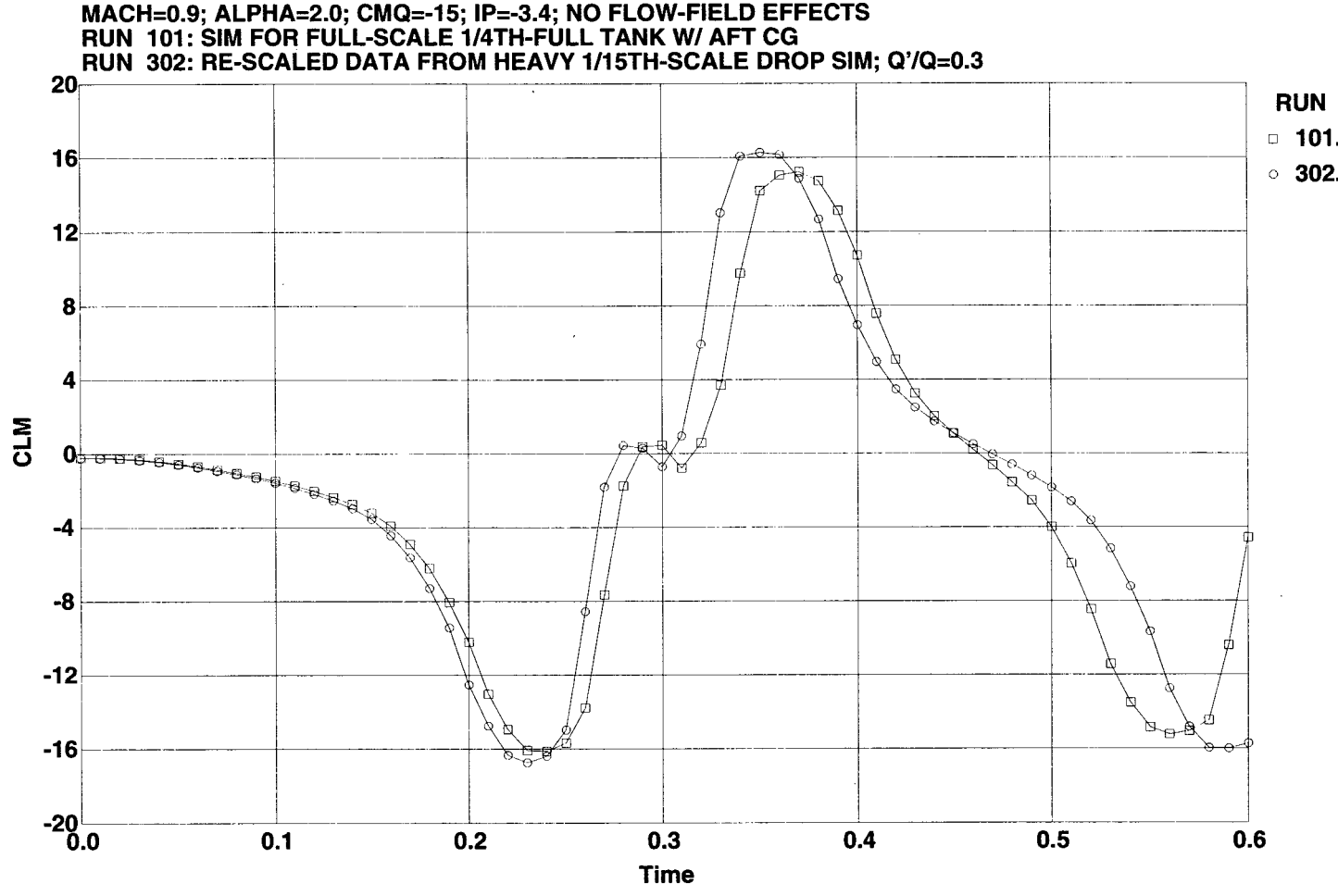

i. Pitching moment coefficient
Figure 11. Continued.

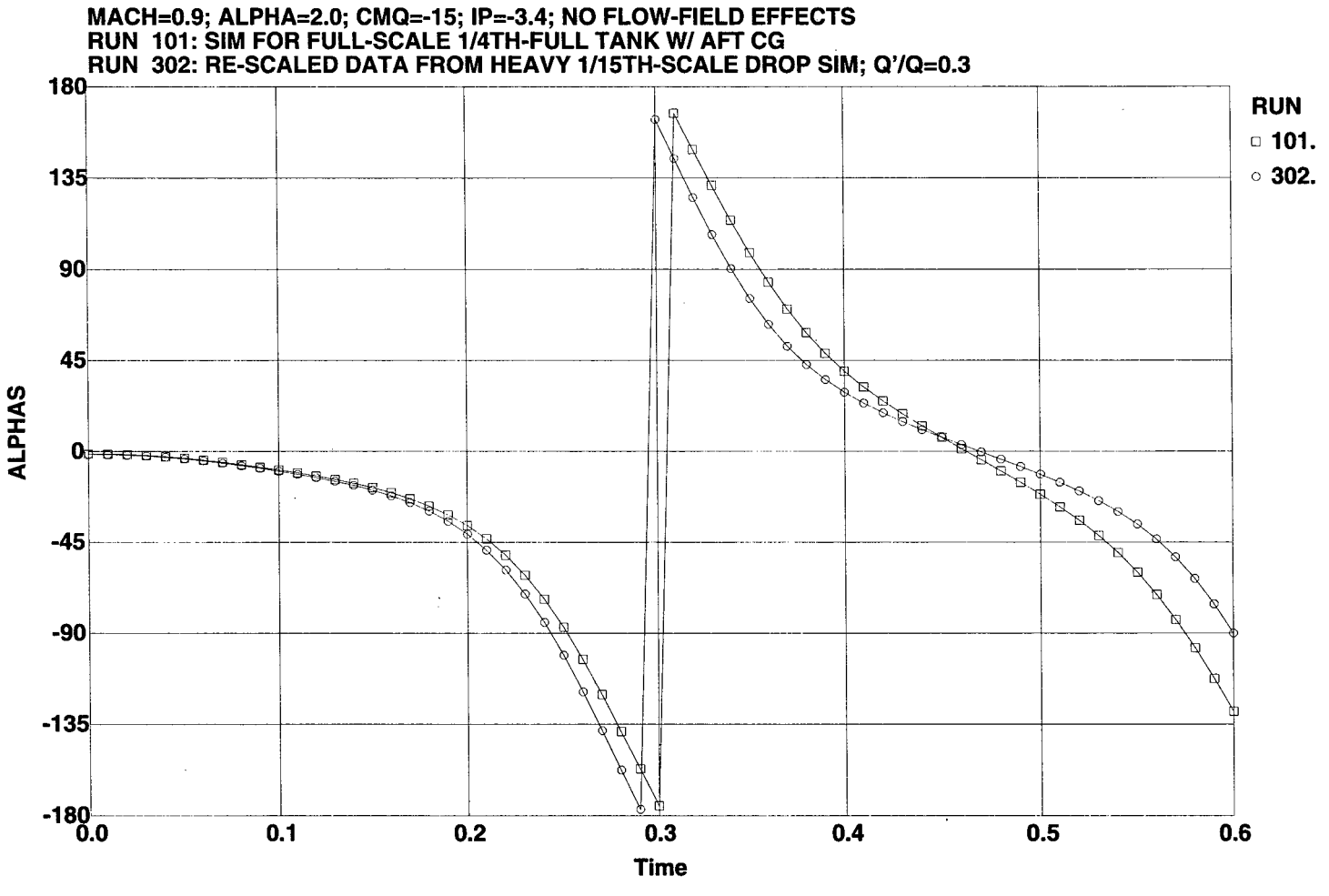

j. Store aerodynamic angle of attack

Figure 11. Concluded.

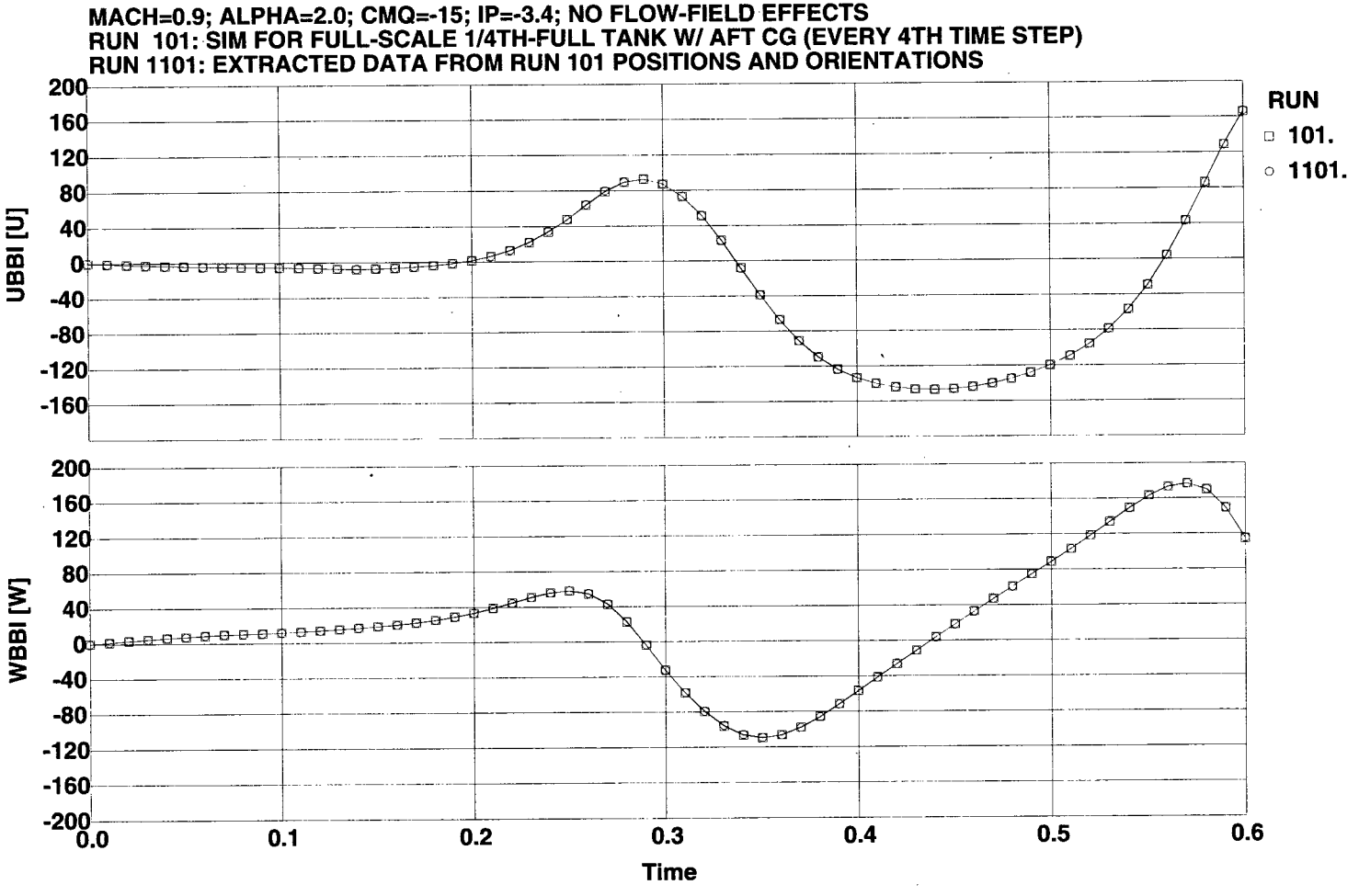

a. Axial and vertical linear velocities

Figure 12. Extracted information from full-scale 1/4th-full tank simulation.

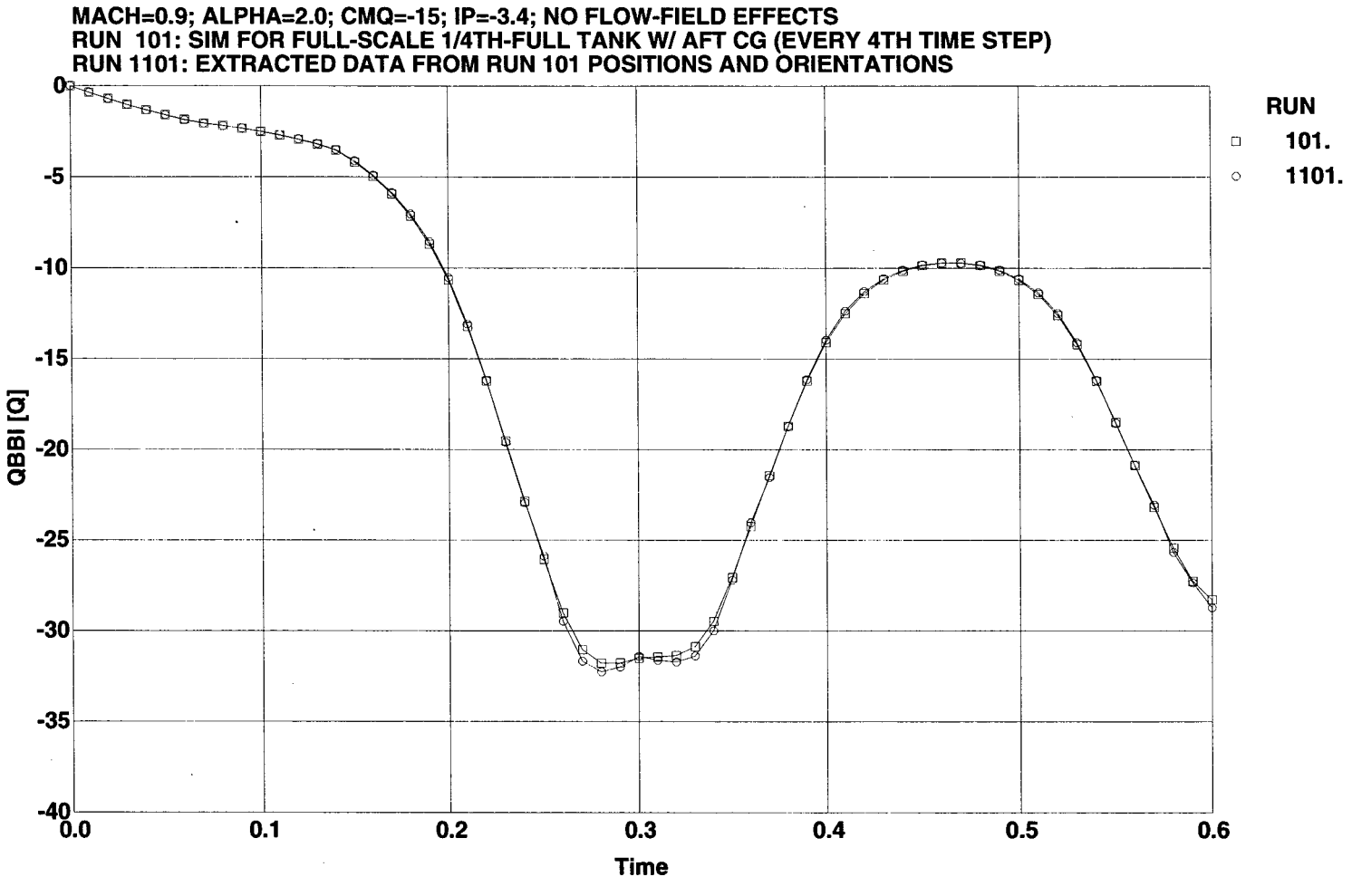

b. Pitch angular velocity
Figure 12. Continued.

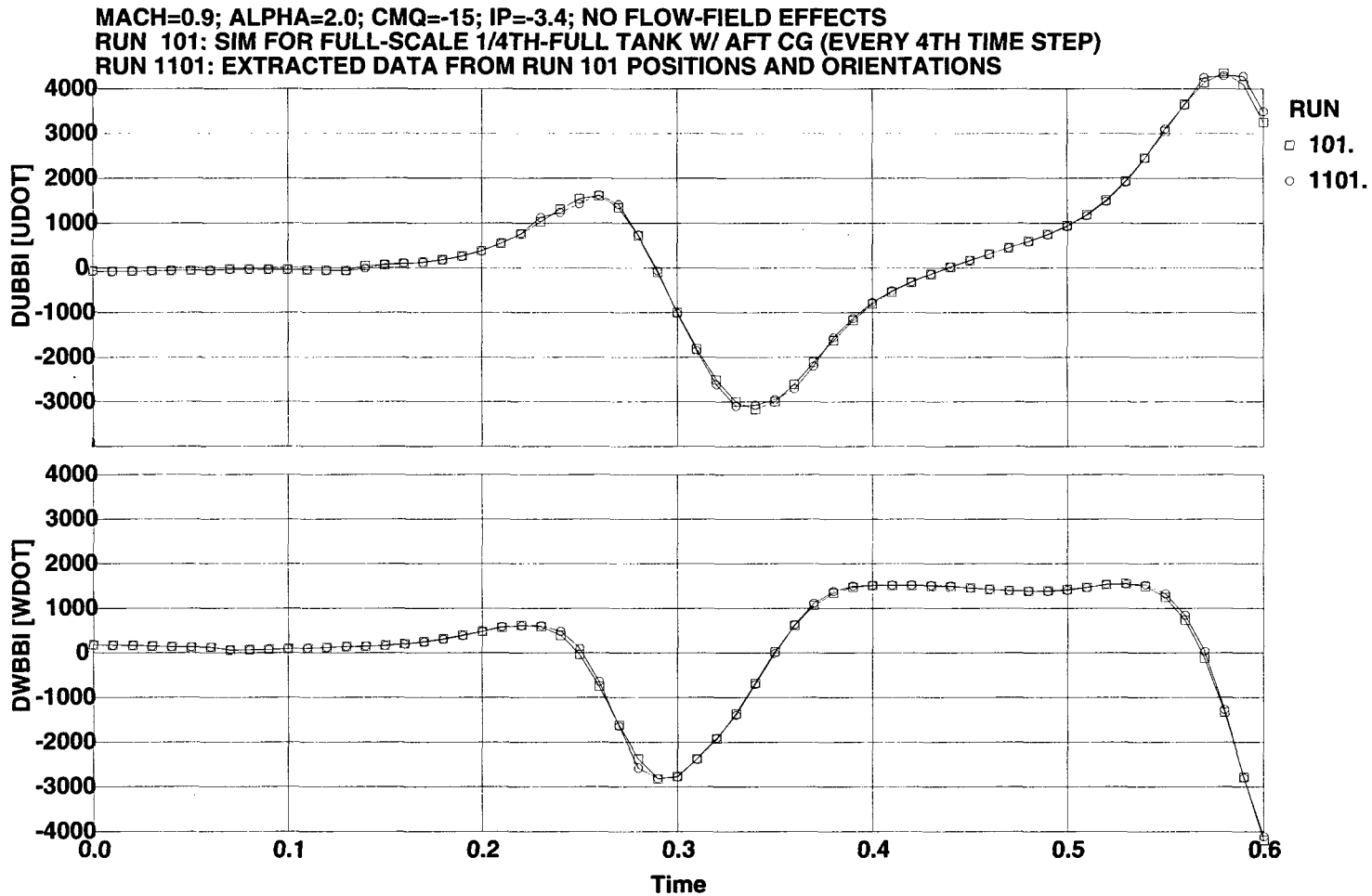

c. Axial and vertical linear velocity derivatives
Figure 12. Continued.

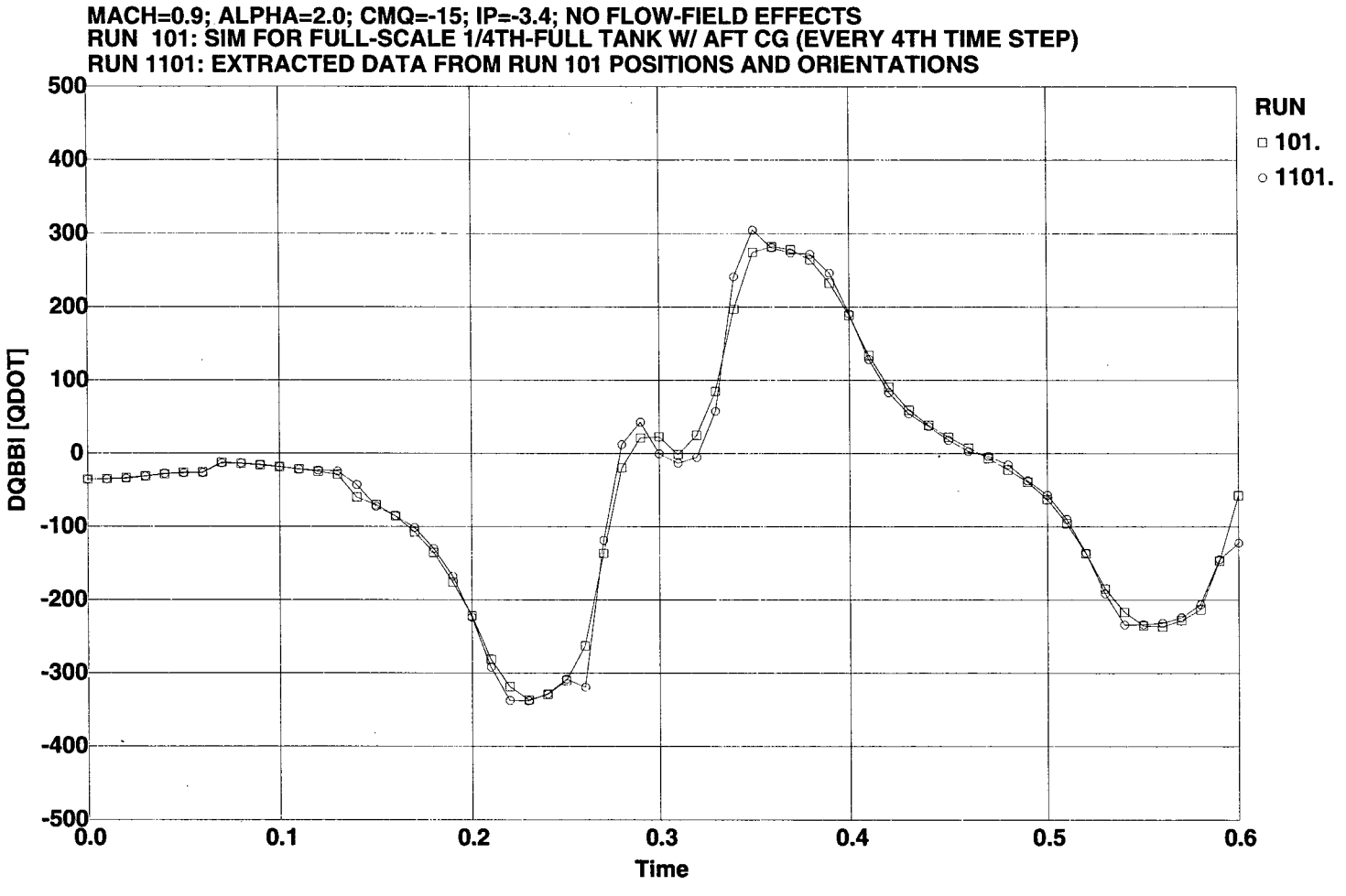

d. Pitch angular velocity derivative

Figure 12. Continued.

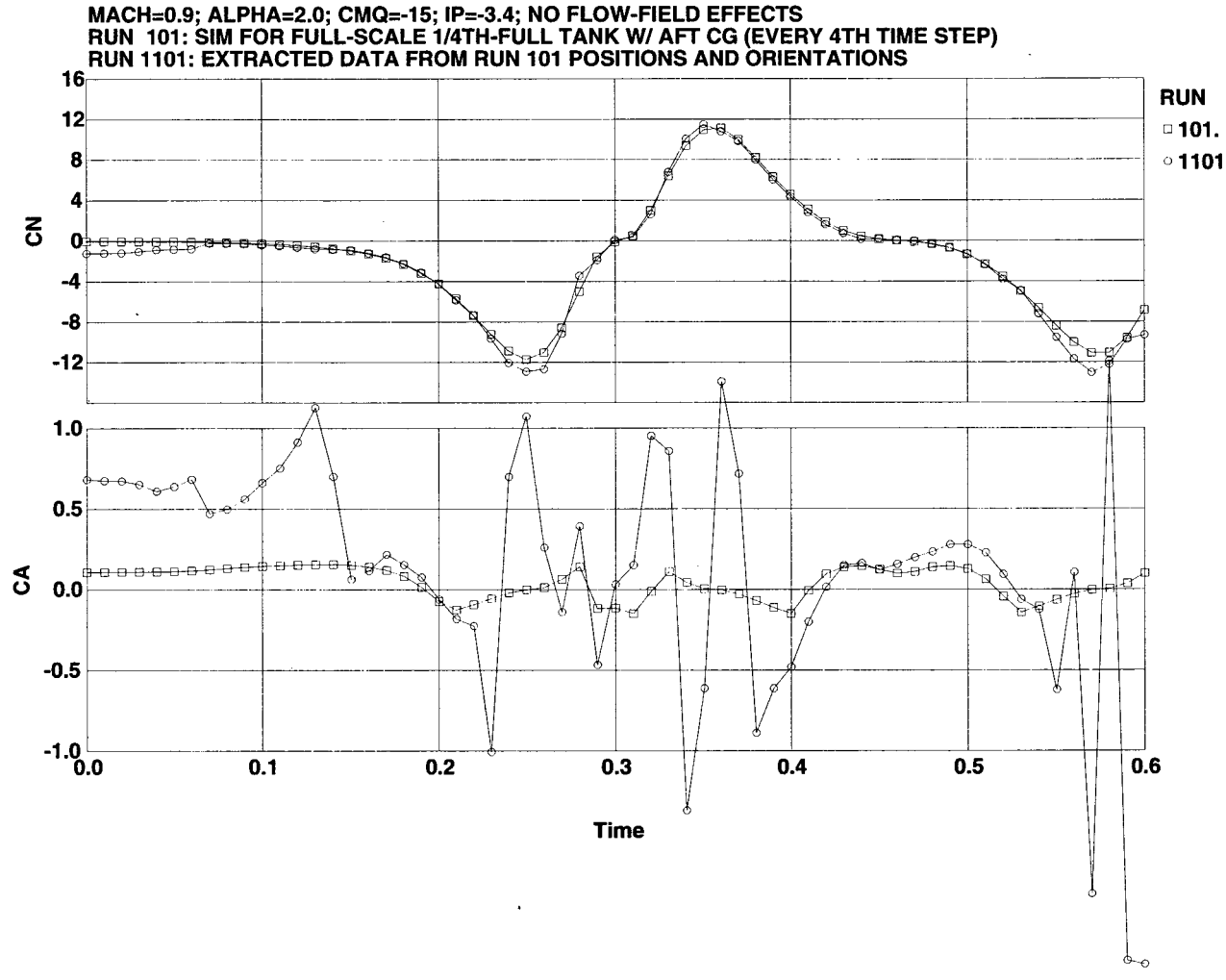

e. Normal and axial force coefficients
Figure 12. Continued.

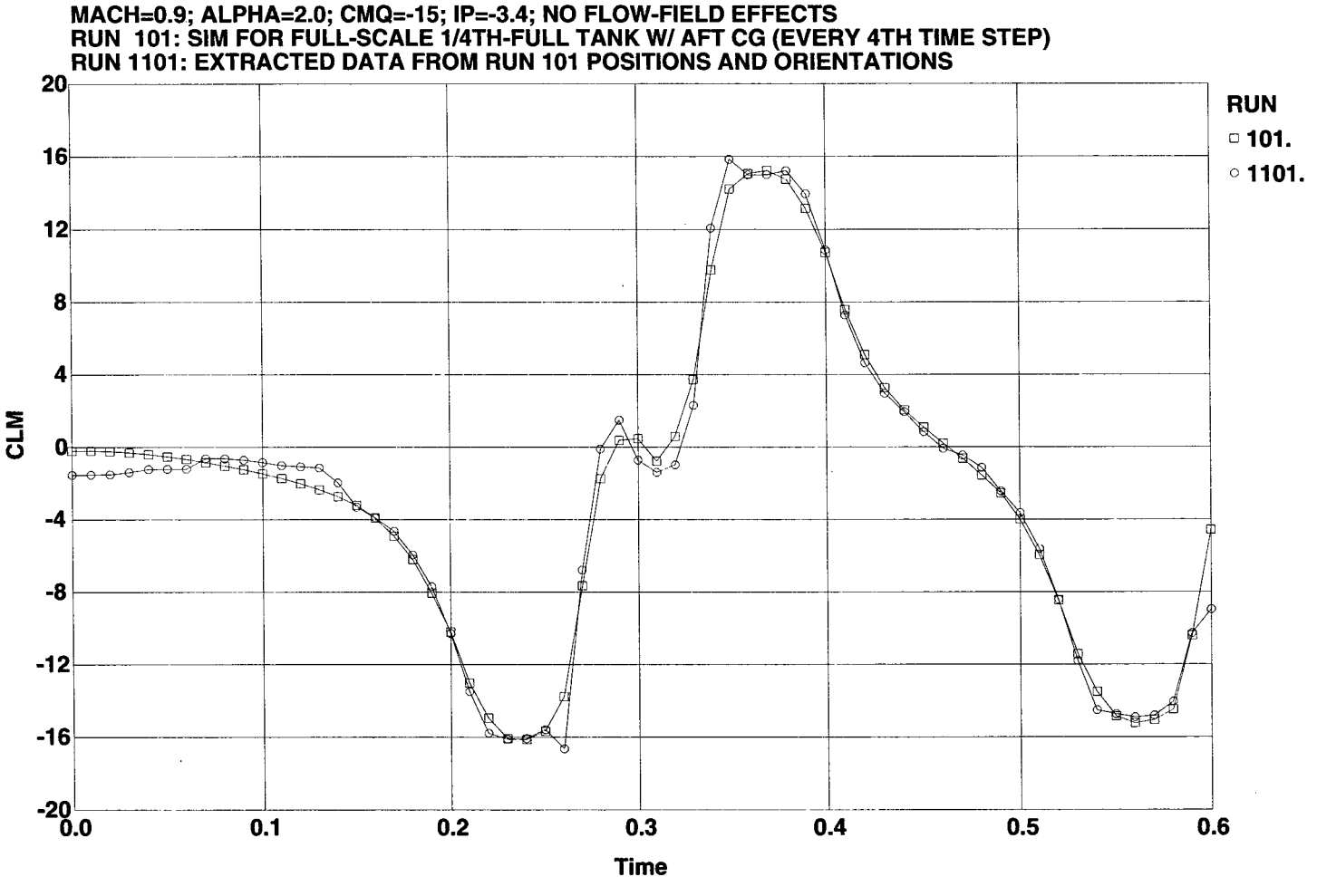

f. Pitching moment coefficient

Figure 12. Concluded.

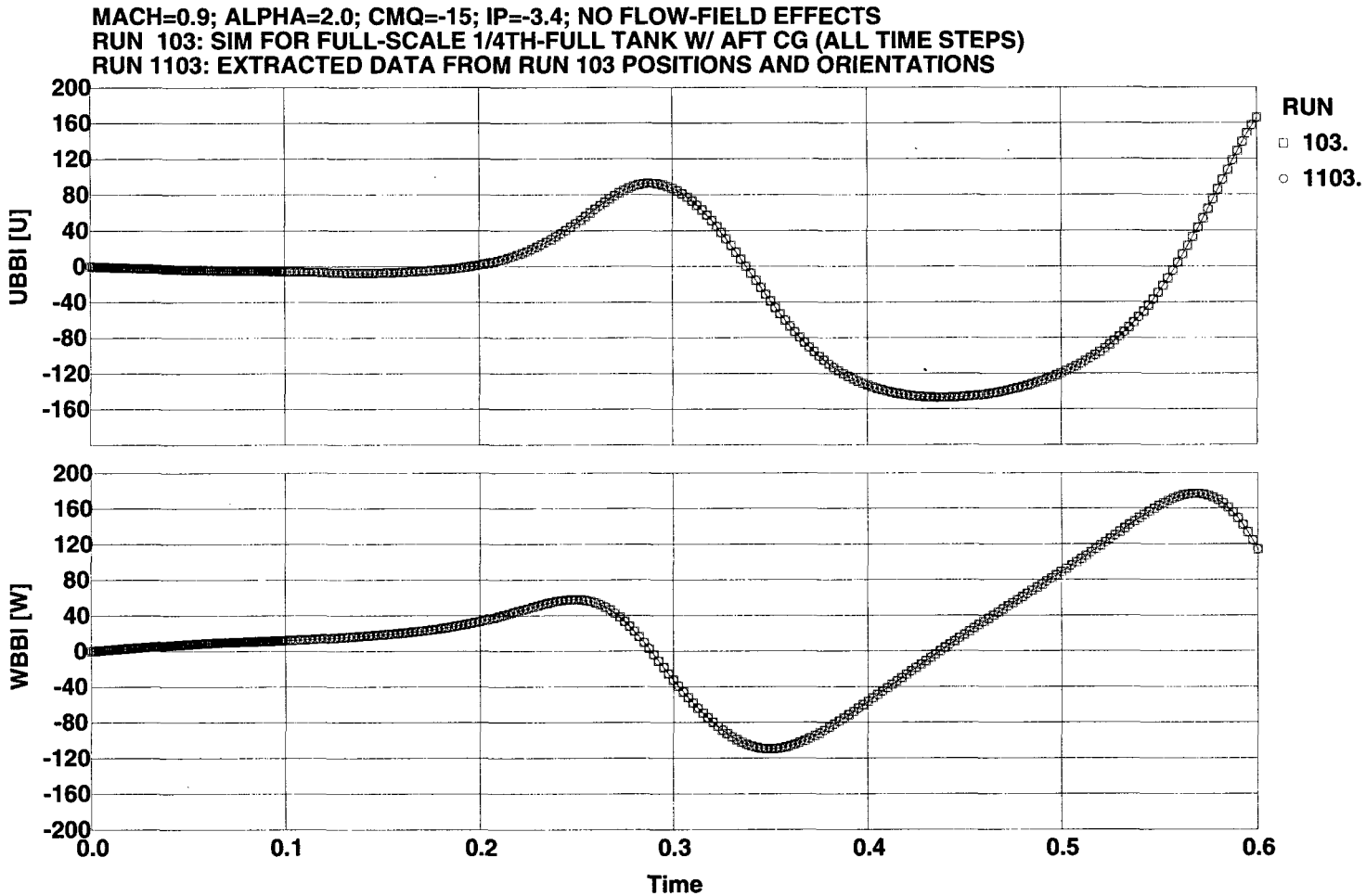

a. Axial and vertical linear velocities

Figure 13. Extracted information from full-scale simulation at finer time step.

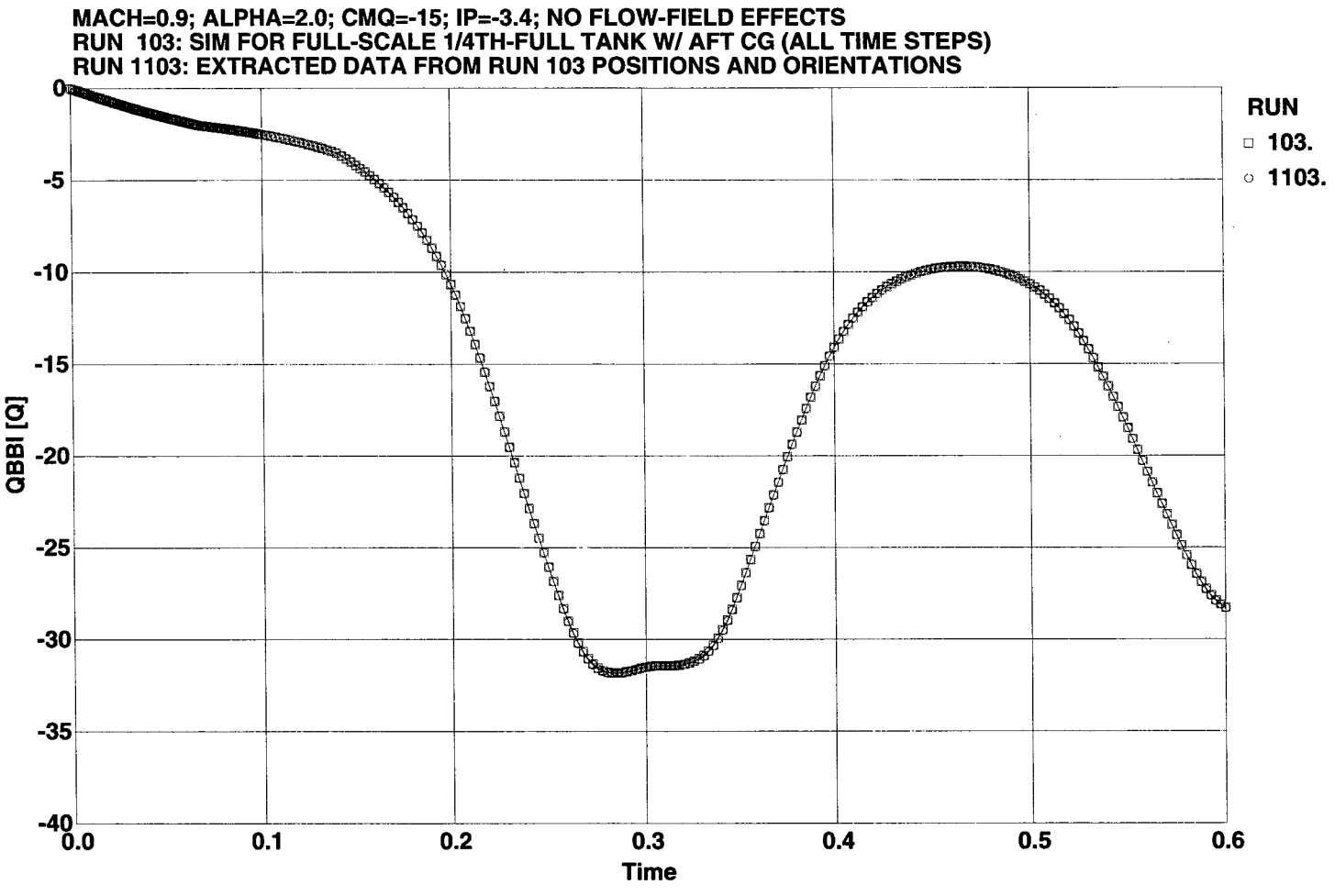

b. Pitch angular velocity
Figure 13. Continued.

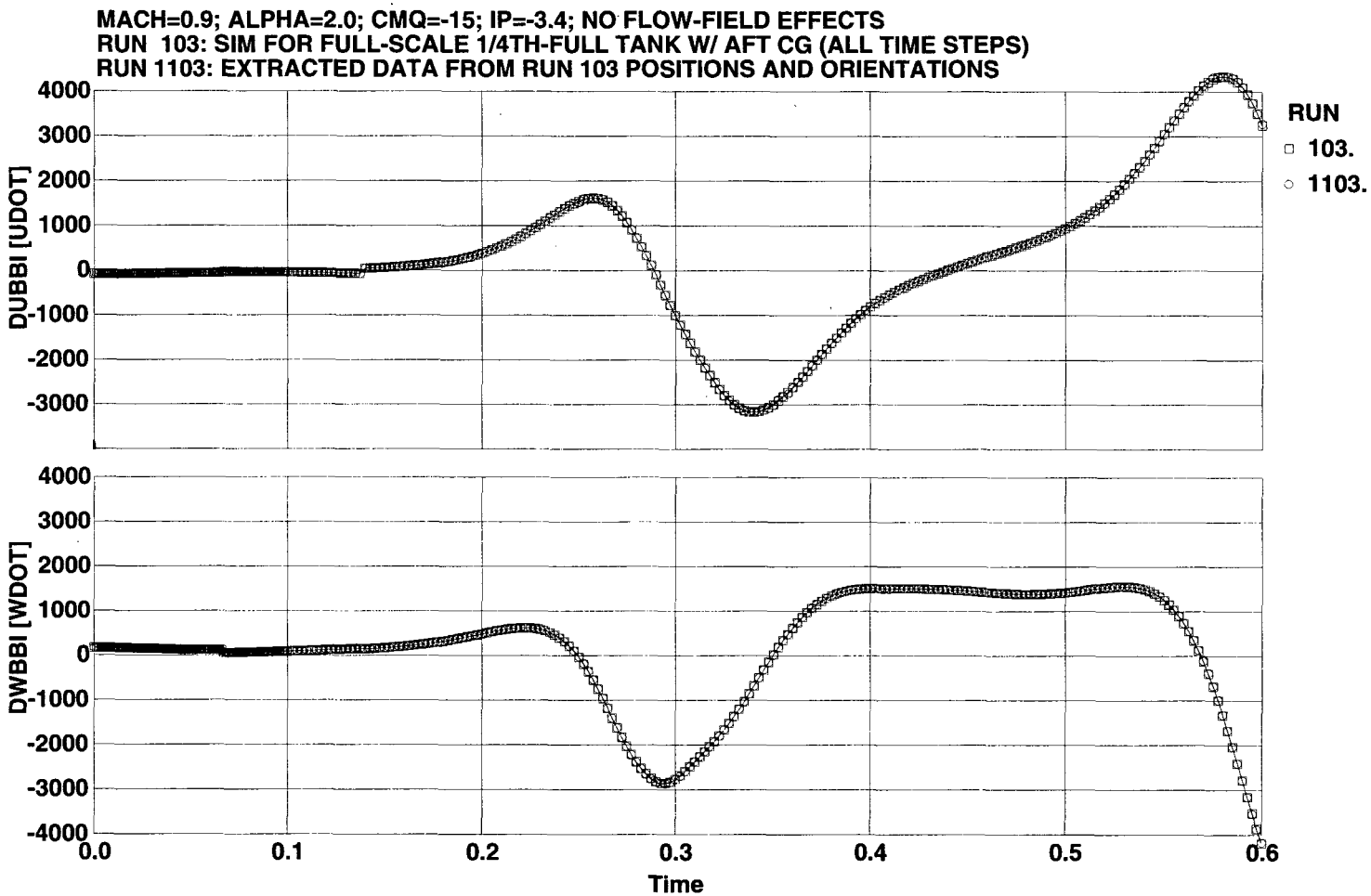

c. Axial and vertical linear velocity derivatives
Figure 13. Continued.

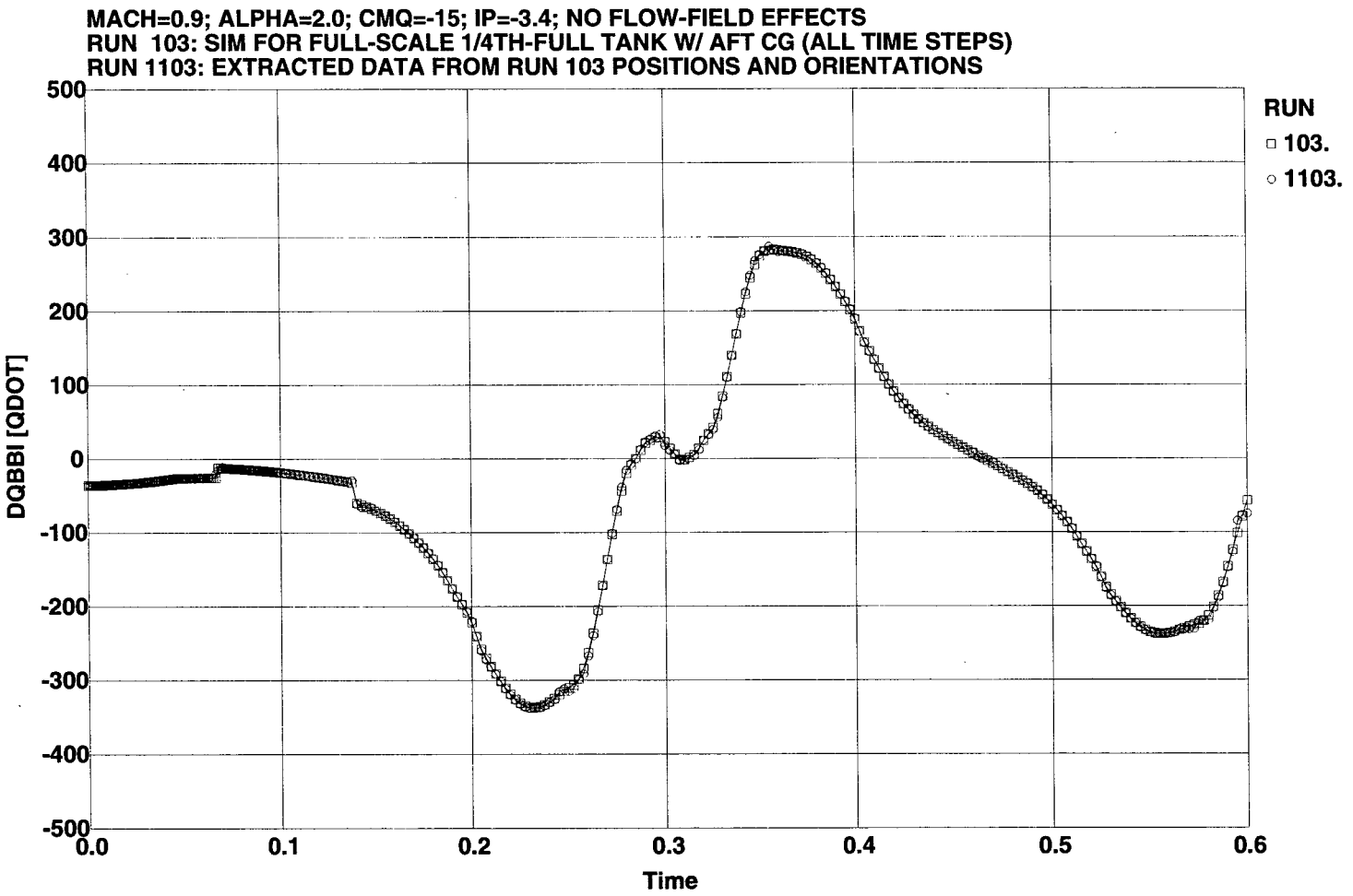

d. Pitch angular velocity derivative

Figure 13. Continued.

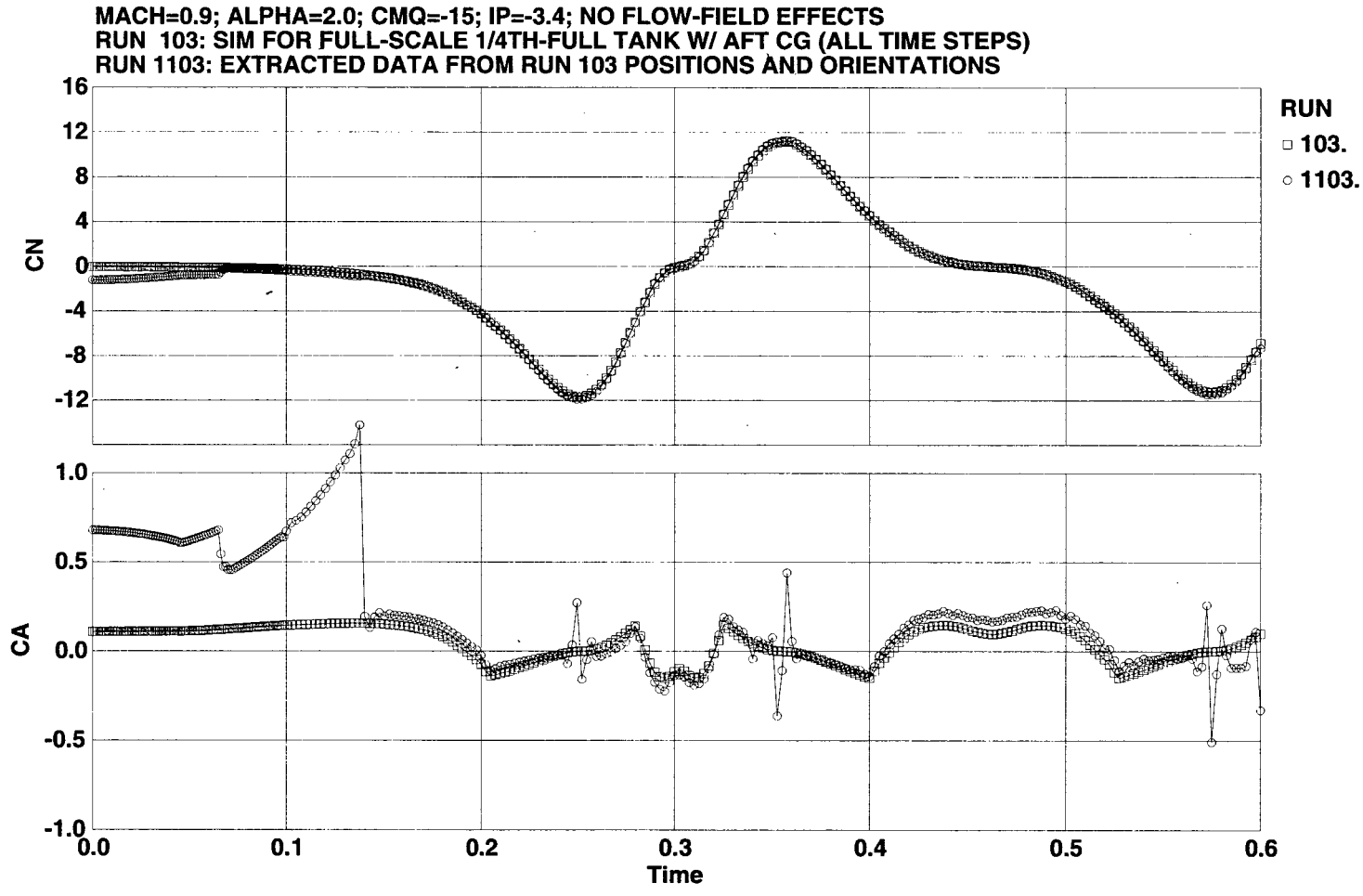

e. Normal and axial force coefficients
Figure 13. Continued.

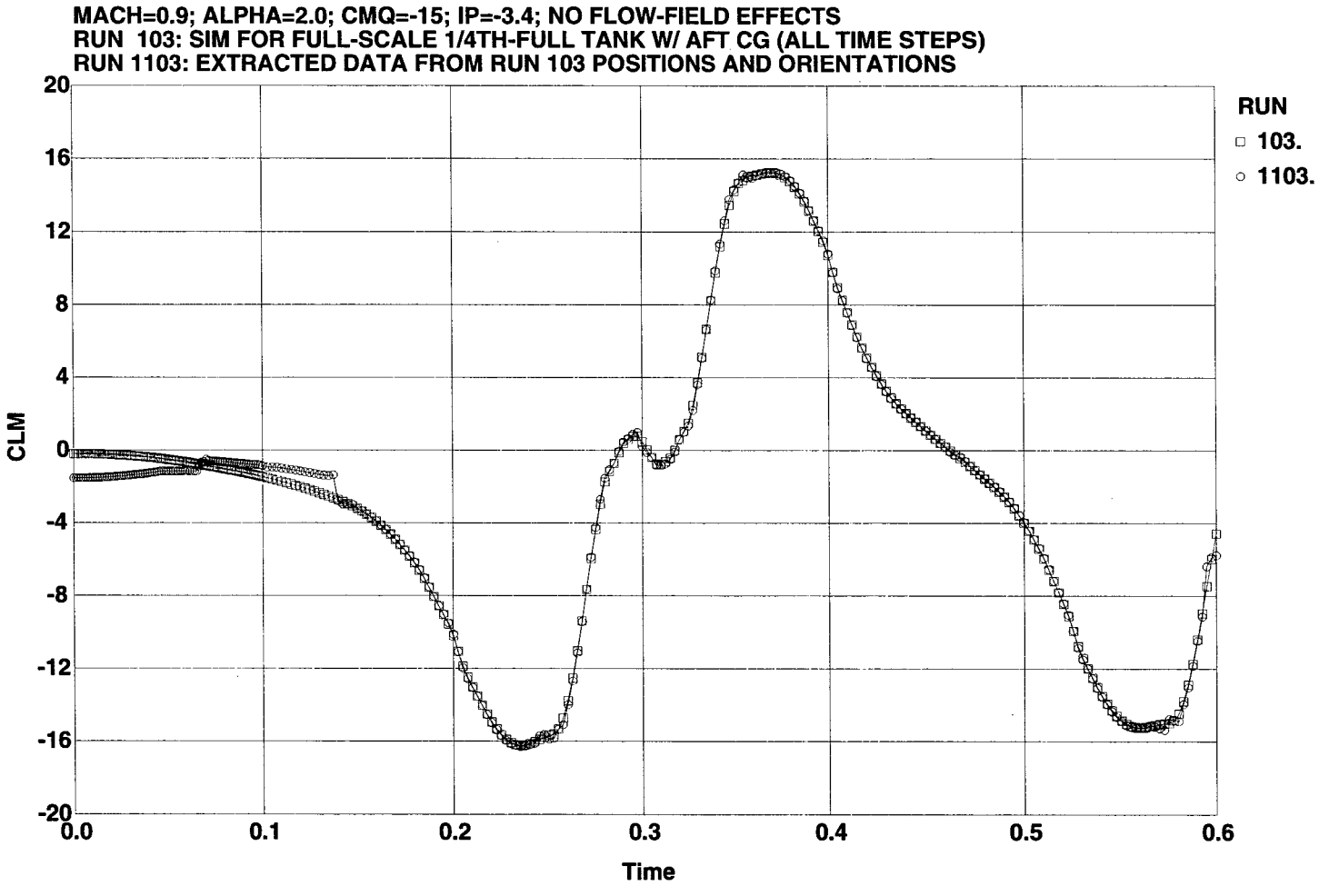

f. Pitching moment coefficient

Figure 13. Concluded.

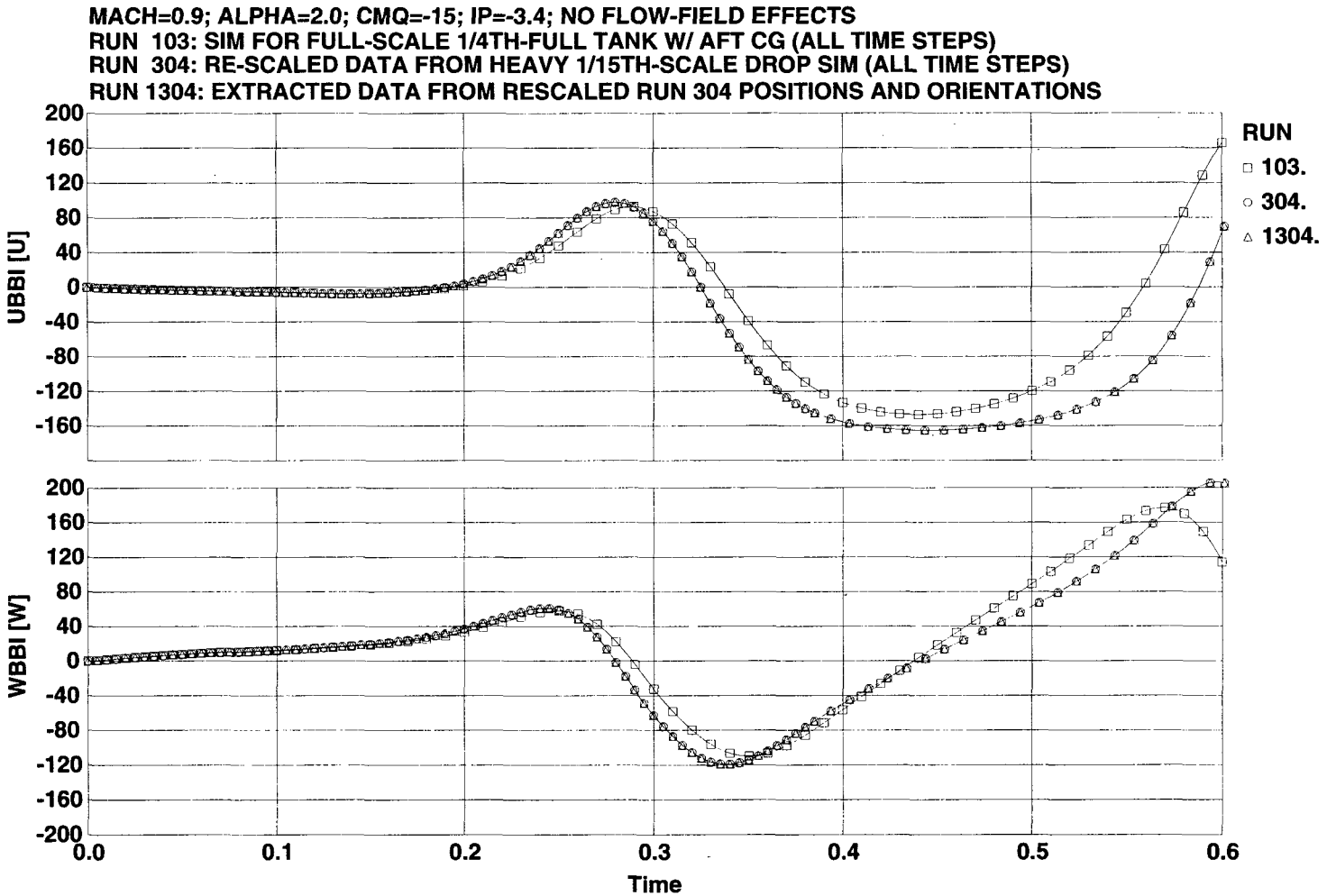

a. Axial and vertical linear velocities

Figure 14. Extracted information from re-scaled 1/15th-scale dynamic simulation.

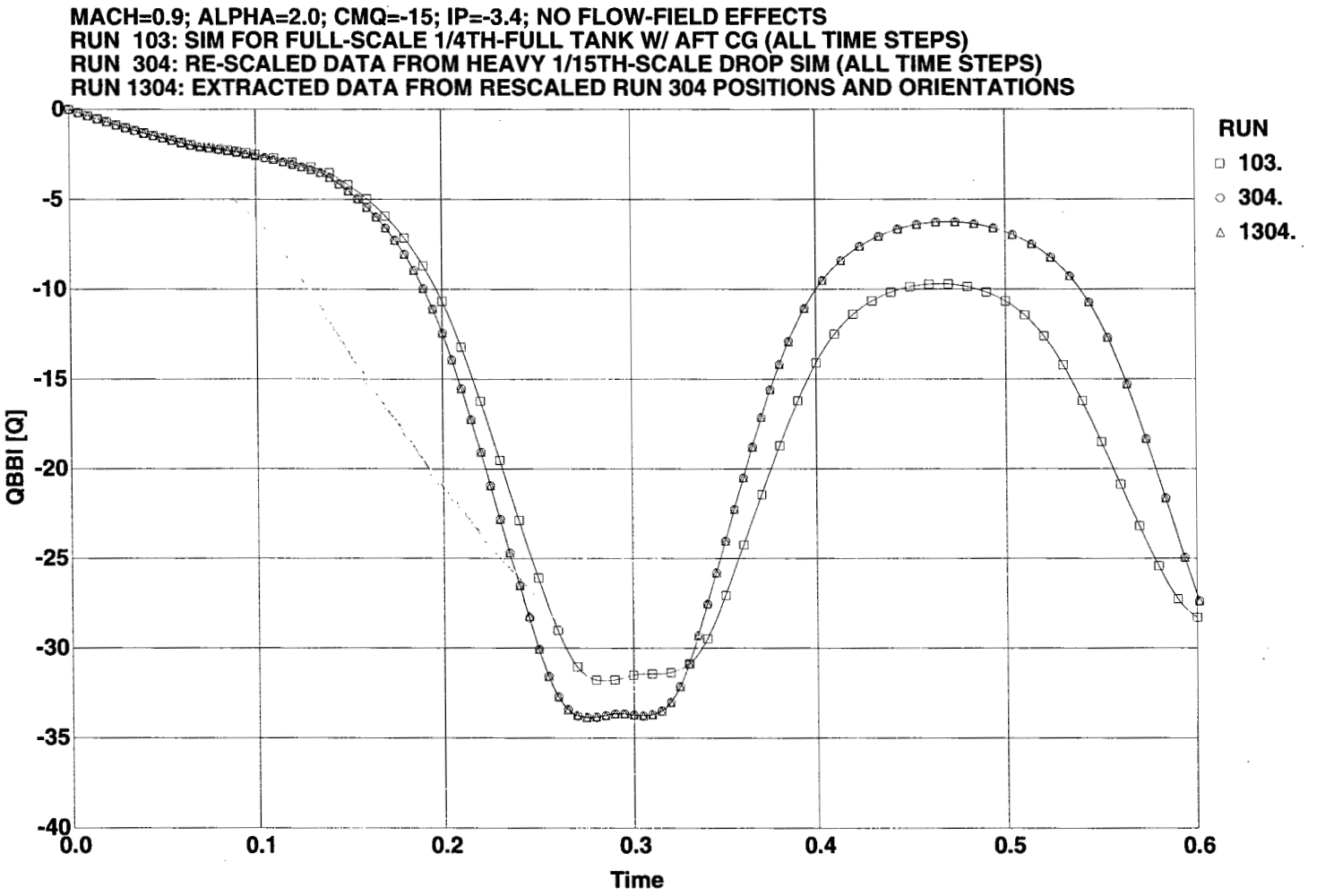

b. Pitch angular velocity

Figure 14. Continued.

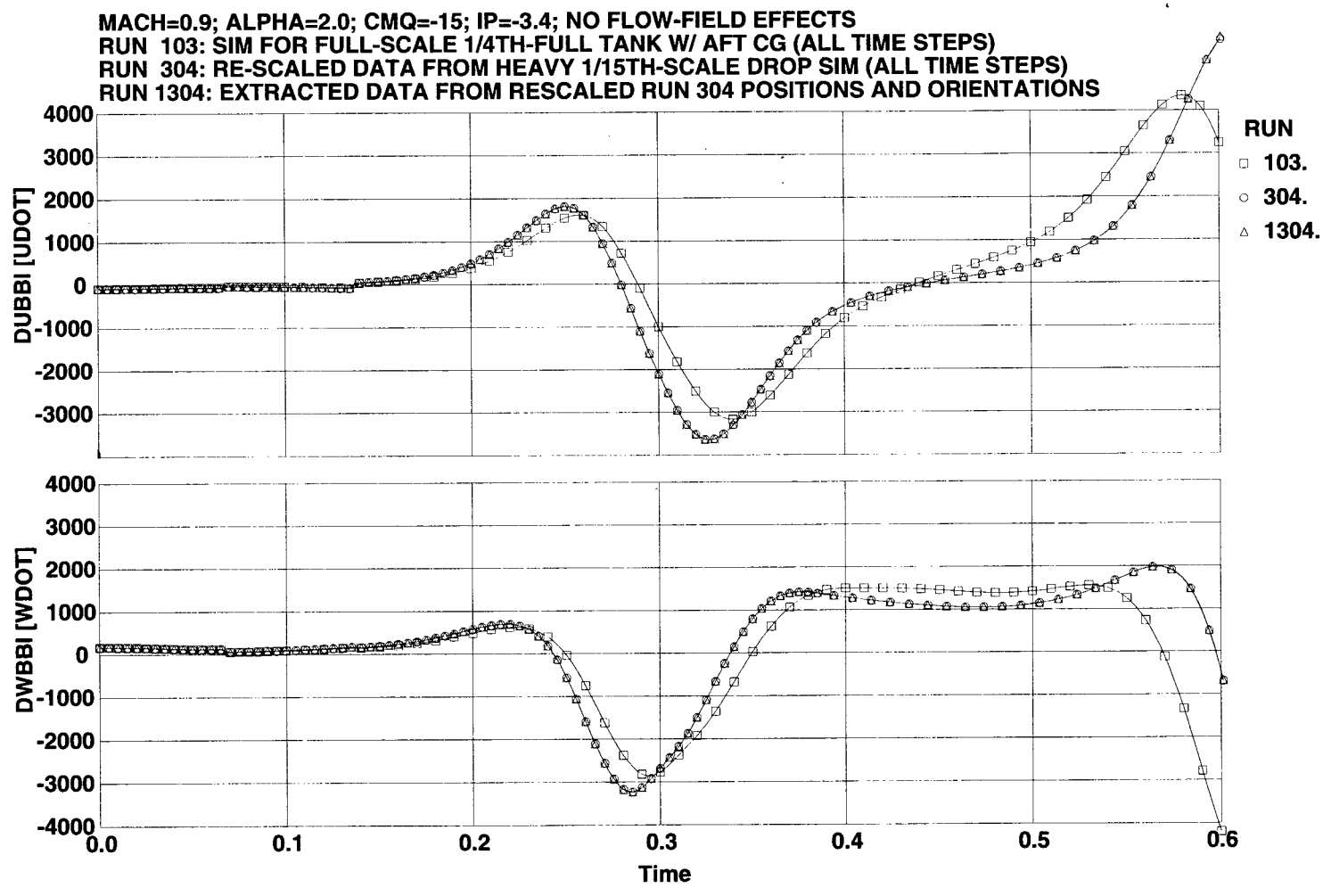

c. Axial and vertical linear velocity derivatives
Figure 14. Continued.

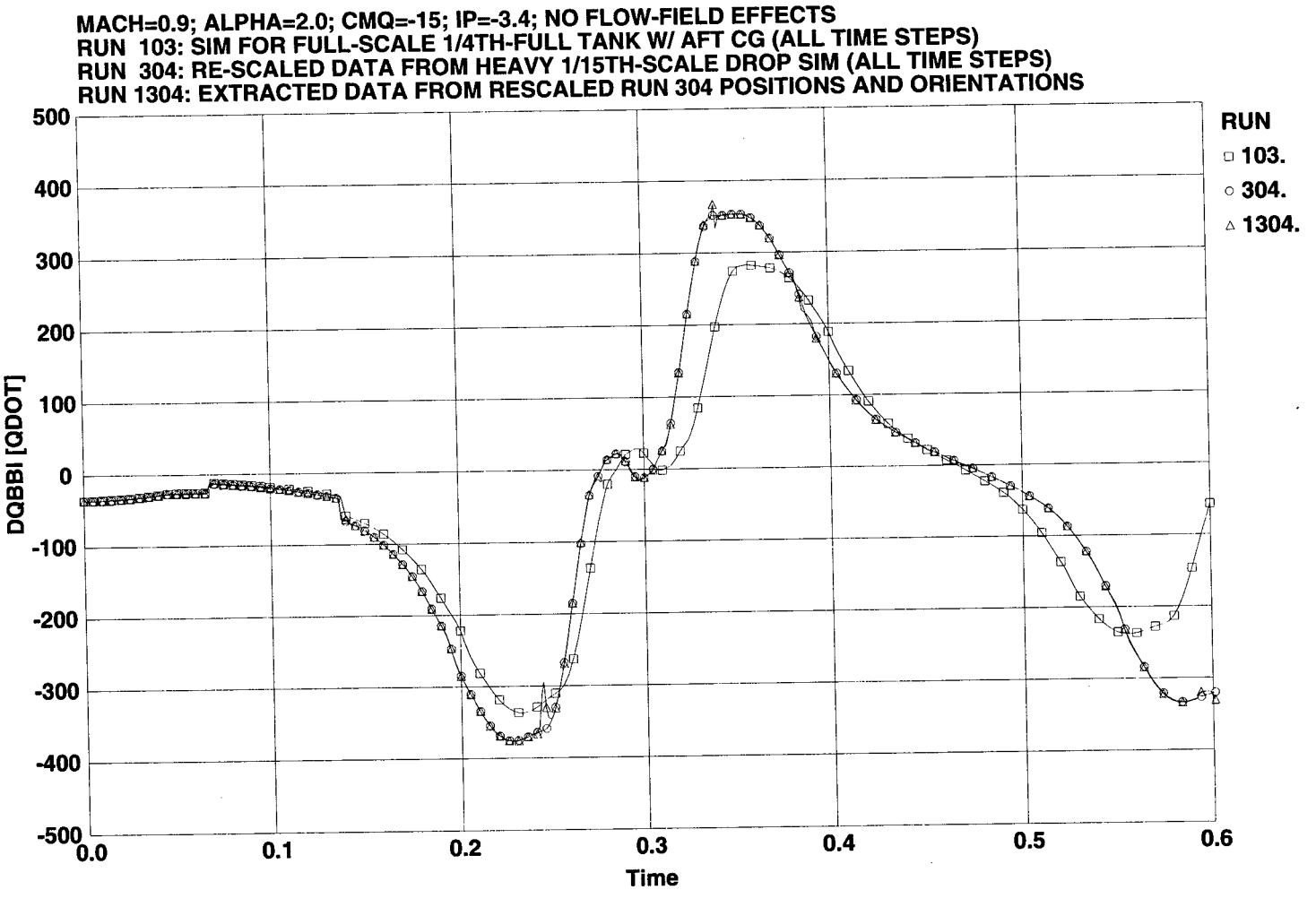

d. Pitch angular velocity derivative

Figure 14. Continued.

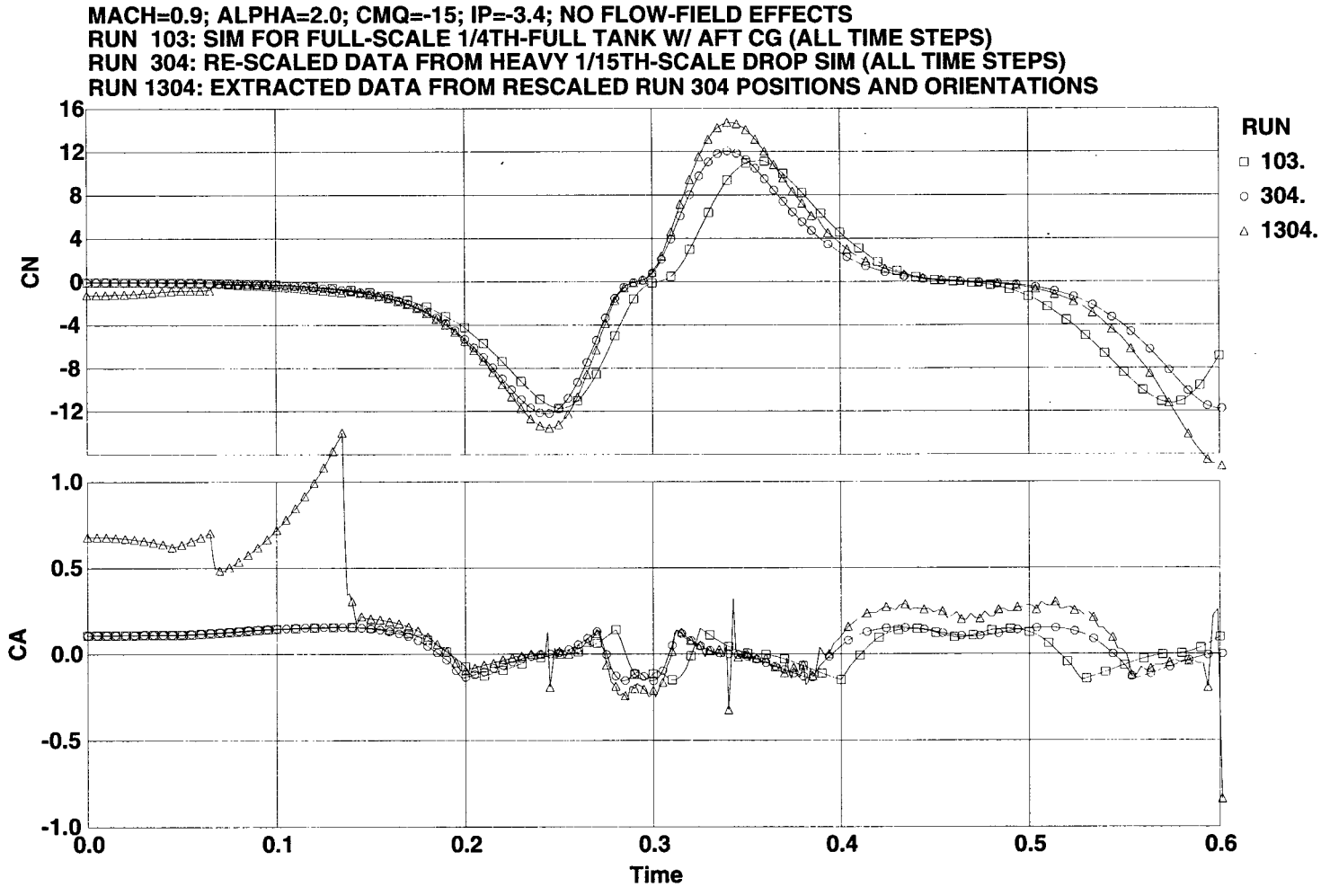

e. Normal and axial force coefficients

Figure 14. Continued.

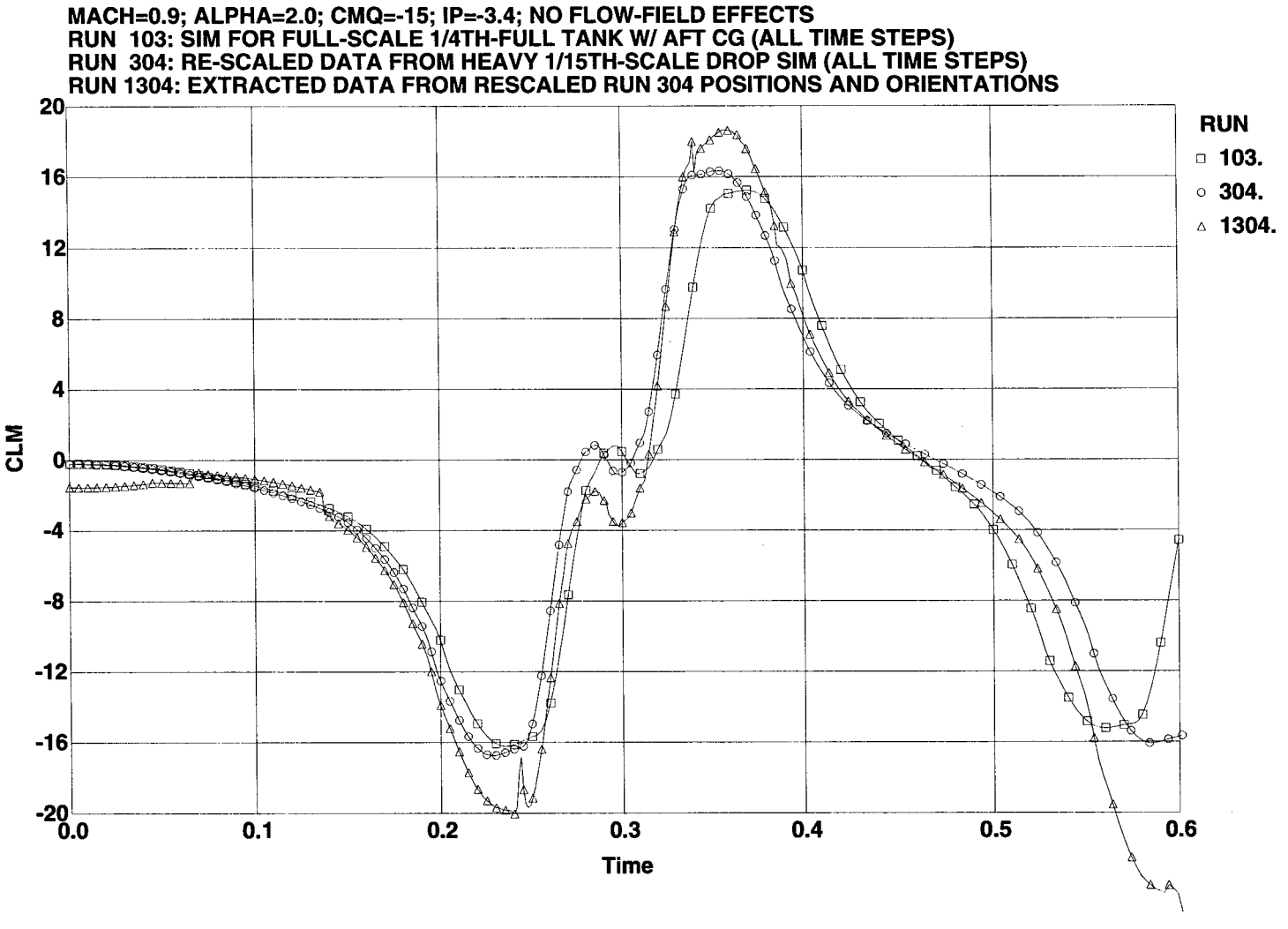

f. Pitching moment coefficient

Figure 14. Concluded.

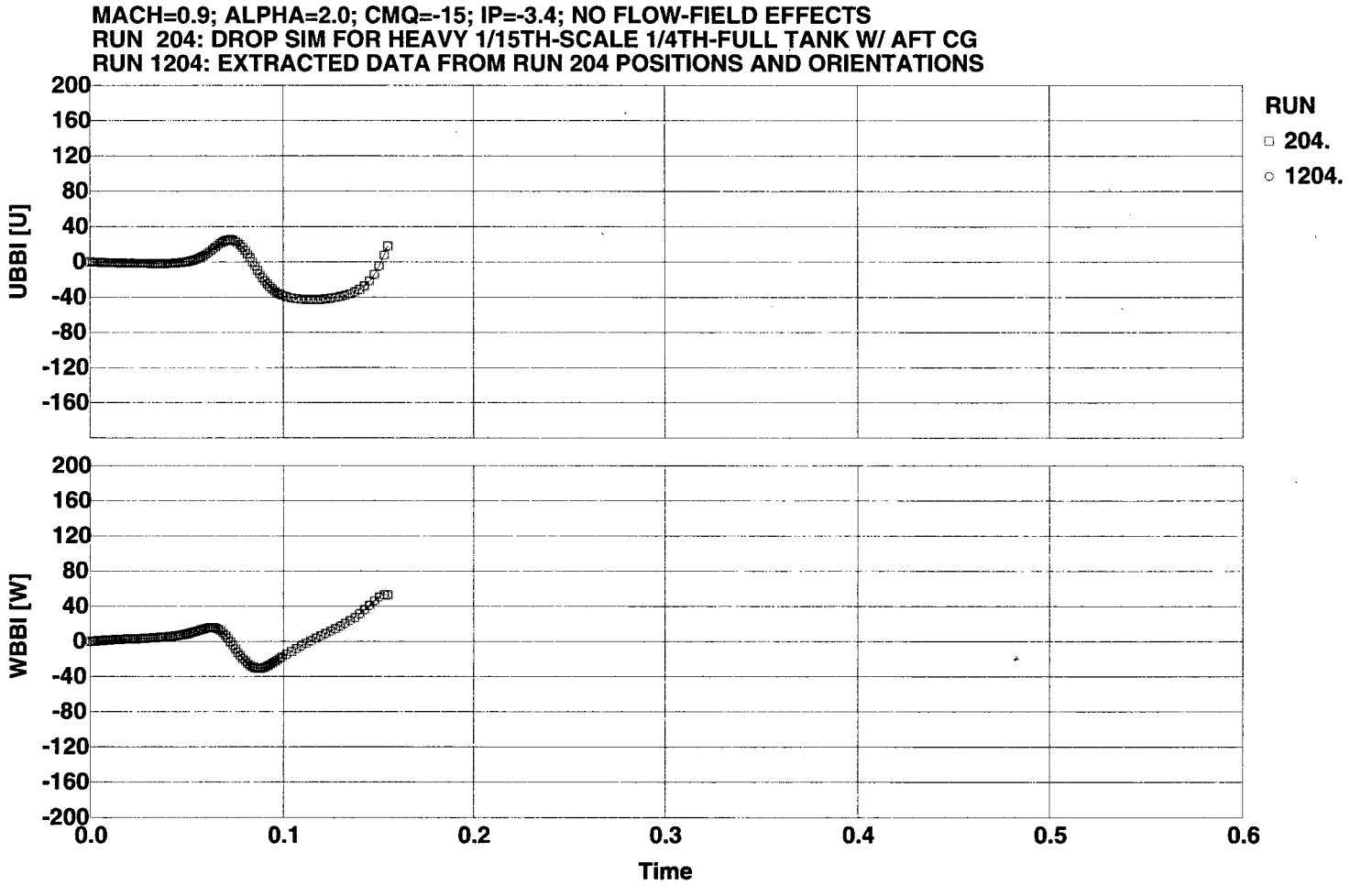

a. Axial and vertical linear velocities

Figure 15. Extracted information from 1/15th-scale dynamic simulation.

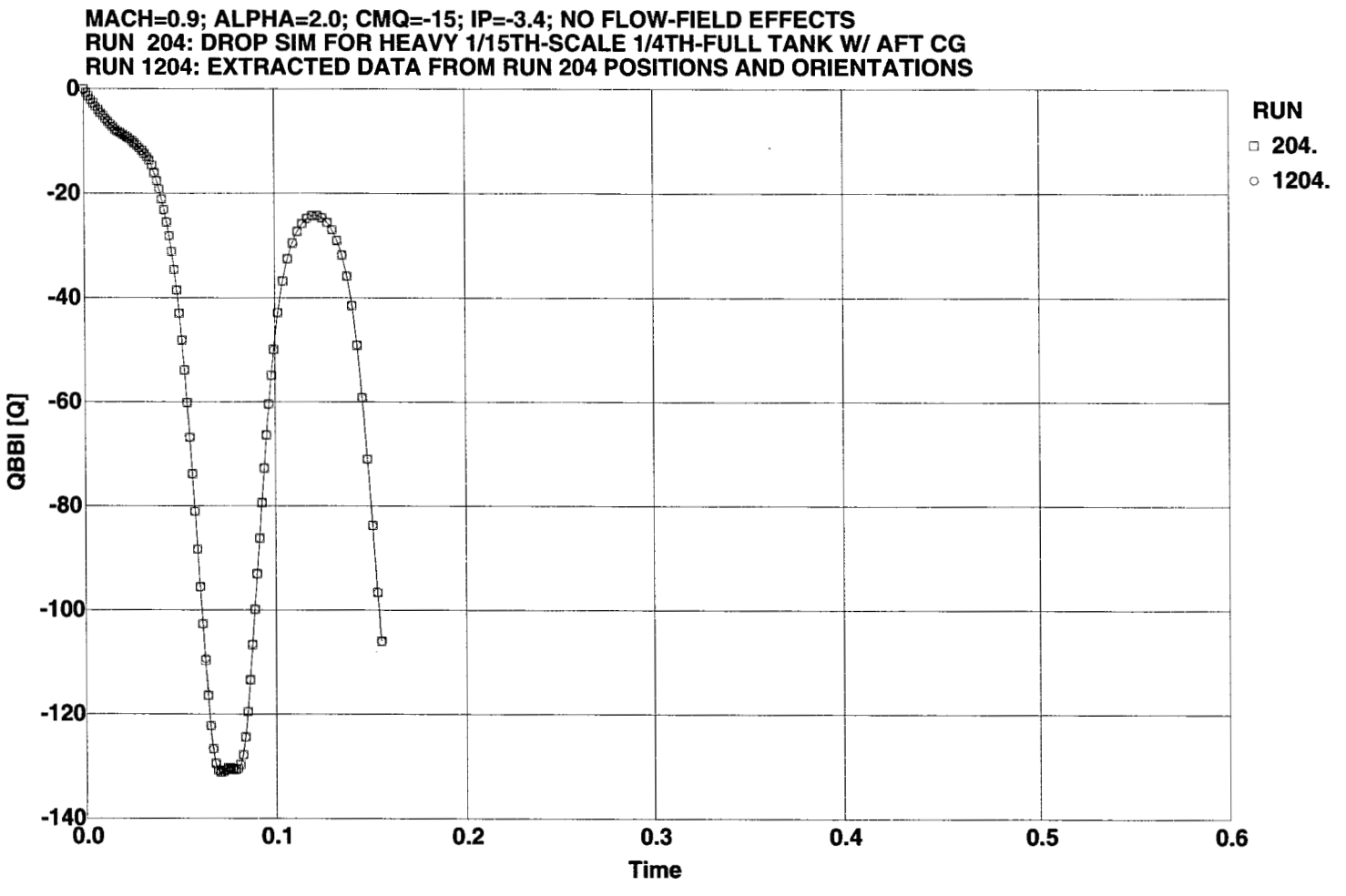

b. Pitch angular velocity

Figure 15. Continued.

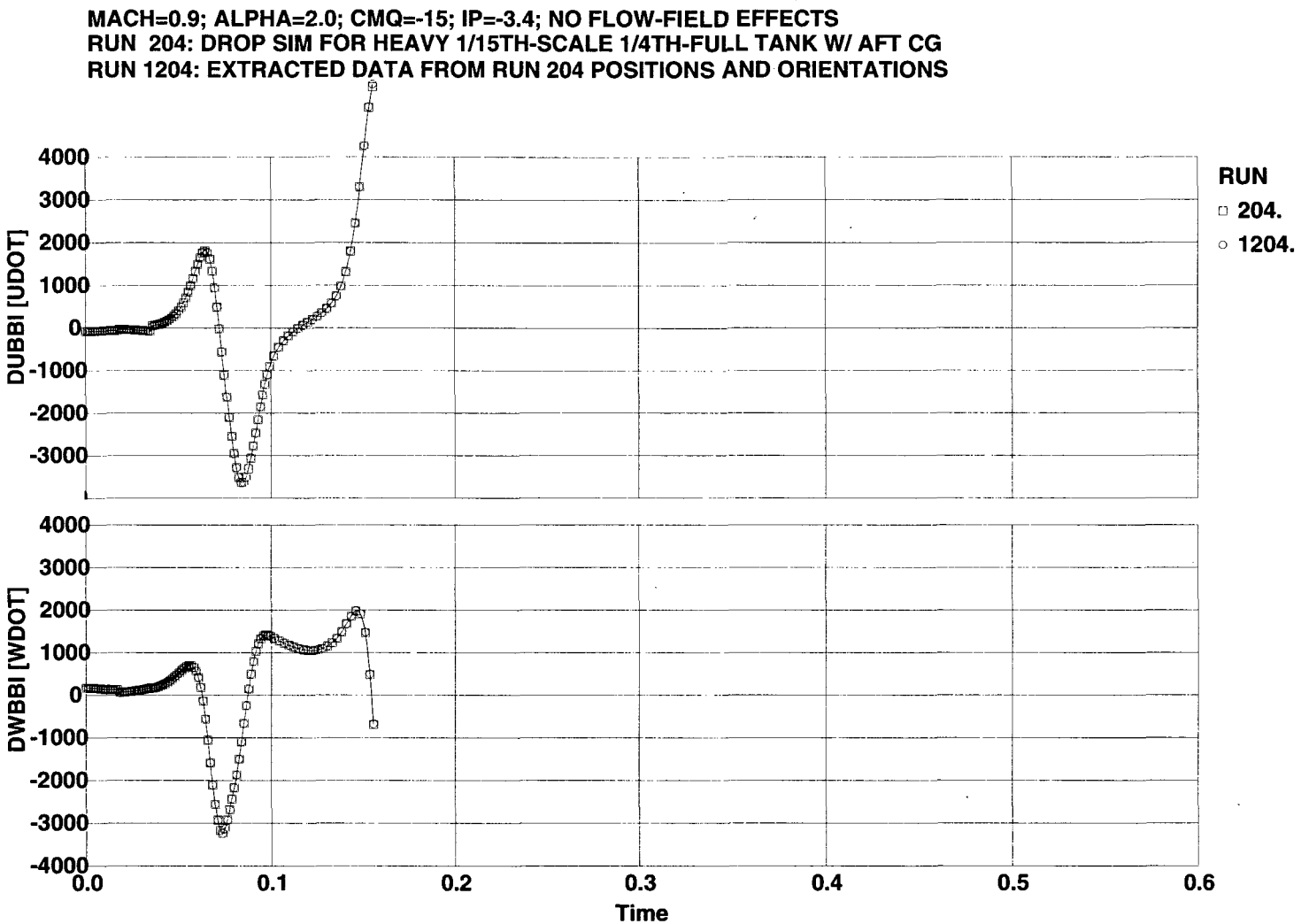

c. Axial and vertical linear velocity derivatives
Figure 15. Continued.

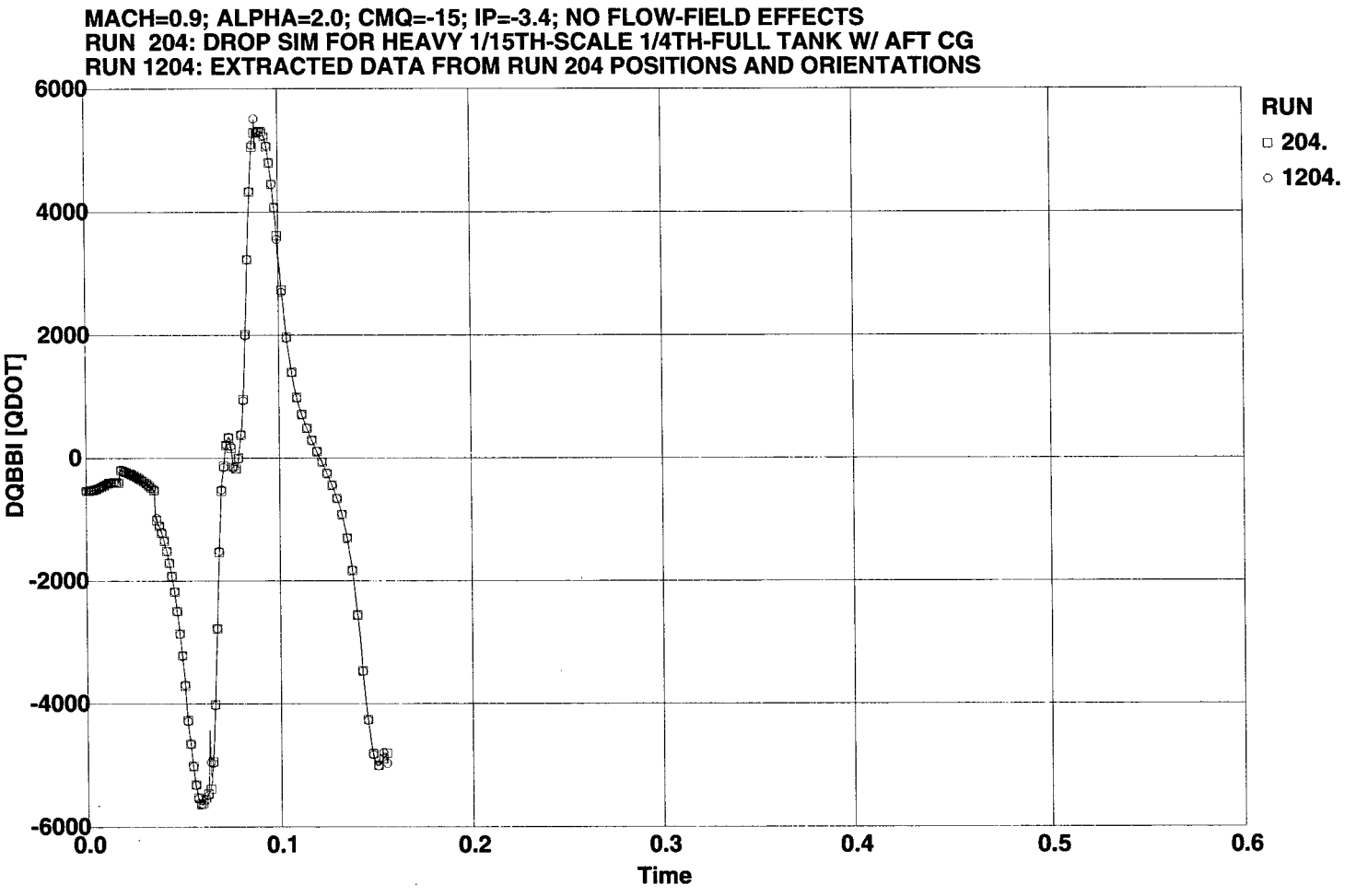

d. Pitch angular velocity derivative

Figure 15. Continued.

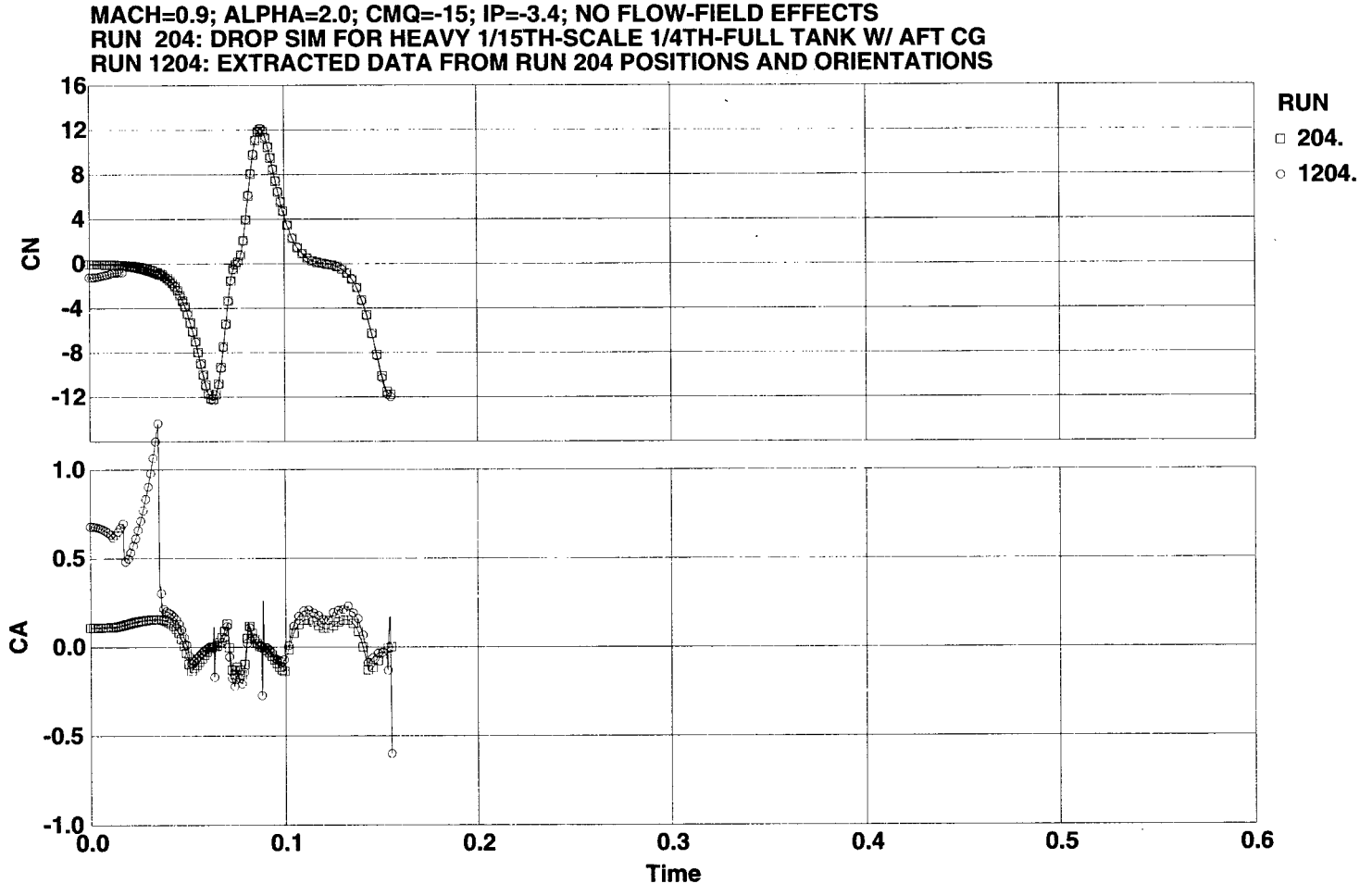

e. Normal and axial force coefficients

Figure 15. Continued.

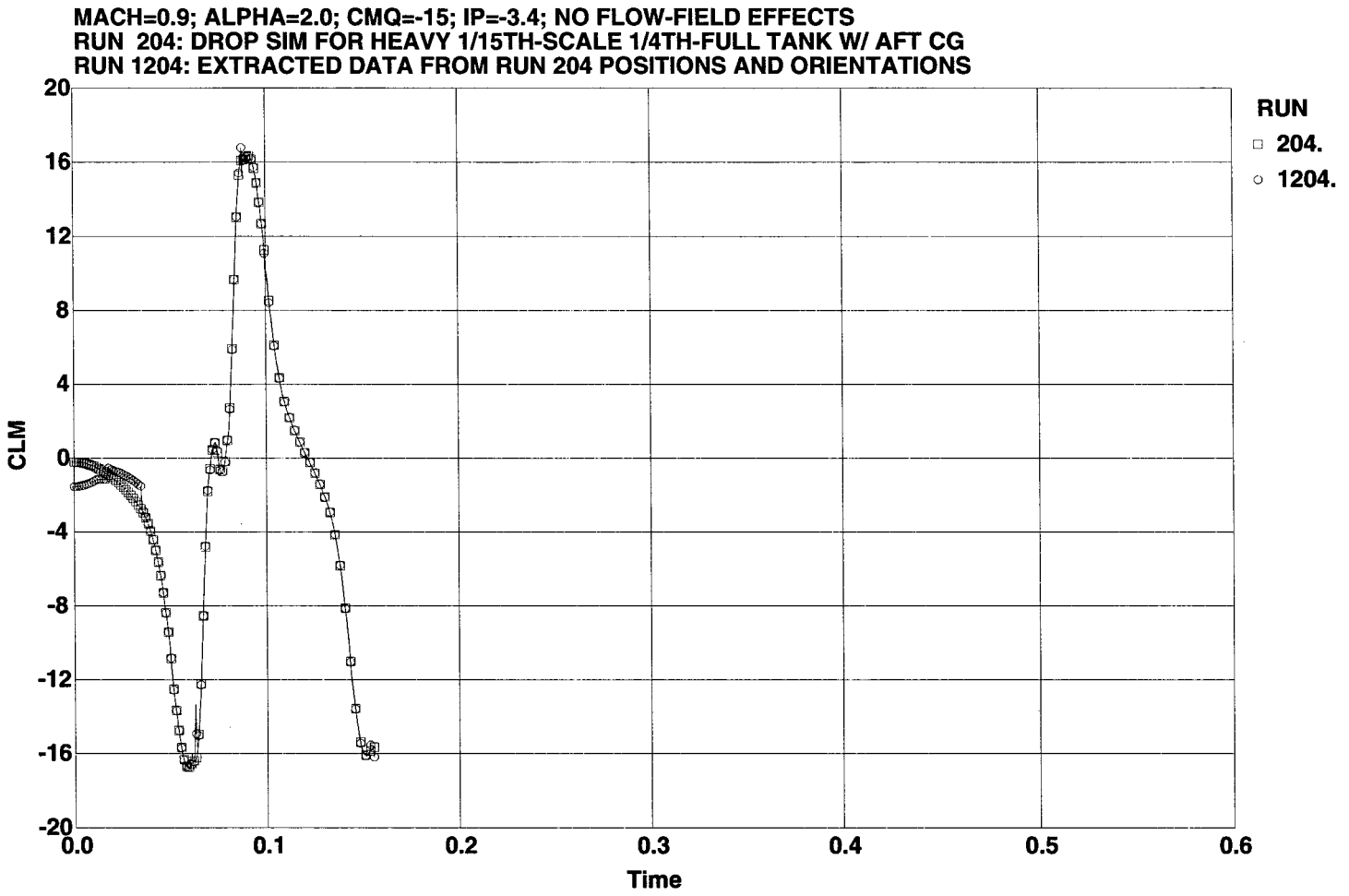

f. Pitching moment coefficient

Figure 15. Concluded.

Table 1. Simulation Mass and Inertial Properties

Run No.	Scale Factor	Integration Time Step, sec	Output Time Step, sec	S ft^2	XLL, XLM, XLN ft	WT, lb	XCG, ft	ZCG, ft	IYY slug-ft^2	Cmq .	Altitude, ft	XBBH [XO], ft	ZBBH [ZO], ft	XFE, ft	Ejector Stroke, ft
101	Full	0.00125	0.01	5.796	2.717	1611	14.458	-0.1	680	-15	5000	4.85	2.183	12.338	0.5
102	Full	0.00125	0.01	5.796	2.717	1611	14.458	-0.1	680	-150	5000	4.85	2.183	12.338	0.5
103	Full	0.00125	0.00125	5.796	2.717	1611	14.458	-0.1	680	-15	5000	4.85	2.183	12.338	0.5
104	Full	0.00125	0.00125	5.796	2.717	4311	11.083	-0.125	3100	-15	5000	8.225	2.158	12.338	0.5
201	0.0667	0.00032275	0.002582	0.02576	0.1811	7.16	0.9639	-0.0067	0.01343	-15	Function of Q'	0.3233	0.1455	0.8225	0.0333
202	0.0667	0.00032275	0.002582	0.02576	0.1811	2.148	0.9639	-0.0067	0.00403	-15	Function of Q'	0.3233	0.1455	0.8225	0.0333
203	0.0667	0.00032275	0.002582	0.02576	0.1811	2.148	0.9639	-0.0067	0.00403	-150	Function of Q'	0.3233	0.1455	0.8225	0.0333
204	0.0667	0.00032275	0.0003275	0.02576	0.1811	2.148	0.9639	-0.0067	0.00403	-15	Function of Q'	0.3233	0.1455	0.8225	0.0333
205	0.0667	0.00032275	0.0003275	0.02576	0.1811	2.148	0.9639	-0.0067	0.00403	-15	Function of Q'	0.3233	0.1455	0.8225	0.0333
206	0.0677	0.00032275	0.0003275	0.02576	0.1811	5.748	0.7389	-0.0083	0.01837	-15	Function of Q'	0.5483	0.1439	0.8225	0.0333

Run No.	Ejector Force First half-stroke, lb	Ejector Force Second half-stroke, lb	Q'inf/Qinf	T'inf/Tinf	Accelerometer Location	Notes
101	8700 - 1400 (stroke)	6250 - 4200 (stroke)	NA	NA	CG	Baseline, 1/4th-full Tank, Full scale
102	8700 - 1400 (stroke)	6250 - 4200 (stroke)	NA	NA	CG	Same as 101 but Cmq x 10
103	8700 - 1400 (stroke)	6250 - 4200 (stroke)	NA	NA	CG	Same as 101 but output every time step.
104	8700 - 1400 (stroke)	6250 - 4200 (stroke)	NA	NA	CG	Full Tank, Full Scale.
201	38.667 - 933.30 (stroke)	27.778 - 2800 (stroke)	1.0	1.0	CG	Same as 101 but for heavy-scaled model: T'inf/Tinf = 1. Q'inf/Qinf = 1.0
202	11.6 - 280 (stroke)	8.33 - 84 (stroke)	0.3	1.0	CG	Same as 101 but for heavy-scaled model: T'inf/Tinf = 1. Q'inf/Qinf = 0.3
203	11.6 - 280 (stroke)	8.33 - 84 (stroke)	0.3	1.0	CG	Same as 202 but Cmq x 10
204	11.6 - 280 (stroke)	8.33 - 84 (stroke)	0.3	1.0	CG	Same as 202 but output every time step.
205	11.6 - 280 (stroke)	8.33 - 84 (stroke)	0.3	1.0	NOSE	Same as 204 but accelerometers at nose instead of CG.
206	11.6 - 280 (stroke)	8.33 - 84 (stroke)	0.3	1.0	CG	Same as 104 but for heavy-scaled model: T'inf/Tinf = 1. Q'inf/Qinf = 0.3

301 - 306 are the same as 201 - 206, but are re-scaled to full scale using inverse scaling laws.

APPENDIX A

OVERVIEW OF DYNAMIC SCALING LAWS

The motion of a model freely dropped in a wind tunnel and an actual store released from an aircraft in flight will be dynamically similar provided two criteria are met. First, the aerodynamic forces and moments on the model store must directly scale to flight forces and moments. Second, the motion responses of the wind tunnel model to the applied forces and moments must be directly scalable to flight motion responses.

A-1.0 AERODYNAMIC FORCE AND MOMENT SCALING

Scaling of forces and moments on a wind tunnel model to the full-scale flight vehicle (the first criteron) is a fundamental requirement of any kind of wind tunnel testing. Aerodynamic scaling is accomplished by exactly reducing the linear dimensions of both the store and the parent aircraft by a constant scale factor (Λ), by exactly matching the angular orientations of the flight store relative to the flow, and by reducing the forces and moments to non-dimensional coefficient form based on the flow dynamic pressure (a measure of the energy available in the flow defined by $Q_\infty = 1/2\rho_\infty V_\infty^2$) and appropriate reference areas and lengths. Force and moment scaling laws take the following forms (using normal force and pitching moment as examples):

$$C_N = -FZB_{AERO}'/(Q_\infty'*S') = -FZB_{AERO}/(Q_\infty*S) \tag{A-1}$$

and

$$C_m = MYB_{AERO}'/(Q_\infty'*S'* XLM') = MYB_{AERO}/(Q_\infty*S* XLM) \tag{A-2}$$

where the primed quantities denote model parameters at wind tunnel conditions. Different reference lengths may be used for pitch-plane or yaw/roll plane moments although for most stores the maximum body diameter and cross-sectional area are usually used.

Force/moment scaling via reduction to coefficients as in Eqs. (A-1) and (A-2) can be accomplished under the condition that flow similarity must be maintained between the tunnel flow and flight flow. Such flow similarity exists when compressibility effects and viscous fluid effects of the wind tunnel and flight flow are identical. Compressibility is quantified by the Mach number, which is defined as the ratio of the free-stream velocity of the flow to the speed of sound in the flow ($M_\infty = V_\infty/a_\infty$). Viscous effects are quantified by the Reynolds number, a ratio of flow density, velocity, coefficient of viscosity, and a reference length ($Re_\infty = l\, V_\infty\rho_\infty/\mu_\infty$). As long as the Mach number and Reynolds number of the flight condition are reproduced in the tunnel, the aerodynamic coefficients of the model will reproduce the flight coefficients if both are placed at the same orientation relative to the flow. In actual practice, however, it is extremely difficult to exactly reproduce flight Reynolds numbers in a wind tunnel while maintaining the Mach number and, therefore, flight Reynolds numbers are not exactly matched in most wind tunnels. (Strict enforcement of the Reynolds number requirement is typically only accomplished in facilities using cryogenic fluids instead of air to simulate the flow.) Fortunately, store aerodynamic proper-

ties are not nearly as dependent on Reynolds number as on Mach number, and some relaxation of the Reynolds number criterion is generally acceptable. In summary, aerodynamic force and moment scaling by dynamic pressure and physical reference length ratios is possible if the following conditions are met:

linear dimensions:	(model coords)' = Λ * (full-scale coords)	(A-3)
orientation relative to flow:	$\alpha_S' = \alpha_S$	
Mach number:	$M_\infty' = M_\infty$	
Reynolds number:	$Re_\infty' = Re_\infty$	

with the caveat that the last condition can only be strictly enforced in specialized wind tunnel facilities.

A-2.0 DYNAMIC MOTION SCALING

The second criterion for dynamic scaling is that the motion of the store model be directly scalable to the flight motion. This implies that the flight positions and angles scale so that the store model separation path emulates the flight separation:

$$X'=X*\Lambda \quad (A\text{-}4)$$
$$Y'=Y*\Lambda$$
$$Z'=Z*\Lambda$$
$$\theta'=\theta$$
$$\Psi'=\Psi$$
$$\phi'=\phi$$

Two approaches may be used to derive the appropriate scaling laws. One commonly used approach is based on the principles of dimensional analysis (Refs. A-1 and A-2). A second and somewhat more rigorous method for deriving the scaling laws (Ref. A-3) involves studying the equations of motion of the separating store. Using this second approach, a clearer understanding of certain aspects of dynamic scaling can be obtained based on studying the motion as a whole. The basic scaling laws arise in the second approach from an examination of the store equations of motion at drop and full scales to determine dynamic simulation relationships between model and full-scale parameters which will satisfy Eq. (A-4). Examining the motions for two simple test cases allows the derivation of the complete scaling laws. The full derivations are presented in the following sections.

A-2.1 ONE-DEGREE-OF-FREEDOM DERIVATION CASE

The first test case for deriving dynamic scaling laws is the classical "drop-a-cannonball-in-a-vacuum" case which is used to derive the basic scaling law for time and which can also be used to illustrate a fundamental contradiction in scaling law development. For this first test case, only gravitational acceleration acts on the store. The position equation-of-motion for vertical fall in a gravity-oriented coordinate system is then:

$$Z = 1/2*g*t^2 \tag{A-5}$$

so that the scaled vertical position equation from Eq. (A-4) becomes:

$$Z' = Z*\Lambda = 1/2*g'*t'^2 = 1/2*g*t^2*\Lambda \tag{A-6}$$

Solving for t', the scaling relationship for time is obtained:

$$t' = t*\sqrt{((g/g')*\Lambda)} \tag{A-7}$$

This very important relationship indicates that events that occur in certain time intervals in flight will occur in greatly compressed time spans in a scaled drop test. The time compression can have significant implications on the data rates necessary for both camera and onboard instrumentation for sub-scale drop tests, as outlined in Section 3.3 of the main body of the report.

An examination of the velocity relations from the "cannonball-in-a-vacuum" derivation for a more realistic situation where the vacuum is replaced by air serves to illustrate a major contradiction in the development of dynamic motion scaling laws. The vertical velocity equation-of-motion of the cannonball (ignoring air friction) is given by:

$$\dot{Z} = g*t \tag{A-8}$$

so that:

$$g*t/\dot{Z} = g'*t'/\dot{Z}' \tag{A-9}$$

or by substituting Eq. (A-7) and solving for $\dot{Z}'$:

$$\dot{Z}' = \dot{Z}*\sqrt{(\Lambda*(g'/g))} \tag{A-10}$$

Assuming (for derivation purposes only) that it is possible to actually drop a cannonball in air without generating aerodynamic loads to resist the gravitational acceleration, $\dot{Z}'$ represents the total free-stream fall velocity for the model-scale cannonball, V_∞'. The free-stream velocity scaling law is then:

$$V_\infty' = V_\infty * \sqrt{(\Lambda*(g'/g))} \tag{A-11}$$

A Mach number for the falling cannonball can be defined as:

$$M_\infty = V_\infty/a_\infty \tag{A-12}$$

where the speed of sound, a_∞, is defined in fluid dynamics as:

$$a_\infty = \sqrt{(\gamma*R*T_\infty)} \tag{A-13}$$

with R representing a universal gas constant, γ the ratio of the specific heats of air, and T_∞ the static free-stream temperature of the air.

Combining Eqs. (A-11), (A-12), and (A-13), the dynamic motion scaling ratio for Mach number becomes:

$$M_\infty' = M_\infty * \sqrt{\Lambda*(g'/g)*((T_\infty)/(T_\infty'))} \tag{A-14}$$

which is in direct contradiction of the requirement identified in Eq. (A-3) that $M_\infty' = M_\infty$ for proper force and moment scaling. This major inconsistency means that it is not possible to simultaneously satisfy aerodynamic scaling and motion scaling. Compromise scaling laws have, therefore, been developed which satisfy certain aspects of scaling at the expense of certain other aspects. The compromise methods will be discussed in Section A-3.

A-2. 2 THREE-DEGREE-OF-FREEDOM DERIVATION CASE

The second test case for derivation of the motion scaling laws is for simple planar motion in the pitch plane. The three-degree-of-freedom (3-DOF) equations of motion are posed in a gravity-oriented coordinate system with origin at the store center-of-gravity at its release position as shown in Fig. A-1. The 3-DOF equations are:

$$m\ddot{X} = -[C_A \cos\theta + C_N \sin\theta]\, Q_\infty S + F_{EZ} \sin\theta \tag{A–15}$$

$$m\ddot{Z} = -[C_N \cos\theta - C_A \sin\theta]\, Q_\infty S + F_{EZ} \cos\theta + WT \tag{A-16}$$

$$I_{YY}\ddot{\theta} = [C_m + C_{mq}\,(XLM\ \dot{\theta}/2V_\infty)]\, Q_\infty S\ XLM + M_{EY} \tag{A-17}$$

For small angular motions, the aerodynamic terms can be expanded in Taylor series form as:

$$C_N = C_{N\alpha}\,(\theta + \dot{Z}/V_\infty) + \Delta C_N \tag{A-18}$$

$$C_m = C_{m\alpha}\,(\theta + \dot{Z}/V_\infty) + \Delta C_m \tag{A-19}$$

where θ represents the geometric angle of the store, ΔC_N and ΔC_m represent the incremental loading effects attributable to the aircraft interference flow field, and $\dot{Z}/V_\infty$ represents the small-angle approximation of the so-called "induced" aerodynamic angle resulting from the store dynamic translational motion. The geometric and induced angles combine to make up the total store (idealized) aerodynamic angles of attack and sideslip (α_S and β_S). For small angles the coefficient slope terms may be considered to be constants. After the coefficient relationships are substituted, and with some rearrangement, the motion equations become:

$$\ddot{X}/g = -\,[C_A \cos\theta + (C_{N\alpha}\,(\theta + \dot{Z}/V_\infty) + \Delta C_N) \sin\theta]\, Q_\infty S/mg + (F_{EZ}/mg)\sin\theta \tag{A–20}$$

$$\ddot{Z}/g = 1 - [(C_{N\alpha}\,(\theta + \dot{Z}/V_\infty) + \Delta C_N) \cos\theta - C_A \sin\theta]\, Q_\infty S/mg + (F_{EZ}/mg)\cos\theta \tag{A-21}$$

$$\ddot{\theta} = [(C_{m\alpha}(\theta + \dot{Z}/V_\infty) + \Delta C_m + C_{mq}(XLM\ \dot{\theta}/2V_\infty] Q_\infty S\ XLM/I_{YY} - M_{EY}/I_{YY} \quad \text{(A-22)}$$

From an examination of the three previous equations, the dynamic simulation relationships that will produce comparable motion on the model and full-scale stores can be deduced. From Eq. (A-4):

$$X' = X^*\Lambda$$

Taking model-scale time derivatives of both sides of Eq. (A-4) and substituting in the relation between model-scale and full-scale time [Eq. (A-7)]:

$$\ddot{X}' = d^2X'/dt'^2 = \Lambda d^2X/dt'^2 = \Lambda d^2X/[(g/g')\Lambda dt^2] = \ddot{X}/(g/g')$$

or:

$$\ddot{X}'/g' = \ddot{X}/g \quad \text{(A-23)}$$

Similarly, for $Z' = Z^*\Lambda$:

$$\ddot{Z}'/g' = \ddot{Z}/g \quad \text{(A-24)}$$

and, for $\theta' = \theta$:

$$\ddot{\theta}' = \ddot{\theta}/[(g/g')\Lambda] \quad \text{(A-25)}$$

After evaluating Eqs. (A-20), (A-21), and (A-22) for model and full-scale properties and substituting into (A-23), (A-24), and (A-25), dynamic similitude is maintained if each term on the left side of the equations is matched by the corresponding term on the right side:

$$C_{N\alpha}' = C_{N\alpha} \quad \text{(A-26)}$$
$$C_{m\alpha}' = C_{m\alpha}$$
$$C_A' = C_A$$
$$C_{mq}' = C_{mq}$$

$$\dot{Z}'/V_\infty' = \dot{Z}/V_\infty \quad \text{(A-27)}$$

$$Q_\infty'A'/m'g' = Q_\infty A/mg \quad \text{(A-28)}$$

$$F_{EZ}'/m'g' = F_{EZ}/mg \quad \text{(A-29)}$$

$$XLM'\ \dot{\theta}'/2V_\infty' = XLM\ \dot{\theta}/2V_\infty \quad \text{(A-30)}$$

$$Q_\infty'A'\ XLM'/I_{YY}' = Q_\infty A\ XLM/[\ I_{YY}(g/g')\Lambda\ ] \quad \text{(A-31)}$$

$$M_{EY}'/I_{YY}' = M_{EY}/[I_{YY}(g/g')\Lambda] \quad \text{(A-32)}$$

Equation (A-26) is satisfied by the aerodynamic force and moment scaling of Section A-1. The relations of Eqs. (A-27) through (A-32) can be used to define the physical properties of the dynamic model needed to emulate the motion of the full-scale store as outlined in the remainder of this section.

Either Eq. (A-27) or Eq. (A-30) can be used to re-derive the free-stream velocity scaling law which was previously derived for the one-degree-of-freedom case in Section A-2.1 Beginning by taking model-scale time derivatives of both sides of the position equation, for example, and substituting in the relation between model-scale and full-scale time [Eq. (A-7)] yields:

$$\dot{Z}' = dZ'/dt' = \Lambda dZ/dt' = \Lambda dZ/[\mathrm{sqrt}[(g/g')\Lambda]dt = \dot{Z}*[\sqrt{((g/g')*\Lambda)}] \quad \text{(A-33)}$$

Substituting Eq. (A-33) into (A-27) then results in the same free-stream velocity relationship deduced earlier for the one-degree-of-freedom case (Eq. (A-11):

$$V_\infty' = V_\infty * \sqrt{(\Lambda*(g'/g))}$$

Alternately, the velocity relationship can also be derived beginning with time derivatives of the pitch orientation relation:

$$\dot{\theta}' = d\theta'/dt' = d\theta/dt' = d\theta/[\mathrm{sqrt}[(g/g')\Lambda]dt = \dot{\theta}/[\sqrt{((g/g')*\Lambda)}] \quad \text{(A-34)}$$

Substituting Eq. (A-34) into (A-30) again results in the free-stream velocity relationship of Eq. (A-11).

The scaling relation for mass can be obtained by solving Eq. (A-28) for m' using (A-11):

$$m' = m\, Q_\infty'S'g/Q_\infty S\, g' = m\, 0.5\, \rho_\infty\, V_\infty'^2\, S'g / 0.5\, \rho_\infty V_\infty^2\, S\, g' = m\, (\rho_\infty'/\rho_\infty)\, (V_\infty'/V_\infty)^2\, (g/g')\Lambda^2 \quad \text{(A-35)}$$

The scaling relation for pitch moment-of-inertia can be obtained by solving Eq. (A-31) for I_{YY}' using (A-11):

$$I_{YY}' = I_{YY}(\rho_\infty'/\rho_\infty)\, (V_\infty'/V_\infty)^2\, (g/g')\Lambda^4 \quad \text{(A-36)}$$

The scaling relation for ejector force can be obtained by solving Eq. (A-29) for F_{EZ}' using (A-11):

$$F_{EZ}' = F_{EZ}(\rho_\infty'/\rho_\infty)\, (V_\infty'/V_\infty)^2\, \Lambda^2 \quad \text{(A-37)}$$

Equation (A-32) provides no additional information beyond that derivable from Eqs. (A-29) and (A-31) because the moment from the ejector is directly related to the ejector force ($M_{EY} = F_{EZ} * X_{E1}$). This completes the derivation of the aerodynamic force and moment and dynamic motion

scaling laws. The only remaining issue is the resolution of the conflict between the Mach number required for aerodynamic scaling, Eq. (A-3), and the Mach number required for motion scaling, Eq. (A-14).

A-3.0 COMPROMISE SCALING LAWS

Because the Mach number required for proper scaling of aerodynamic forces and moments differs from the Mach number required for proper scaling of dynamic motions, some form of compromise must be introduced into the scaling laws. Three primary types of compromise scaling laws are generally available and are described in the next sections.

A-3.1 FROUDE SCALING

One possible compromise to the scaling laws is simply to set the reduced Mach number required for motion scaling, Eq. (A-14), and accept the errors in the model aerodynamics that result from the improperly-simulated compressibility effects through Eq. (A-3). This compromise, of course, is only valid if the compressibility effects are small or, in other words, the simulation is only valid at low subsonic Mach numbers. As such, the Froude scaling laws are not very useful for store separations from high-performance fighter/bomber aircraft, but are often selected for releases from slow-moving aircraft such as helicopters and cargo planes. Froude scaling is also often used by hobbyists for radio-controlled model aircraft. The complete Froude relations may be obtained by assuming g' = g, evaluating the velocity relation, Eq. (A-11), and substituting the free-stream velocity relation into the other relations for the physical properties of the dynamic model:

Gravitational acceleration:

$$g' = g \tag{A-38}$$

Time from Eq. (A-7):

$$t' = t^* \sqrt{(\Lambda)} \tag{A-39}$$

Free-stream velocity from (A-11):

$$V_\infty' = V_\infty^* \sqrt{(\Lambda)} \tag{A-40}$$

Mach number from (A-14):

$$M_\infty' = M_\infty^* \sqrt{(\Lambda(T_\infty'/T))} \tag{A-41}$$

Mass from A35 and (A-40):

$$m' = m^*(\rho_\infty'/\rho_\infty)^*\Lambda^3 \tag{A-42}$$

or (since WT = m*g):

$$WT' = WT^*(\rho_\infty'/\rho_\infty)^*\Lambda^3 \tag{A-42b}$$

Moments of inertia from (A-36) and (A-40):

$$I_{YY}' = I_{YY}^*(\rho_\infty'/\rho_\infty)^*\Lambda^5 \tag{A-43}$$

Ejector forces from (A-37) and (A-40):

$$F_{EZ}' = F_{EZ}^*(\rho_\infty'/\rho_\infty)^*\Lambda^3 \tag{A-44}$$

Froude scaling maintains the ratio of store mass density (m/l^3) to air density (ρ_∞) as can be seen by an examination of Eq. (A-42). Because Froude-scaled stores maintain the same mass per unit volume as the full-scale store (at unity air density ratio), the Froude store may be comprised of

the same materials as the full-scale store in the same proportions by volume. If, for example, ρ_∞' and ρ_∞ are identical and the full-scale store is comprised of 1000 cubic inches of solid steel, then a 1/10th-scale Froude model would be comprised of 1 cubic inch of the same type of steel. Froude scaling is so named because the Froude number (a property defined by $V_\infty^2/g\ l$, which is used most often in hydrodynamic studies to relate bouyancy forces to inertial forces) remains constant.

If the physical properties of the dynamic model are set by the relations of Eqs. (A-38) through (A-44), then the dynamic motion properties of the model are related to those of the full-scale store by the relations:

Linear translations from Eq. (A-4): (A-45)

$Z' = Z^*\Lambda$

Linear velocities from (A-33):

$\dot{Z}' = \dot{Z}\ ^*\sqrt{(\Lambda)}$

Linear accelerations or velocity derivatives from (A-23):

$\ddot{Z}' = \ddot{Z}$

Angles from (A-4):

$\theta' = \theta$

Angular rates from (A-34):

$\dot{\theta}' = \dot{\theta}/\sqrt{(\Lambda)}$

Angular accelerations or velocity derivatives from (A-25):

$\ddot{\theta}' = \ddot{\theta}/\Lambda$

and the drop event will be in error relative to the full-scale flight event to the extent that the store aerodynamics are influenced by the improperly simulated Mach number.

A-3.2 "HEAVY" MACH SCALING

The second compromise scaling law again assumes g' = g but involves setting the Mach number required for aerodynamic scaling, Eq. (A-3), at the expense of compromises to the Mach-number requirements for dynamic motion scaling, Eq. (A-14). Arbitrarily setting the Mach number for aerodynamic scaling results [through Eq. (A-12)] in a free-stream velocity that is too large for proper motion scaling by a factor approximately equal to the square root of the scale factor [compare Eq. (A-40) with (A-49)]. The dynamic motion simulation is, therefore, compromised in each of the motion terms involving free-stream velocity, particularly the induced angles, Eq. (A-27), and the non-dimensional rotational rates, Eq. (A-30). Equations (A-27) and (A-30) are essentially removed from the development of the dynamic scaling laws. The heavy-scaled simulation will be in error to the extent that the aerodynamic forces and moments (which ultimately drive the store motion) are sensitive to the small induced angle errors, and will also tend to over-rotate (angular motion amplitudes will be too large) because of the reduction in damping moments brought about by the larger value of free-stream velocity in the denominator of the non-dimensional angular rate term of Eq. (A-30). The larger amplitudes of the angular

oscillations will also have secondary effects on store positions in the aircraft flow field because of the dependence on the store aerodynamic angles of the store aerodynamic coefficients which drive the store motion. Typical errors for a tumbling fuel tank model are presented in Section 3.2 of the main body of the current report. Fortunately, however, the errors involved in heavy scaling are usually conservative in that the under-damped rotational motions observed on a scaled model would be expected to be somewhat more severe than would actually occur in flight, and the induced angle errors for transonic/supersonic flight usually represent small errors in small angles. The heavy scaling laws are:

Gravitational acceleration:

$$g' = g \tag{A-46}$$

Time from Eq. (A-7) (unchanged):

$$t' = t * \sqrt{(\Lambda)} \tag{A-47}$$

Mach number:

$$M_\infty' = M_\infty \tag{A-48}$$

Free-stream velocity from (A-48), (A-12), and (A-13):

$$V_\infty' = V_\infty * \sqrt{(T_\infty'/(T_\infty))} \tag{A-49}$$

Mass from (A-35), (A-49), (A-12), and (A-13):

$$m' = m*(Q_\infty'/Q_\infty)*\Lambda^2 \tag{A-50}$$

or (since WT = m * g):

$$WT' = WT*(Q_\infty'/Q_\infty)*\Lambda^2 \tag{A-50b}$$

Moments of inertia from (A-36), (A-49), (A-12), and (A-13):

$$I_{YY}' = I_{YY}*(Q_\infty'/Q_\infty)*\Lambda^4 \tag{A-51}$$

Ejector forces from (A-37), (A-49), (A-12), and (A-13):

$$F_{EZ}' = F_{EZ}*(Q_\infty'/Q_\infty)*\Lambda^2 \tag{A-52}$$

The connotation "heavy scaling" is a consequence of the mass relationship [Eq. (A-50) compared to Eq. (A-42)]. All else being equal, the mass of heavy-scaled models will be larger than that for Froude-scaled models by a factor of $1/\Lambda$ because of the choice to match the Mach number required for aerodynamic scaling at the expense of the Mach number for motion scaling. In other words, if the Q ratio is unity in Eq. (A-50) and the full-scale store is made up of 1000 cubic inches of solid steel, then the heavy-scaled store must consist of 1 cubic inch of something ten times denser than steel. It can easily be realized that it might not even be possible to find an adequate model-construction material to allow "heavy" scaling of models at the small scales necessary for smaller wind tunnels. For example, a small 1/30th-scale drop model would have to be constructed of a super-dense material 30 times more dense than the full-scale item. (The unavailable super-dense material is often referred to as "unobtainium" in free-drop circles.) For this reason, "light" scaling, as outlined in the next section, is almost universally used in smaller wind tunnels. Heavy scaling tends to be used primarily in larger tunnels where scale factors of about 1/20th scale or larger are possible.

If the physical properties of the dynamic model are set by the heavy scaling relations of Eqs. (A-46) through (A-52), then the dynamic motion properties of the model are related to those of the full-scale store by relations identical to those for Froude scaling:

Linear translations from Eq. (A-4): (A-53)

$Z' = Z * \Lambda$

Linear velocities from (A-33):

$\dot{Z}' = \dot{Z} * \sqrt{(\Lambda)}$

Linear accelerations or velocity derivatives from (A-23):

$\ddot{Z}' = \ddot{Z}$

Angles from (A-4):

$\theta' = \theta$

Angular rates from (A-34):

$\dot{\theta}' = \dot{\theta} / \sqrt{(\Lambda)}$

Angular accelerations or velocity derivatives from (A-25):

$\ddot{\theta}' = \ddot{\theta} / \Lambda$

and the drop event will be in error relative to the full-scale flight event to the extent that the store aerodynamics are influenced by the improperly simulated non-dimensional rotational rates and induced angles.

The scaling laws are derived in this appendix from the viewpoint of the total store motion and are derived by comparing terms in the store equations of motion at full and drop scale. It is also possible to derive similar scaling laws using the principles of dimensional analysis. Several such derivations are available in published literature (for example, Refs. A-1 and A-2). In some published derivations (not the ones cited above) of the scaling laws from the dimensional analysis viewpoint, however, the heavy laws are (somewhat prematurely) declared to be inferior to other laws (such as light scaling which will be described in the next section). The perceived conflict arises because different scaling laws are developed for linear motion velocities than are developed for free-stream velocity. This, rightly, seems a violation of dimensional analysis considerations, and the heavy laws have, on occasion, been declared to be mathematically invalid. Such (almost religious) convictions ignore the fact that light scaling laws also involve compromises to the simulated store motion. It happens that dimensional analysis principles are not violated by the particular set of compromises used in the light scaling derivation as will be shown in the next section. (All the terms in light scaling, for instance, have correct and consistent *units* - the light-scaling compromise is that the *magnitudes* of gravitational terms are incorrect by the scale factor.) Any dogmatic statement that one scaling law is better than another should be viewed as a fundamental non-understanding that all scaling laws are the result of compromises to full-scale flight 'truth'.

A-3.3 "LIGHT" MACH SCALING

Both Froude and heavy scaling assume that $g' = g$, as it is not yet possible to change gravitational acceleration for a model in a ground test facility. If such an artificial gravity field were possible, however, the gravity ratio of Eq. (A-14) could be adjusted so that the Mach numbers for aerodynamic and motion scaling could be achieved simultaneously. The required artificial gravi-

tational acceleration is derived by beginning with Eq. (A-14) and substituting in (A-12) and (A-13):

$$(V_\infty'/V_\infty)^2 (a_\infty'/a_\infty)^2 = \Lambda (g'/g)(T_\infty/T_\infty') = (V_\infty'/V_\infty)^2 (T_\infty/T_\infty')$$

and then solving for g':

$$g' = g(V_\infty'/V_\infty)^2/\Lambda \tag{A-54}$$

Given that V_∞'/V_∞ is typically near unity, the gravitational acceleration needed for proper light scaling from Eq. (A-54) is directly related to the scale factor. Thus, for a 1/30th-scale model, the acceleration of gravity needed would have to be thirty times the nominal 1 "gee" value available on the earth. The so-called "light" scaling laws can then be derived by substituting Eq. (A-54) into (A-7), (A-11), and (A-35) through (A-37).

Time from Eq. (A-7):

$$t' = t*(\Lambda / (V_\infty'/V_\infty)) \tag{A-55}$$

Mach number from (A-14), (A-12), and (A-13):

$$M_\infty' = M_\infty \tag{A-56}$$

Free-stream velocity from (A-56), (A-12), and (A-13):

$$V_\infty' = V_\infty * \sqrt{(T_\infty'/(T_\infty))} \tag{A-57}$$

Mass from (A-35), (A-57), (A-12), and (A-13):

$$m' = m*(\rho_\infty'/\rho_\infty)*\Lambda^3 \tag{A-58}$$

Moments of inertia from (A-36), (A-52), (A-12), and (A-13):

$$I_{YY}' = I_{YY}*(\rho_\infty'/\rho_\infty)*\Lambda^5 \tag{A-59}$$

Ejector forces from (A-37), (A-58), (A-12), and (A-13):

$$F_{EZ}' = F_{EZ}*(Q_\infty'/Q_\infty)*\Lambda^2 \tag{A-60}$$

Light scaling like Froude scaling maintains the ratio of store mass density (m/l^3) to air density (ρ_∞) as can be seen by an examination of Eq. (A-58).

The difficulty with light scaling is, of course, how to simulate the required model-scale gravitational acceleration. Three approaches have been proposed and to some extent demonstrated in various test environments. All but one of the approaches involve great complexity or mechanical difficulty, however. The first approach is to simply run the experiment at normal gravity and either accept the errors arising from the improper gravity simulation or make some attempt to add correction factors for vertical acceleration errors. If the errors are simply accepted, it must be realized that the error in vertical acceleration of the store away from the aircraft because of the missing artificial gravity component will lead to a velocity error that linearly grows in time and a quadratically growing error in the vertical position of the store relative to the aircraft in the flow field. The light-scaled store typically matches full-scale angular orientations better but may also result in premature collisions with the aircraft because the store does not accelerate away from the aircraft properly in the vertical direction. The drop simulation will then also be in error to the

extent that the aircraft flow-field effects on store aerodynamics are a strong function of the incorrect vertical position relative to the aircraft. The correction factors developed to correct for the lack of the increased gravitational acceleration generally involve some additional force in the ejector model (Ref. A-3) so that the combination of adjusted ejector acceleration and the actual 1-gee earth gravitational acceleration matches the sum of g' and the acceleration derived from the properly scaled ejector forces, Eq. (A-60). The second approach to simulating artificial gravity is an approach used by the British in which the aircraft model is mounted on a separate support and is vertically accelerated upward relative to the store at release so that the relative acceleration between store and aircraft emulates g'. For a 1/30th-scale model, the aircraft must be accelerated upwards at approximately 29 g's. Such a vertical plunging motion of the aircraft can, however, greatly effect the aircraft flow field which, in turn, effects the aerodynamic loads on the store model within the flow field and the resulting motion of the store. The plunging aircraft flow-field effects are sometimes partially corrected for by dynamically changing the aircraft pitch angle during its vertical plunging motion. There are, however, obvious logistical difficulties involved in coordinating the aircraft model pitching and plunging to such an extent that the resulting aircraft flow environment is "equivalent" to that of a steady-state flight condition. A third approach to simulating artificial gravity involves attempting to generate a magnetic field around the wind tunnel test section which emulates g' on a magnetically balanced store model. This third approach requires a magnetically non-conductive wind tunnel and very sophisticated magnets.

If the physical properties of the dynamic model are set by the light scaling relations of Eqs. (A-54) through (A-60), then the dynamic motion properties of the model are related to those of the full-scale store by relations identical to those for Froude and heavy scaling:

Linear translations from Eq. (A-4): (A-61)

$Z' = Z^*\Lambda$

Linear velocities from (A-33):

$\dot{Z}' = \dot{Z} * \sqrt{(\Lambda)}$

Linear accelerations or velocity derivatives from (A-23):

$\ddot{Z}' = \ddot{Z}$

Angles from (A-4):

$\theta' = \theta$

Angular rates from (A-34):

$\dot{\theta}' = \dot{\theta} / \sqrt{(\Lambda)}$

Angular accelerations or velocity derivatives from (A-25):

$\ddot{\theta}' = \ddot{\theta} / \Lambda$

and either (1) the drop event will be in error relative to the full-scale flight event to the extent that the store aerodynamics are influenced by the improperly simulated position of the store relative to the aircraft which results from the improperly simulated gravitational acceleration if uncorrected light scaling is used, or (2) the drop event will be in error relative to the full-scale flight event to the extent that the store aerodynamics are influenced by the improperly simulated plunging aircraft flow-field environment if the vertically accelerated aircraft approach is used, or

(3) light scaling would not be compromised at all relative to full scale if a true artificial gravity simulation were available (magnetic or otherwise).

REFERENCES

A-1. Deitchman, S. J. "Similarity Laws for Dynamic Model Testing." Cornell Aeronautical Laboratories, Report No. CAL GC-910-C-14, September 1956.

A-2. Sandahl, C. A. and Faget, M. A. "Similitude Relations for Free-Model Wind tunnel Studies of Store-Dropping Problems." National Advisory Committee for Aeronautics, Technical Note No. TN-3907, January 1957.

A-3. Marshal, John C. "Analytic Evaluation of the Limitations of the Various Scaling Laws for Freedrop Store Separation Testing." Paper presented at the Fourth JTCG Aircraft/Stores Compatibility Symposium, Ft. Walton Beach, FL, October 12-14, 1977.

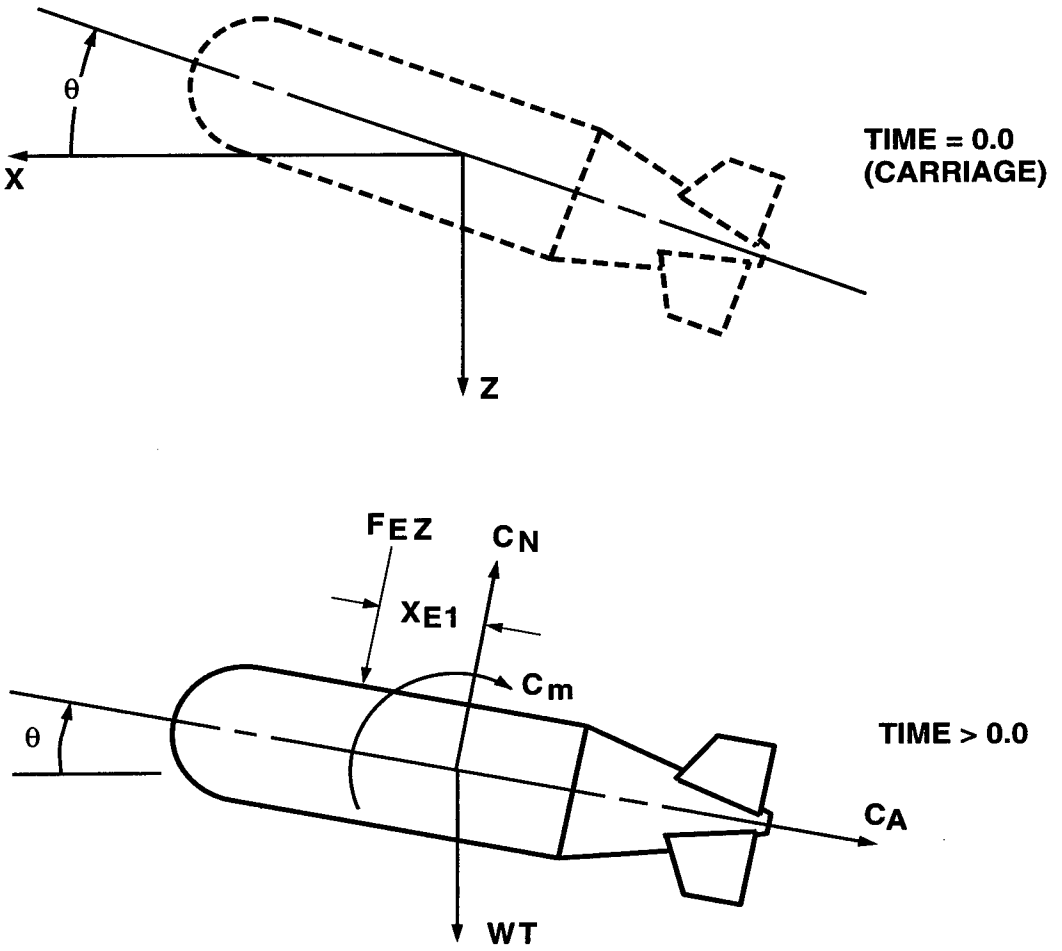

Figure A-1. Three-DOF coordinate notation.

NOMENCLATURE

The superscript prime (ô) when applied to any of the following parameter names indicates that a parameter normally defined at full scale is defined at model scale (e.g., XLM'=Λ*XLM). This nomenclature makes use of an extended variable-naming convention developed in Ref. 4 - whenever possible, however, the more-traditional but less-descriptive names commonly used in wind tunnel testing are also indicated in square brackets.

ALPHA, α, α_p	Parent aircraft angle of attack relative to the aircraft free-stream flight velocity vector, positive when the aircraft nose is raised relative to the free-stream velocity vector, angle between the projection of the free-stream velocity on the aircraft horizontal reference plane and the aircraft longitudinal axis, deg
ALPHAS, α_S	Store aerodynamic angle of attack relative to the idealized store flight velocity vector (vector sum of the aircraft flight velocity and the separation velocity of the store relative to the aircraft), positive when the store nose is raised relative to the idealized flight velocity, angle between the projection of the idealized flight velocity on the store X_B–Z_B plane and the X_B axis, deg
BETA, β	Parent aircraft angle of sideslip relative to the aircraft free-stream flight velocity vector, positive when the aircraft nose is rotated to the left relative to the free-stream velocity vector, angle between the free-stream velocity vector and the projection of the velocity vector on the aircraft horizontal reference plane, deg
BETAS, β_S	Store aerodynamic angle of sideslip relative to idealized store flight velocity vector, positive when the store nose is rotated to the left relative to the idealized flight velocity, angle between the idealized flight velocity vector and the projection of the vector on the store X_B–Z_B plane, deg
cg	Store center of gravity (moment center)
CAT, C_A	Store axial-force coefficient, positive in the negative X_B direction; = aerodynamic axial force/(Q_∞*S)
CLL, C_l	Store rolling-moment coefficient, positive rotation vector in the positive X_B direction; = aerodynamic rolling moment/(Q_∞*S*XLL)
CLM, C_m	Store pitching-moment coefficient, positive rotation vector in the positive Y_B direction; = aerodynamic pitching moment/(Q_∞*S*XLM)
CLN, C_n	Store yawing-moment coefficient, positive rotation vector in the positive Z_B direction; = aerodynamic yawing moment/(Q_∞*S*XLN)

C_{lp}	Dynamic stability derivative in rolling moment caused by rolling velocity, roll-damping coefficient, per rad; = dCLL/d{ (PBBI*XLL)/(2*V_∞) }
C_{mq}	Dynamic stability derivative in pitching moment caused by pitching velocity, pitch-damping coefficient, per rad; = dCLM/d{ (QBBI*XLM)/(2*V_∞) }
$C_{m\alpha}$	Static stability derivative in pitching moment with respect to aerodynamic angle of attack, per rad: = dCLM/dα_S
CN, C_N	Store normal-force coefficient, positive in the negative Z_B direction; = aerodynamic normal force/(Q_∞*S)
C_{nr}	Dynamic stability derivative in yawing moment caused by yawing velocity, yaw-damping coefficient, per rad; = dCLN/d{ (RBBI*XLN)/(2*V_∞) }
CY, C_Y	Store side-force coefficient, positive in the positive Y_B direction; = aerodynamic side force/(Q_∞*S)
DE0BI - DE3BI	Derivatives of the Euler parameters describing the orientation of the body axis system relative to the inertial axis system
DPBBI [pdot]	Derivative of the X_B component of the rotational velocity of the store body axis system relative to the inertial axis system, rad/sec^2
DQBBI [qdot]	Derivative of the Y_B component of the rotational velocity of the store body axis system relative to the inertial axis system, rad/sec^2
DRBBI [rdot]	Derivative of the Z_B component of the rotational velocity of the store body axis system relative to the inertial axis system, rad/sec^2
DUBBI [udot]	Derivative of the X_B component of the velocity of the store body axis system relative to the inertial axis system, ft/sec^2
DVBBI [vdot}	Derivative of the Y_B component of the velocity of the store body axis system relative to the inertial axis system, ft/sec^2
DWBBI [wdot]	Derivative of the Z_B component of the velocity of the store body axis system relative to the inertial axis system, ft/sec^2
DXFBF	Derivative of the axial separation distance of the store cg from the trajectory origin in the X_F direction, derivative of the X_F component of the position of the store body-axis system relative to the flight axis system, positive forward as seen by the pilot, ft/sec

DYFBF	Derivative of the lateral separation distance of the store cg from the trajectory origin in the Y_F direction, derivative of the Y_F component of the position of the store body axis system relative to the flight axis system, positive to the right as seen by the pilot, ft/sec
DZFBF	Derivative of the vertical separation distance of the store cg from the trajectory origin in the Z_F direction, derivative of the Z_F component of the position of the store body axis system relative to the flight axis system, positive downward as seen by the pilot, ft/sec
E0BI - E3BI	Euler parameters describing the orientation of the body axis system relative to the inertial axis system
FEXB [FEX]	X_B -component of sum of external applied ejector forces on store, lb (ejector contribution to FXB)
FEYB [FEY]	Y_B -component of sum of external applied ejector forces on store, lb (ejector contribution to FYB)
FEZB [FEZ]	Z_B -component of sum of external applied ejector forces on store, lb (ejector contribution to FZB)
FXB [FX]	X_B -component of sum of external applied forces on store, lb (subscript AERO denotes aerodynamic only contribution)
FYB [FY]	Y_B -component of sum of external applied forces on store, lb (subscript AERO denotes aerodynamic only contribution)
FZB [FZ]	Z_B -component of sum of external applied forces on store, lb (subscript AERO denotes aerodynamic only contribution)
g	gravitational acceleration, ft/sec^2 (nominally 32.174 ft/sec^2)
GAXMBBI	body-axis X_B-component of the measured portion of the acceleration of the body axis system relative to the inertial axis system, g's
GAYMBBI	body-axis Y_B-component of the measured portion of the acceleration of the body axis system relative to the inertial axis system, g's
GAZMBBI	body-axis Z_B-component of the measured portion of the acceleration of the body axis system relative to the inertial axis system, g's
GAXMBNI	body-axis X_B-component of the measured portion of the acceleration of the nose point (nose axis system) relative to the inertial axis system, g's

GAYMBNI	body-axis Y_B-component of the measured portion of the acceleration of the nose point (nose axis system) relative to the inertial axis system, g's
GAZMBNI	body-axis Z_B-component of the measured portion of the acceleration of the nose point (nose axis system) relative to the inertial axis system, g's
H	Simulated pressure altitude at store release, ft
IP	Pitch incidence angle of active store at carriage relative to the aircraft, angle between the store longitudinal body axis (X_B) at carriage and its projection in the X_A–Y_A plane, positive when the store nose is raised relative to the aircraft, deg
IR	Roll incidence angle of active store at carriage relative to the aircraft, angle between the store lateral body axis (Y_B) at carriage and the intersection of the Y_B–Z_B and X_A–Y_A planes, positive for clockwise rotation relative to the aircraft when looking forward, deg
IY	Yaw incidence angle of active store at carriage relative to the aircraft, angle between the projection of the store longitudinal axis (X_B) at carriage in the X_A–Y_A plane and the X_A axis, positive when the store nose is rotated to the right relative to the aircraft, deg
IYY	Moment of inertia about the store Y_B axis, slug-ft^2
$[\,I\,]_{BB}$	Tensor matrix of inertias about the store body axes
LAMBDA, Λ	Model linear scale factor
M_∞, M	Free-stream Mach number
m	Store mass, slugs
MEXB [MEX]	X_B -component of resultant moment about the store center of gravity of applied ejector forces on store, ft-lb (ejector contribution to MXB)
MEYB [MEY]	Y_B - component of resultant moment about the store center of gravity of applied ejector forces on store, ft-lb (ejector contribution to MYB)
MEZB [MEZ]	Z_B - component of resultant moment about the store center of gravity of applied ejector forces on store, ft-lb (ejector contribution to MZB)
MXB [MX]	X_B -component of sum of external applied moments about the store center of gravity, ft-lb (subscript AERO denotes aerodynamic only contribution)

MYB [MY]	Y_B -component of sum of external applied moments about the store center of gravity, ft-lb (subscript AERO denotes aerodynamic only contribution)
MZB [MZ]	Z_B -component of sum of external applied moments about the store center of gravity, ft-lb (subscript AERO denotes aerodynamic only contribution)
PBBI [p]	Store roll rate, X_B component of the rotational velocity of the store body axis system relative to the inertial axis system, rad/sec
Q_∞	Free-stream dynamic pressure, lb/ft^2 ; = $1/2\rho_\infty(V_\infty)^2$
QA	Idealized store flight dynamic pressure, lb/ft^2 ; =$1/2\rho_\infty$ (VTOTBW)^2
QBBI [q]	Store pitch rate, Y_B component of the rotational velocity of the store body axis system relative to the inertial axis system, rad/sec
RBBI [r]	Store yaw rate, Z_B component of the rotational velocity of the store body axis system relative to the inertial axis system, rad/sec
RXB [RX]	X_B -component of external applied reaction force at restraint point on store, lb
RYB [RY]	Y_B -component of external applied reaction force at restraint point on store, lb
RZB [RZ]	Z_B -component of external applied reaction force at restraint point on store, lb
RLB [RL]	X_B -component of external applied reaction moment at restraint point on store, ft-lb
RMB [RM]	Y_B -component of external applied reaction moment at restraint point on store, ft-lb
RNB [RN]	Z_B -component of external applied reaction moment at restraint point on store, ft-lb
RUN	Sequential indexing number for referencing data. A constant for each trajectory, free-stream, grid, or flow-field probe sweep
ρ_∞	Free-stream air density, $slug/ft^3$
S	Store reference area, ft^2
t, T, TIME	Time from first store motion, sec
T_∞	Free-stream static temperature, °R

[TRNBI(3,3)]	Three-by-three direction cosine matrix describing the orientation of the body-axis system relative to inertial axes (projects inertial-axis quantities to body-axis quantities)
[TRNIE(3,3)]	Three-by-three direction cosine matrix describing the orientation of the inertial-axis system relative to earth axes (projects earth-axis quantities to inertial-axis quantities)
UBBI [u]	Store separation velocity in the X_B direction, X_B component of the velocity of the store body axis system relative to the inertial axis system, ft/sec
UBBW [VX]	X_B component of the velocity of the store body axis system relative to the wind mass, ft/sec
UBIW	X_B component of the velocity of the inertial axis system relative to the wind mass, ft/sec
UIIW	X_I component of the velocity of the inertial axis system relative to the wind mass, aircraft flight velocity at release instant, ft/sec
VBBI [v]	Store separation velocity in the Y_B direction, Y_B component of the velocity of the store body axis system relative to the inertial axis system, ft/sec
VBBW [VY]	Y_B component of the velocity of the store body axis system relative to the wind mass, ft/sec
VBIW	Y_B component of the velocity of the inertial axis system relative to the wind mass, ft/sec
V_∞	Free-stream velocity, ft/sec (= UIIW for the aircraft; = VTOTBW for the store)
VTOTBW [UR]	Idealized store flight velocity (vector sum of UIIW, UBBI, VBBI, and WBBI), ft/sec
WBBI [w]	Store separation velocity in the Z_B direction, Z_B component of the velocity of the store body axis system relative to the inertial axis system, ft/sec
WBBW [VZ]	Z_B component of the velocity of the store body axis system relative to the wind mass, ft/sec
WBIW	Z_B component of the velocity of the inertial axis system relative to the wind mass, ft/sec
WL	Manufacturer-defined aircraft vertical coordinate (waterline), positive up when the aircraft is at zero pitch and roll angles, in.

WT	Store weight, lb
WXB	Body-axis X_B-component of the store weight, lb
WYB	Body-axis Y_B-component of the store weight, lb
WZB	Body-axis Z_B-component of the store weight, lb
XBBH [XO]	Body-axis X_B-component of the position of the store body-axis system relative to the hook/hanger/pivot axis system for restrained motion, ft
XBNB	Body-axis X_B-component of the position of the nose point (nose-axis system) relative to the body axis system, ft
XLL	Store reference length for rolling moment coefficient, ft
XLM	Store reference length for pitching moment coefficient, ft
XLN	Store reference length for yawing moment coefficient, ft
YBBH [YO]	Body-axis Y_B-component of the position of the store body-axis system relative to the hook/hanger/pivot axis system for restrained motion, ft
YBNB	Body-axis Y_B-component of the position of the nose point (nose-axis system) relative to the body axis system, ft
ZBBH [ZO]	Body-axis Z_B-component of the position of the store body-axis system relative to the hook/hanger/pivot axis system for restrained motion, ft
ZBNB	Body-axis Z_B-component of the position of the nose point (nose-axis system) relative to the body axis system, ft

BODY-AXIS-SYSTEM DEFINITIONS

Coordinate Directions

X_B	Parallel to the store longitudinal axis defined by the store manufacturer, positive upstream at store release
Y_B	Perpendicular to the X_B and Z_B directions, positive to the right looking upstream when the store is at zero yaw and roll angles
Z_B	Perpendicular to the X_B direction and parallel to the aircraft plane of symmetry when the store and aircraft are at zero yaw and roll angles, positive downward as seen by the pilot when the store is at zero pitch and roll angles

Origin

The store body-axis-system origin is coincident with the store center of gravity at all times. The X_B, Y_B, and Z_B coordinate axes rotate with the store in pitch, yaw, and roll so that mass moments-of-inertia about the three axes are not time-varying quantities.

INERTIAL-AXIS-SYSTEM DEFINITIONS

Coordinate Directions

X_I — Parallel to the aircraft flight path direction at the instant of release, positive forward as seen by the pilot

Y_I — Perpendicular to the X_I and Z_I directions, positive to the right as seen by the pilot

Z_I — Parallel to the aircraft plane of symmetry and perpendicular to the aircraft flight path direction at the instant of release, positive downward as seen by the pilot

Origin

The inertial-axis-system origin is coincident with the store center-of-gravity location at the instant of release. The origin translates parallel to the aircraft flight path direction at the instant of release at the aircraft free-stream flight velocity at the instant of release. The origin is not fixed with respect to either the aircraft or the store (both of which may be in motion relative to the inertial system). The coordinate axes do not rotate during aircraft maneuvers.

Store Positions

XIBI [XI] — Axial separation distance of the store cg from the inertial-axis origin in the X_I direction, X_I component of the position of the store body-axis system relative to the inertial axis system, positive forward as seen by the pilot, ft

YIBI [YI] — Lateral separation distance of the store cg from the inertial-axis origin in the Y_I direction, Y_I component of the position of the store body axis system relative to the inertial axis system, positive to the right as seen by the pilot, ft

ZIBI [ZI] — Vertical separation distance of the store cg from the inertial-axis origin in the Z_I direction, Z_I component of the position of the store body axis system relative to the inertial axis system, positive downward as seen by the pilot, ft

Store Attitudes (Yaw-Pitch-Roll Sequence)

PSIBI, Ψ_{BI} [PSII, Ψ_I] — Yaw angle of the store body axis system relative to the inertial axis system, angle between the projection of the store longitudinal (X_B) axis in the X_I–Y_I plane and the X_I–axis, positive for store nose to the right as seen by the pilot, deg

THABI, θ_{BI} [THAI, θ_I] Pitch angle of the store body axis system relative to the inertial axis system, angle between the store longitudinal (X_B) axis and its projection in the X_I–Y_I plane, positive when the store nose is raised as seen by the pilot, deg

PHIBI, ϕ_{BI} [PHII, ϕ_I] Roll angle of the store body axis system relative to the inertial axis system, angle between the store lateral (Y_B) axis and the intersection of the Y_B–Z_B and X_I–Y_I planes, positive for clockwise rotation when looking upstream, deg

Store Attitudes (Pitch-Yaw-Roll Sequence)

NUBI, ν_{BI} [NUI, ν_I] Pitch angle of the store body axis system relative to the inertial axis system, angle between the projection of the store longitudinal (X_B) axis in the X_I–Z_I plane and the X_I–axis, positive when the store nose is raised as seen by the pilot, deg

ETABI, η_{BI} [ETAI, η_I] Yaw angle of the store body axis system relative to the inertial axis system, angle between the store longitudinal (X_B) axis and its projection in the X_I–Z_I plane, positive when the store nose is raised as seen by the pilot, deg

OMGBI, ω_{BI} [OMEGAI, ω_I] Roll angle of the store body axis system relative to the inertial axis system, angle between the store vertical (Z_B) axis and the intersection of the Y_B–Z_B and X_I–Z_I planes, positive for clockwise rotation when looking upstream, deg

FLIGHT-AXIS-SYSTEM DEFINITIONS

Coordinate Directions

X_F — Parallel to the current aircraft flight path direction, positive forward as seen by the pilot

Y_F — Perpendicular to the X_F and Z_F directions, positive to the right as seen by the pilot

Z_F — Parallel to the aircraft plane of symmetry and perpendicular to the current aircraft flight path direction, positive downward as seen by the pilot

Origin

The flight-axis-system origin is coincident with the store center-of-gravity location at the instant of release. The origin is fixed with respect to the aircraft (not the store) and, thus, translates parallel to the current aircraft flight path at the aircraft free-stream flight velocity. The coordinate axes rotate during an aircraft maneuver to maintain alignment of the X_F axis with the current aircraft flight path direction. Inertial and flight axes are coincident at the instant of release but flight axes may, thereafter, translate and rotate with the aircraft relative to inertial axes if the aircraft is maneuvering.

Store Positions

XFBF [X] — Axial separation distance of the store cg from the flight-axis origin in the X_F direction, X_F component of the position of the store body-axis system relative to the flight axis system, positive forward as seen by the pilot, ft

YFBF [Y] — Lateral separation distance of the store cg from the flight-axis origin in the Y_F direction, Y_F component of the position of the store body axis system relative to the flight axis system, positive to the right as seen by the pilot, ft

ZFBF [Z] — Vertical separation distance of the store cg from the flight-axis origin in the Z_F direction, Z_F component of the position of the store body axis system relative to the flight axis system, positive downward as seen by the pilot, ft

Store Attitudes (Yaw-Pitch-Roll Sequence)

PSIBF, Ψ_{BF} [PSI, ψ] Yaw angle of the store body axis system relative to the flight axis system, angle between the projection of the store longitudinal (X_B) axis in the X_F–Y_F plane and the X_F–axis, positive for store nose to the right as seen by the pilot, deg

THABF, θ_{BF} [THA, θ] Pitch angle of the store body axis system relative to the flight axis system, angle between the store longitudinal (X_B) axis and its projection in the X_F–Y_F plane, positive when the store nose is raised as seen by the pilot, deg

PHIBF, ϕ_{BF} [PHI, ϕ] Roll angle of the store body axis system relative to the flight axis system, angle between the store lateral (Y_B) axis and the intersection of the Y_B–Z_B and X_F–Y_F planes, positive for clockwise rotation when looking upstream, deg

Store Attitudes (Pitch-Yaw-Roll Sequence)

NUBF, ν_{BF} [NU, ν] Pitch angle of the store body axis system relative to the flight axis system, angle between the projection of the store longitudinal (X_B) axis in the X_F–Z_F plane and the X_F–axis, positive when the store nose is raised as seen by the pilot, deg

ETABF, η_{BF} [ETA, η] Yaw angle of the store body axis system relative to the flight axis system, angle between the store longitudinal (X_B) axis and its projection in the X_F–Z_F plane, positive when the store nose is raised as seen by the pilot, deg

OMGBF, ω_{BF} [OMEGA, ω] Roll angle of the store body axis system relative to the flight axis system, angle between the store vertical (Z_B) axis and the intersection of the Y_B–Z_B and X_F–Z_F planes, positive for clockwise rotation when looking upstream, deg

AIRCRAFT-AXIS-SYSTEM DEFINITIONS

Coordinate Directions

X_A — Parallel to the aircraft manufacturer-defined longitudinal reference (fuselage station) axis, positive forward as seen by the pilot

Y_A — Parallel to the aircraft manufacturer-defined lateral reference (buttock line) axis, positive to the right as seen by the pilot

Z_A — Parallel to the aircraft manufacturer-defined vertical reference (waterline) axis, positive downward as seen by the pilot

Origin

The aircraft-axis-system origin is coincident with the store center-of-gravity location at the instant of release and is coincident with the flight-axis-system origin at all times. The origin is fixed with respect to the aircraft and, thus, translates parallel to the current aircraft flight path at the aircraft free-stream flight velocity. The coordinate axes rotate with the aircraft during a maneuver to maintain constant angular orientation relative to the aircraft.

Store Positions

XABA [XA] — Axial separation distance of the store cg from the flight-axis origin in the X_A direction, X_A component of the position of the store body axis system relative to the aircraft axis system, positive forward as seen by the pilot, ft

YABA [YA] — Lateral separation distance of the store cg from the flight-axis origin in the Y_A direction, Y_A component of the position of the store body axis system relative to the aircraft axis system, positive to the right as seen by the pilot, ft

ZABA [ZA] — Vertical separation distance of the store cg from the flight-axis origin in the Z_A direction, Z_A component of the position of the store body axis system relative to the aircraft axis system, positive downward as seen by the pilot, ft

Store Attitudes (Yaw-Pitch-Roll Sequence)

PSIBA, Ψ_{BA} [DPSIA, $\Delta\psi_A$] — Yaw angle of the store body axis system relative to the aircraft axis system, angle between the projection of the store longitudinal (X_B) axis in the X_A–Y_A plane and the X_A–axis, positive for store nose to the right as seen by the pilot, deg

THAAP, θ_{BA} [DTHAA, $\Delta\theta_A$] — Pitch angle of the store body axis system relative to the aircraft axis system, angle between the store longitudinal (X_B) axis and its projection in the X_A–Y_A plane, positive when the store nose is raised as seen by the pilot, deg

PHIBA, ϕ_{BA} [DPHIA, $\Delta\phi_A$] — Roll angle of the store body axis system relative to the aircraft axis system, angle between the store lateral (Y_B) axis and the intersection of the Y_B–Z_B and X_A–Y_A planes, positive for clockwise rotation when looking upstream, deg

Store Attitudes (Pitch-Yaw-Roll Sequence)

NUBA, ν_{BA} [DNUA, $\Delta\nu_A$] — Pitch angle of the store body axis system relative to the aircraft axis system, angle between the projection of the store longitudinal (X_B) axis in the X_A–Z_A plane and the X_A–axis, positive when the store nose is raised as seen by the pilot, deg

ETABA, η_{BA} [DETAA, $\Delta\eta_A$] — Yaw angle of the store body axis system relative to the aircraft axis system, angle between the store longitudinal (X_B) axis and its projection in the X_A–Z_A plane, positive when the store nose is raised as seen by the pilot, deg

OMGBA, ω_{BA} [DOMEGAA, $\Delta\omega_A$] — Roll angle of the store body axis system relative to the aircraft axis system, angle between the store vertical (Z_B) axis and the intersection of the Y_B–Z_B and X_A–Z_A planes, positive for clockwise rotation when looking upstream, deg

PYLON-AXIS-SYSTEM DEFINITIONS

Coordinate Directions

X_P — Parallel to the store longitudinal (X_B) axis at the instant of release and at constant angular orientation with respect to the aircraft, positive forward as seen by the pilot

Y_P — Perpendicular to the X_P direction and parallel to the X_A–Y_A plane, positive to the right as seen by the pilot

Z_P — Perpendicular to the X_P and Y_P directions, positive downward as seen by the pilot

Origin

The pylon-axis-system origin is coincident with the store center-of-gravity location at the instant of release and is coincident with the flight-axis-system origin at all times. The origin is fixed with respect to the aircraft and, thus, translates parallel to the current aircraft flight path at the aircraft free-stream flight velocity. The coordinate axes rotate with the aircraft during a maneuver to maintain constant angular orientation relative to the aircraft.

Store Positions

XPBP [XP] — Axial separation distance of the store cg from the flight-axis origin in the X_P direction, X_P component of the position of the store body axis system relative to the pylon axis system, positive forward as seen by the pilot, ft

YPBP [YP] — Lateral separation distance of the store cg from the flight-axis origin in the Y_P direction, Y_P component of the position of the store body axis system relative to the pylon axis system, positive to the right as seen by the pilot, ft

ZPBP [ZP] — Vertical separation distance of the store cg from the flight-axis origin in the Z_P direction, Z_P component of the position of the store body axis system relative to the pylon axis system, positive downward as seen by the pilot, ft

Store Attitudes (Yaw-Pitch-Roll Sequence)

PSIBP, Ψ_{BP} [DPSI, $\Delta\psi$] — Yaw angle of the store body axis system relative to the pylon axis system, angle between the projection of the store longitudinal (X_B) axis in the X_P–Y_P plane and the X_P–axis, positive for store nose to the right as seen by the pilot, deg

THABP, θ_{BP} [DTHA, $\Delta\theta$] — Pitch angle of the store body axis system relative to the pylon axis system, angle between the store longitudinal (X_B) axis and its projection in the X_P–Y_P plane, positive when the store nose is raised as seen by the pilot, deg

PHIBP, ϕ_{BP} [DPHI, $\Delta\phi$] — Roll angle of the store body axis system relative to the pylon axis system, angle between the store lateral (Y_B) axis and the intersection of the Y_B–Z_B and X_P–Y_P planes, positive for clockwise rotation when looking upstream, deg

Store Attitudes (Pitch-Yaw-Roll Sequence)

NUBP, ν_{BP} [DNU, $\Delta\nu$] — Pitch angle of the store body axis system relative to the pylon axis system, angle between the projection of the store longitudinal (X_B) axis in the X_P–Z_P plane and the X_P–axis, positive when the store nose is raised as seen by the pilot, deg

ETABP, η_{BP} [DETA, $\Delta\eta$] — Yaw angle of the store body axis system relative to the pylon axis system, angle between the store longitudinal (X_B) axis and its projection in the X_P–Z_P plane, positive when the store nose is raised as seen by the pilot, deg

OMGBP, ω_{BP} [DOMEGA, $\Delta\omega$] — Roll angle of the store body axis system relative to the pylon axis system, angle between the store vertical (Z_B) axis and the intersection of the Y_B–Z_B and X_P–Z_P planes, positive for clockwise rotation when looking upstream, deg